Development and Experimental Validation of Simple Methodologies for Modelling of Flow Boiling in Microchannels with Large Pressure Drop

A Thesis Submitted in
Partial Fulfillment of the Requirements
for the Degree of

Doctor of Philosophy

by

Ashif Iqbal

Department of Mechanical Engineering
Indian Institute of Technology Guwahati
Guwahati - 781 039
October 2019

Declaration

I declare that the work contained in the thesis entitled **Development and Experimental Validation of Simple Methodologies for Modelling of Flow Boiling in Microchannels with Large Pressure Drop** is done under the suprvison of **Professor Manmohan Pandey**, in the Department of Mechanical Engineering, Indian Institute of Technology Guwahati for the award of the degree of Doctor of Philosophy and this work has not been submitted elsewhere for a degree.

Ashif Iqbal
Research Scholar
Department of Mechanical Engineering
Indian Institute of Technology Guwahati

11th September 2019

Certificate

This is certified that the work contained in the thesis entitled **Development and Experimental Validation of Simple Methodologies for Modelling of Flow Boiling in Microchannels with Large Pressure Drop** and authored by **Ashif Iqbal**, a student in the Department of Mechanical Engineering, Indian Institute of Technology Guwahati for the award of the degree of Doctor of Philosophy has been carried out under my supervision and that this work has not been submitted elsewhere for a degree.

Dr. Manmohan Pandey
Professor
Department of Mechanical Engineering
Indian Institute of Technology Guwahati

11th September 2019

DEDICATED TO MY PARENTS

Acknowledgement

A PhD work can only be accomplished through a lot of support, encouragement and inspiration from the well-wishers. At the outset I thank the Almighty for blessing me with the strength and patience required to complete a PhD work. I take this opportunity to thank from the core of my heart all those people who have directly or indirectly contributed in this direction.

Words are not enough to express my gratitude towards my PhD supervisor, Prof. Manmohan Pandey. He has been a constant source of support, inspiration and invaluable guidance. I thank him from the bottom of my heart for imparting the basics of the relevant subjects in the best possible way before I embarked on my thesis-work. He has imbibed in me the habit of scientific thinking and systematic analysis. this juncture, I also take the opportunity to express my sincere thanks to Prof. Pandey' family members for being very affectionate and for their kind hospitality.

I thank the members of my Doctoral Committee, Prof. Niranjan Sahoo, Dr. Dipankar N. Basu (Department of Mechanical Engineering) and Prof. Subrat K. Majumdar (Department of Chemical Engineering) for their invaluable comments and suggestions during my progress seminars.

I would like to acknowledge Department of Mechanical Engineering, Indian Institute of Technology Guwahati for providing me with fund and facilities for carrying out my research. I am thankful to SERB, DST India providing me partial financial support during my research work. I am also grateful to the technical officers and staff– Mr. Rituraj Saikia and Nipjoyti Borah, Shaifuddin Ahmed, Manuranjan Dowarah, Joytirmoi Kakokti and all the workshop staff for their support and help.

I thank the reviews and editors of International Journal of Multiphase Flow and International Journal of Thermal Sciences for their valuable comments and suggestion which certainly improve the quality and presentation of this thesis.

I deeply thank my wife, Sultana Sehnaz (Barsha) for her constant love, sacrifice, support, encouragement and patience during the course of my thesis-work. All my family members have immensely contributed directly or indirectly towards the smooth completion of my Ph.D. I believe that the prayers and wishes from my grandfather Late Keramat Ali and grandmother Ms Nurunnesha always keep me in the right path. My father, Seikh Mamat instilled in me strong values, self-belief and a thirst for knowledge. My mother,

Sobiha Naznin taught me the importance of sincerity, hard work and honesty. I I thank my sister Rulia and my brother-in-law Jiyabul for their constant support and encouragement. I also thank my cousin brothers Mozibar and Wasim, my cousin sisters Najin and Jerifa and sister-in-law Pinky and my nice Nishi. I gratefully acknowledge the encouragement of my father-in-law and mother-in-law and Masum.

A special thanks to Mr. Sandip Kumar Sarma and Mr. Subhra Sankar Kalita for lifting up the confidence during difficult times and act like catalyst during solving any issue. The encouragements and suggestions form Dr. Paragmoni Kalita Sir, Dr. Bhaskor Jyoti Bora and Mr. Debarshi Mallick help every aspects of my life. I am lucky to have friends like Mr. Ujjwol Barman, Mr. Shahnawaz Ahmed, Mr. Vineet Kumar, Mr. Dhrubojyoti Kashyap, Dr. Kalpojoyti Borah, Mr. Subhas Matta, Mr. Arvind Kumar, Mr. Ratiram, Mr. Kiran Saikia, Ms. Baisalini Sethy, Mr. Rajesh Gupta, Mr. Kalule Ramanzani, Mr. Pratik Sondkar. Mr. Rohit Kumar, , Dr. Daya Sankar, Dr. Jai Manik, Dr. Hakeem Niyaz Dr. Vijay Mishra, and many more, who all have been my co-research-scholars in the Department of Mechanical Engineering. They have always provided me great help and support. The motivation, support from my friends- Mr. Prayash Barua, Mr.Sambaran Kapil, Dr.Kukil Khanikar, Dr. Bisawadev Sarma, Mr. Debajit Sarma, Mr. Ashim Kumar,Mr.Pallab Barman, Dr. Upama Dutta, Dr. Namrata Talukadar, Ms. Munmi Saikia always inspired me during this time.

I am grateful to Prof. Amit Agarwal and Dr. P.K. Saha and the Department of Mechanical Engineering, IIT Bombay for allowing me to work in the Microfluidics Lab. I convey my gratitude to Dr. Vijay Duryodhan, Mr. Ayyaz Siddique, Dr. Anvesh Gaddam, Mr. Somnath Dey, and all the supporting staff of CEN, IIT Bombay for their help and support during test section fabrication.

I feel fortunate to have received the love, cooperation and support from so many people in the completion of my PhD that it would not be possible for me to name them all. I thank all of them from the core of my heart.

Ashif Iqbal
Indian Institute of Technology Guwahati

Abstract

"Everything should be made as simple as possible but not simpler." Inspired by Albert Einstein's famous quote, this thesis proposes simple but accurate approaches to model the complex interplay between the various thermophysical phenomena occurring in flow boiling. The proposed methodologies incorporate the effect of flashing and local thermophysical properties on two-phase pressure drop evaluation, and hence on heat transfer prediction. The governing equations are derived in an elegant close form, consisting of a system of ODEs, and their simulation is computationally inexpensive. The new modelling approaches are validated by conducting experiments on a microchannel with a large pressure drop.

Dissipating high amount of heat flux is an important issue of modern thermal management with the ever-increasing demands for high performance and miniaturization. Flow boiling in microchannel heat sinks has emerged as one of the most effective solutions for cooling high and ultrahigh heat flux devices such as high-performance computer chips, laser diodes and nuclear fusion and fission reactors. Design of these miniature devices requires a proper estimation of the two-phase heat transfer, which, in turn, necessitates an accurate prediction of pressure drop in flow boiling. Two-phase pressure drop in microchannels is relatively high as compared to conventional channels, due to their very small sizes and moderate mass fluxes, the latter being so in order to achieve reasonable heat transfer coefficients. Due to the large pressure gradient, the saturation temperature drops, and hence the effects of flashing and axial variation of thermophysical properties become significant.

An extensive review is done on flow and heat transfer in microchannels, and the existing predictive methods are assessed using experimental data. The existing approach for modelling flow boiling pressure drop evaluates thermophysical properties at the system pressure and neglects the effect of flashing. To develop the flow boiling heat transfer coefficient, the existing methods assume a linear pressure profile to estimate local saturation temperature. These methods give fairly accurate predictions for small pressure drop cases, but not in cases where a relatively large pressure drop occurs. It indicates the need for improvements in predictive approaches for flow boiling pressure drop and heat transfer, especially for large pressure drop. To fill this gap, a new modelling approach has been developed for comprehensive evaluation of pressure drop along a microchannel with flow boiling. It is based on the separated flow model, incorporating the evaluation of thermophysical properties at local pressure, the effect of flashing on thermodynamic quality, and

the effect of heat flux on the two-phase multiplier. For the fluids with ideal gas behaviour of the vapour phase, the Clausius-Clapeyron equation is used to relate local pressure and temperature. A modified form of the Clausius-Clapeyron equation is developed to characterize the saturation line on the P-T plane for fluids whose vapour phase has nearly constant compressibility factor in the range of operation. On the basis of existing literature, it can also be inferred that there is a need for different predictive tools for pressure drop calculation in flow boiling as opposed to those for condensing and adiabatic flows. Therefore, for the non-adiabatic case, the two-phase multiplier is modified incorporating the heating effect.

The existing method of evaluation of local flow boiling heat transfer coefficient using a linear pressure profile assumption gives good predictions if the pressure drop is low but shows significant errors for large pressure drop cases. Using the new modelling approach of pressure drop prediction, local saturation pressure is evaluated for both large and small pressure drop cases. Estimation of the local heat transfer coefficient is found to be accurate when compared to experimental data from the literature with local pressure measurements in microchannels. A new methodology is suggested to develop correlations for flow boiling heat transfer coefficient with correct calculation of experimental heat transfer coefficient and accurate estimation of the variables associated with the correlations.

To validate these new modelling approaches for flow boiling pressure drop and heat transfer in microchannel, experiments are conducted on a single microchannel with hydraulic diameter of 111 μm. The fabrication of the test sections is done using microfabrication facility available at CEN, IIT Bombay. Heat loss calibration and uncertainty analysis is carried out to ensure the correctness of the measurements. Development of correlations for two phase pressure drop and heat transfer requires corresponding correlations for single phase flow. Therefore, single phase pressure drop and heat transfer in a trapezoidal microchannel are investigated. A new sample correlation of friction factor for the trapezoidal microchannel with non-adiabatic condition is developed. For heat transfer, the correlation of Wu and Cheng (2003) gives good agreement with the present experimental data.

Flow boiling experiments are performed using two working fluids (water and FC-72) with mass flux 205-690 kg/m^2s and heat flux 4.5-19.5 kw/m^2. The pressure drops observed for both the working fluids are large, facilitating validation of the new modelling approaches. The new predictive approaches for flow boiling pressure drop are validated for both the fluids. Comparison with experimental data demonstrates the effectiveness of the new pressure drop predictive approach relative to the existing approach. The new modelling approach for flow boiling heat transfer is illustrated by developing a sample correlation using experimental data from the literature and validating with experimental data. Another sample correlation is formulated using linear pressure profile assumption,

and it is found that the correlation formulated with the new methodology predicts the data more accurately for both the fluids.

Flow boiling heat transfer experiments are conducted in the same microchannel for both the fluids (water and FC-72) and the local heat transfer coefficient is evaluated at 16 mm from the inlet. To illustrate the new modelling approach for flow boiling heat transfer, a sample correlation was formulated by modifying a randomly chosen existing correlation using the experimental data from the literature. It was found that the correlation formulated with the new modelling approach improves the prediction over the original existing correlation chosen, for both the fluids. The new sample correlation was tested for experimental data from literature, and it was observed that the predictions were better for some data sets but poor for some other data sets, thus implying the need for further improvement in the correlation of h_{TP} considering extensive data sets for different ranges of fluid properties, shape, size, surface properties, and pressure drop.

The main contributions of the thesis are the new methodologies to predict pressure drop and heat transfer for flow boiling in microchannels. This is accomplished by relaxing some of the assumptions made in the existing predictive methods and validating the results by conducting experiments.

List of Publications

Publications from the Present Thesis

Journals

- Ashif Iqbal and Manmohan Pandey, 2018. Effect of local thermophysical properties and flashing on flow boiling pressure drop in microchannels, International Journal of Multiphase Flow. 106, 311-324.

  DOI: https://doi.org/10.1016/j.ijmultiphaseflow.2018.05.020

- Ashif Iqbal and Manmohan Pandey, 2018. A simple methodology to incorporate flashing and variation of thermophysical properties for flow boiling pressure drop in a microchannel. International Journal of Thermal Sciences. 132, 137-145.

  DOI: https://doi.org/10.1016/j.ijthermalsci.2018.05.046

.

Conferences

- Ashif Iqbal, Sandip Kumar Sarma and Manmohan Pandey, 2018. Non-adiabatic Flow Characteristics of Dielectric Fluids in Trapezoidal Microchannel, Proceedings of the 7th International and 45th National Conference on Fluid Mechanics and Fluid Power December 10-12, IIT Bombay, Mumbai, India

- Ashif Iqbal and Manmohan Pandey, 2016. Heat Transfer Model for Flow Boiling in Microchannel with the Effect of Pressure Profile and Variable Thermophysical Properties, Proceedings of the 6th International and 43rd National Conference on Fluid Mechanics and Fluid Power December 15-17, MNNITA, Allahabad, U.P., India. Paper No 107

- Ashif Iqbal and Manmohan Pandey, 2015. Two-phase slip flow pressure drop modeling in microchannels with variable physical properties, 42st National Conference on Fluid Mechanics and Fluid Power, December 12-14, NIT Suratkal, India. Paper No: FMFP2015-273

- Ashif Iqbal, and Manmohan Pandey, 2013. Modeling of pressure drop in microchannel flow boiling. Proceedings of the 22nd National and 11th International ISHMT-ASME Heat and Mass Transfer Conference, December 28-31, IIT Kharagpur, and India. Paper code: HMTC1300773

Contents

List of Figures

List of Tables

Nomenclature

A	Area of cross-section (m^2)
Bd	$\frac{(\rho_f-\rho_g)gL^2}{\sigma}$ (Bond number)
Bo	$\frac{q_{eff}}{Gh_{fg}}$ (Bond number)
C	Chisholm parameter
Co	$\sqrt{\frac{\sigma}{(\rho_f-\rho_g)gL^2}}$ (Confinement number)
C_p	Specific heat at constant pressure (J/kgK)
D_H	Hydraulic diameter (m)
Fa	$\frac{(\rho_f-\rho_g)\sigma}{G^2D_H}$ (Fang number)
f	Friction factor
F	Enhancement factor
G	Mass flux, kg/m^2s
H	Height (m)
h	Enthalpy (J/kg)
h_{fg}	Latent heat of vaporization (J/kg)
k	Thermal conductivity (W/mK)
L	Total length (m)
$\dot{m}$	Mass flow rate, kg/s
M	Molecular mass kg/mol
MAE	Mean absolute error
n	Number of channels
$N_{\mu TP}$	$\mu_{TP}/\left(\rho_{TP}\sigma\sqrt{\frac{\sigma}{g\Delta\rho}}\right)$ (Two-phase viscosity number)
Nu	Nusselt number
p	Pressure (Pa)
Pr	Prandtl number
p_{ref}	Reference Pressure (Pa)
P_F	Wetted perimeter (m)
P_H	Heated perimeter (m)
Δp	Pressure drop (Pa)

q	Heat input (W)
q_{eff}	Effective heat flux (W/m^2)
R	Universal gas constant (J/K kg)
Re_{fo}	Liquid only Reynolds number
Re_{go}	Gas only Reynolds number
S	Suppression factor
Su	Suratman number
T	Temperature (K)
T_f	Mean fluid temperature (K)
T_{ref}	Reference temperature (K)
v	Specific volume (m^3/kg)
W	Width (m)
We	$\frac{\nu G^2 L}{\sigma}$ (Weber number)
x	Thermodynamic equilibrium quality
z	Stream-wise coordinate (m)
Z	Compressibility Factor

Greek Symbols

α	Void fraction
β	Aspect ratio $(min(W,H)/max(W,H))$
μ	Coefficient of dynamic viscosity (Ns/m^2)
ν	Coefficient of kinematic viscosity (m^2/s)
ρ	Density of the fluid
σ	Surface Tension (N/m)
ϕ	Two-phase multiplier
Φ	Percentage predicted within $\pm$30%
X	Surface Tension (N/m)

Subscripts

a	Acceleration

amb	Ambient
b	Bottom
CB	Convective Boiling
exp	Experimental (measured)
in	Inlet
f	Liquid
fo	Liquid only
fr	Friction
g	Saturated vapor
go	Gas only
$Header$	Inlet header
NB	Nucleate Boiling
o	Outlet
$pred$	predicted
r	Reduced
s	Solid
sat	Saturation
SP	Single-phase
TP	Two-phase
T	Temperature
t	Top
tc	Thermocouple
w	wall
vv	Laminar liquid - laminar vapor

Chapter 1

Introduction

Focus on miniaturisation in today's world has increased the need for compact heat exchangers. Though our understanding of high-performance small scale cooling devices has increased tremendously in recent years, knowledge about flow boiling in microchannels is still not complete. In this chapter, the background, definition of microchannels, motivation for doing research in this field and basic phenomenon in flow boiling in microchannels are explained.

1.1 Introduction

1.1.1 Background

Miniaturization has recently become the keyword in many advanced technologies as well as traditional industries. Compact and micro heat exchangers, micro heat pipes, micro-fabricated fluidic systems and microelectronic devices are being progressively employed in the commercial sectors. Micro Thermal Mechanical Systems (MTMS), which includes heat exchangers, cooling assemblies and thermal systems implementing such devices, are used as micro-cooling elements for electronic components, portable computer chips, radar and aerospace avionics components and microchemical reactors. Along with single-phase, numerous two-phase (evaporation) cooling applications have also been identified. In two-phase flow, the phase change process enhances the heat transfer in cooling systems of electronic devices, thus allowing the device to function at high power densities.

The landmark study by Tuckerman and Pease (1981) was the first attempt to use a microchannel heat sink for electronic cooling. This opened the door for further investigations in that area. Since then, much effort has been devoted to improving the capabilities of microchannel heat sinks to remove the heat generated by electronic chips. Improvements in the development of microchannel heat sinks include the use of different microchannel geometries such as circular, rectangular, triangular, and trapezoidal designs to increase the area available for heat transfer. They also used different materials with high thermal conductivity such as copper, aluminium, and silicon to make the microchannell heat sinks. Due to the non-uniformity in the heat flux, hot spots in electronics chips are observed. This has motivated researchers to develop new heat sinks that can be directly embedded on the back of the heat source for uniform heat flux removal. Such a heat sink is usually made of silicon, with a silicon oxide layer to keep the component electrically insulated (Asadi et al., 2014). The increase in the rate of the heat generated by increasingly powerful electronics that continued to decrease in size forced designers to search for alternative coolants with better heat removal capabilities better than the abilities provided by air, and one alternative is liquid coolants (Adham et al., 2013). Liquid coolants (water, dielectric fluids) in single-phase as well as in two-phase, have been used in electronics cooling because of their relatively high heat removal capabilities.

1.1.2 Definition of Microchannels

The definition of microchannels has not been generally agreed. The attempts made by the researchers to differentiate between macro and micro-scale can be divided into two categories. One is based on fixed ranges of diameter or surface area per unit volume. Kandlikar and Grande (2003) used the hydraulic diameter for classification of single-phase

and two-phase heat exchangers as,

$$\begin{cases} \text{Microchannels} & : 10\mu m \leq D_H \leq 200\mu m \\ \text{Minichannels} & : 200\mu m \leq D_H \leq 3mm \\ \text{Conventional Channels} & : D_H \geq 3mm \end{cases}$$

Shah and Sekulic (2003) used the surface area density (β_s) and Mehendale et al. (2000) used hydraulic diameter as a criterion to differentiate between macro, compact, meso and micro heat exchangers. When the values of β_s are converted into hydraulic diameter, similar ranges are obtained as given by Mehendale et al. (2000).

Recently, many researchers argued that the criterion ought to be based on thermohydraulic properties rather than on channel dimension alone and do not seem representative for two-phase flows because they do not consider the physical mechanisms, different fluids or other flow effects (Karayiannis and Mahmoud (2017)). However, the bubble confinement looks like a suitable criterion for identifying the threshold between micro- and macro scale, the discrepancy is significant. Fukano and Kariyasaki (1993) found the critical diameter, at which the surface tension surpasses gravity, to be between 5 to 9 mm and the effect of diameter dominated over the flow direction when the hydraulic diameters were smaller than 6 mm. These conclusions agreed with the criterion of Kew and Cornwell (1997). They found that two-phase flow exhibits different flow and heat transfer characteristics when the confinement number is greater than 0.5. Confinement of a growing bubble is represented by the restriction of channel size on bubble growth, such that the bubble length is greater than the channel diameter. This dimensionless number depends on the diameter as well as surface tension and density of the liquid and vapor.Harirchian and Garimella (2010) derived the condition experimentally, under which microscale confinement effects are exhibited in flow boiling. Relation was based on convective confinement number ($Bd^{0.5}Re$) and is considered for present study, is given by Equation (1.1).

$$Bd^{0.5}Re < 160 \tag{1.1}$$

The other non-dimensional criterion for the transition from macro to micro scale were (a) Eotvos number $E\ddot{o} = 4\pi^2$ (Brauner and Maron (1992)) (b) Bond number $Bd^{0.3} \leq 0.3$ by Suo and Griffith (1964) (c)Laplace constant $La = D_H$ by Triplett et al. (1999) and (d) $E\ddot{o} = 1.6$ by Ullmann and Brauner (2007).

Flow pattern observation also reveals some deferences between macro and microchannels. Tibirica and Ribatski (2015) proposed two criteria for the transition from macro to micro scale flow. The first one was based on a mechanistic model for plug flow in a circular channel, and the transition was assumed to occur when stratified flow no longer existed. The second criterion was based on the uniformity of the liquid film thickness in annular

flow.

Chen et al. (2006) investigated flow boiling patterns for R134a in four vertical metallic tubes having inner diameters of 4.26, 2.88, 2.01 and 1.1 mm and found that the flow patterns in 4.26 mm and 2.88 mm diameter channels are similar to those observed in conventional channels. When the diameter was decreased to 2.01 mm, the flow patterns experienced small tube characteristics where the liquid film around the long bubble became thinner, and the liquid-vapour interface in churn flow became less chaotic. Also in the 2.01 mm tube, confined bubbles appeared first at 6 bar system pressure and were established at all pressures 6-14 bar when the diameter was decreased further to 1.1 mm. Since the 2.01 mm tube showed both small tube characteristics and conventional tube characteristics, they concluded that the threshold diameter between small and conventional tubes might be of the order of 2 mm.

Karayiannis and Mahmoud (2017) summarized the transition criterion and rewritten in a simple form to give the threshold diameter as a function of the Laplace constant (La) and presented a discussion connecting the flow pattern and the values associated with the criterion. Karayiannis and Mahmoud (2017) stated that the value given by Chen et al. (2006) agrees with the value predicted by the first criterion ($D_H = La\sqrt{8cos(\theta)}$) given by Tibirica and Ribatski (2015) and the criterion ($D_H = 2.94La$) given by Ong and Thome (2011) and is near to the values given by the criterion ($D_H = 2La$) of Cornwell and Kew (1993). Another important observation was that the values predicted by the two criteria ($D_H = La\sqrt{8cos(\theta)}$ and $D_H = La\sqrt{1/20}$) given by Tibirica and Ribatski (2015) were completely different. This may be attributed to the fact that they were based on two different ideas and two different flow regimes. This creates another complexity in the identification of the threshold diameter because it seems that there is a threshold for each flow regime. Additionally, the dependence of the different criteria on fluid properties and operating conditions make the definition of the threshold diameter very complex.

Karayiannis and Mahmoud (2017) also demonstrated the effect of saturation temperature (fluid R134a and water) and observed that some criteria demonstrate small dependence on the saturation temperature, while others indicate a strong dependence. Still there is a need for more systematic experiments with a wide range of diameters and different fluids to precisely estimate the transition criteria for the macro to microchannels.

1.1.3 Motivation

The capacity of integrated circuits is traditionally increased by adding more transistors on the surface of the chip. The number of transistor on integrated circuits doubles approximately every two years, according to Moore's law. However, the 2010 update to the International Technology Roadmap for Semiconductors suggests that for the first time in more than half a century, this trend will begin to slow near the end of 2013, after which

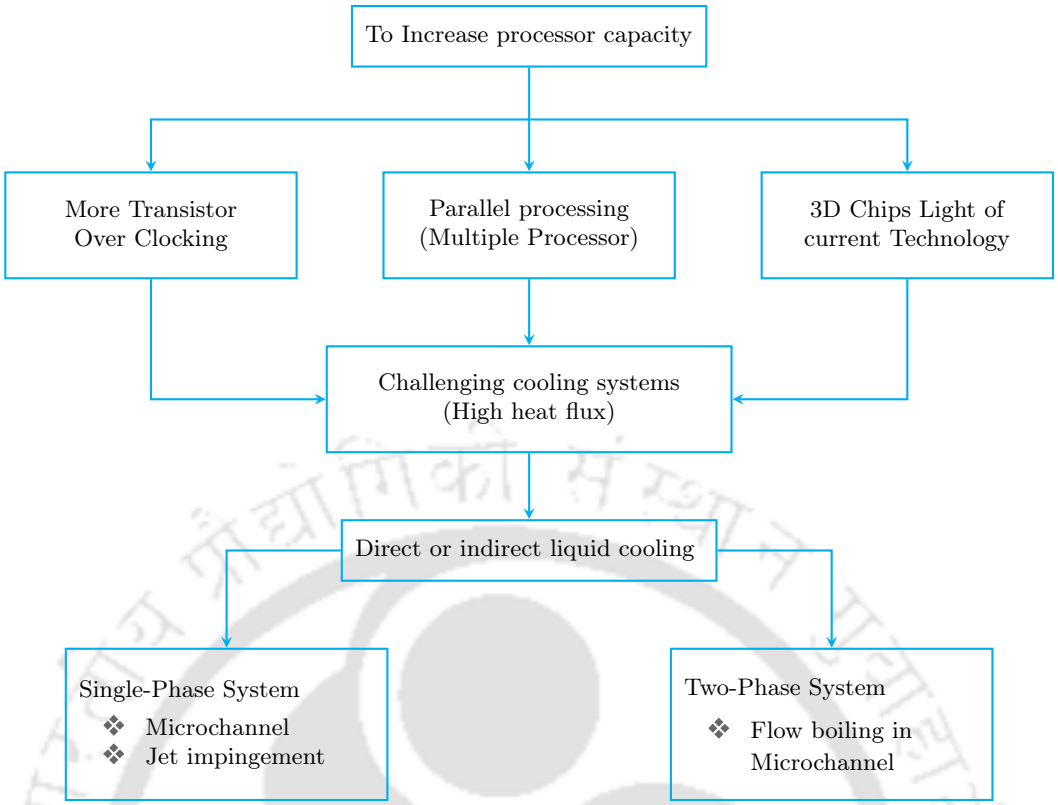

Fig. 1.1: Cooling system problem statement flow diagram

time transistor counts and densities are to double only every three years (Galvis and Culham, 2012). This drastic change from Moore's law is an indication of the limitation on the heat dissipation capacity of current cooling systems. Alternative techniques, such as Core technology or other novel techniques, are expected to increase chip performance. However, they are currently limited by the available cooling technologies. Therefore, new novel cooling technologies are required to allow for advances in chip performance. Figure 1.1 summarizes the cooling system problem flow diagram. In order to increase chip capacity, several techniques are used (more transistors, parallel processing or long term solutions). Unfortunately, many of these performance enhancements result in excessive heat generation that cannot be controlled by present-day cooling solutions. Therefore, new cooling strategies are required.

Boiling is one of the most capable heat transfer mechanisms for electronics cooling, but the understanding of the boiling process mechanisms in microchannels is still a challenge for the future development of two-phase cooling systems. An understanding of heat transfer mechanisms associated with microchannels boiling is not well understood, and this uncertainty is further complicated in microchannels where capillarity forces, and experimental accuracy, among other factors are more crucial. Design of the flow boiling miniature devices requires a proper estimation of two-phase heat transfer, which, in turn, necessitates accurate prediction of pressure drop in flow boiling. Flow boiling pressure drop

in microchannels is relatively high as compared to conventional channels, due to their very small sizes and moderate mass fluxes, the latter being so in order to achieve reasonable heat transfer coefficients. Due to the large pressure gradient, the saturation temperature — and hence the thermophysical properties — vary along the length, and the effect of flashing becomes significant. Therefore, the incorporation of these effect during prediction make the design more realistic. To ensure the efficient and computationally inexpensive design methodology, a physically sound and yet easy to implement an approach to evaluate flow boiling pressure drop and heat transfer is essential. All observations, analysis and modelling approach presented in this research are expected to help with a better understanding of the physical mechanisms during flow boiling in microchannels which is a key factor in the development of cooling systems for future high heat flux applications.

1.1.4 Flow Boiling in Miniature Channels

Boiling is the process in which heat transfer leads to a phase change of a substance from a liquid to a gas. Boiling will not occur if the wall temperature is below the saturation temperature. Saturation flow boiling occurs when the bulk liquid reaches saturation temperature, and sub-cooled flow boiling exists when the bulk liquid temperature remains below its saturation value, but the surface is hot enough for bubbles to form. There are two types of boiling: pool boiling refers to boiling from a heated surface submerged in a large volume of stagnant liquid, where the fluid flow is caused by a natural convective phenomenon only, and flow boiling, where the boiling occurs in a fluid which is flowing over a heated surface. Flow boiling is considerably more complicated than pool boiling, owing to the coupling between hydrodynamics and the boiling heat transfer process.

There are three different boiling heat transfer mechanisms: in nucleate boiling, bubbles form at the heat transfer surface and then break away to be carried into the main stream of the fluid. There is also convective boiling, where heat is conducted through the liquid which evaporates at the liquid-vapour interface. Finally, in film boiling, the heat is transferred by conduction and radiation through a film of vapor that covers the heated surface and the liquid vaporizes at the vapor-liquid interface.

Boiling is first initiated at the Onset of Nucleate Boiling, ONB, when some of the bubbles forming on crevices can survive condensation (e.g. no collapse of the vapor bubble). As the vaporization process proceeds, the vapor content of the flow increases with the distance along the tube and different flow pattern such as bubbly, plug, annular, and mist flow are observed as shown in Figure 1.2.

For conventional channels, depending on the flow conditions, regimes of slug, stratified, or wavy flow was observed. The qualitative axial variation of the heat transfer coefficient is also shown in Figure 1.2 The heat transfer coefficient, often (but not always) increases with the downstream distance prior to the onset of dry-out. Furthermore, as the wetted fraction

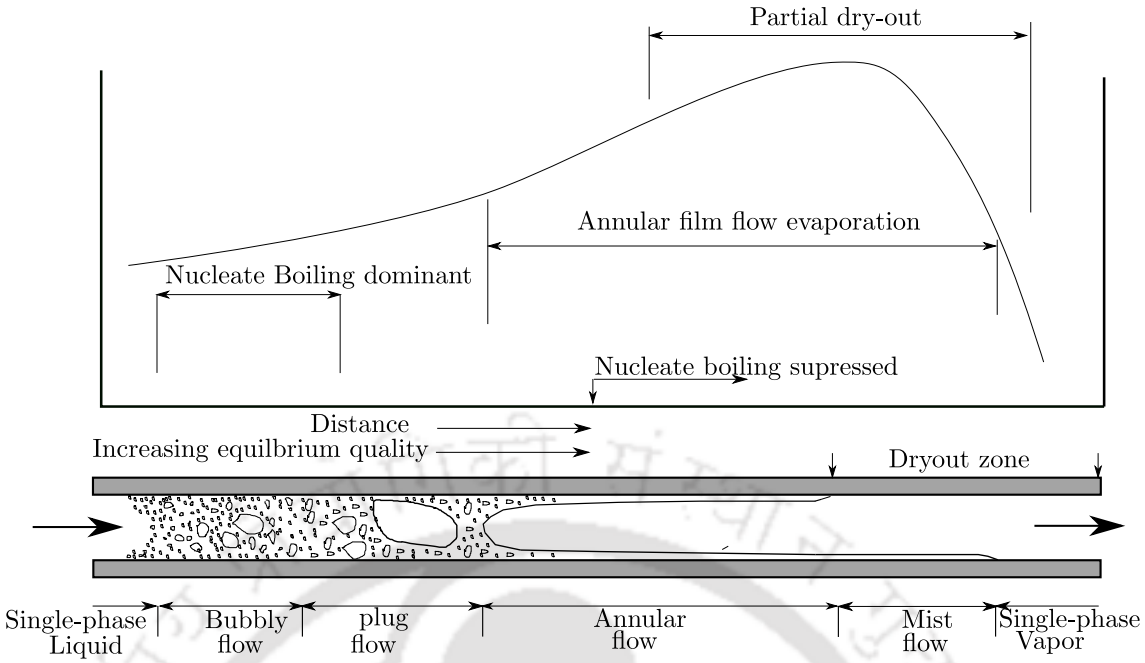

Fig. 1.2: Flow and heat transfer regimes in a uniformly heated horizontal tube with moderate heat flux

of the wall decreases with downstream distance, more of the wall becomes drier, and the heat transfer coefficient progressively decreases. Nucleate boiling is usually the dominant heat transfer mechanism near the ONB and at low equilibrium quality. As the liquid film on the wall thins, film evaporation may become so effective that it is the dominant mechanism. Between low and moderated qualities, both mechanisms may be important (Galvis and Culham, 2012).

In miniature channels, Kim and Mudawar (2012) explored dryout limits that constitute important boundaries to flow boiling heat transfer in small channels. Dryout is closely associated with the annular flow regime prevalent in saturated flow boiling in mini/microchannels. However, the axial span of the annular flow is highly dependent on working fluid and operating conditions. Two distinct heat transfer regimes have been identified based on mechanisms that dominate the largest fraction of channel length upstream of the dryout location. Shown in Figure 1.3(a) is Nucleate boiling dominant heat transfer, where a significant fraction of the channel length is dominated by bubbly, and slug flow and the heat transfer coefficient decreases monotonically due to gradual suppression of nucleate boiling. During the annular flow region, due to a decrease in film thickness h_{TP} increase to the inception of dryout. Figure 1.3(b) shows the second, Convective Boiling Dominant heat transfer, where a significant fraction of the channel length is dominated by annular flow and the heat transfer coefficient increases along the channel due to gradual thinning of the annular liquid film. Dryout of the annular film constitutes an important operational limit for both heat transfer types. But because of a lack of symmetry in the formation

and consumption of the annular film, initial dry patches begin to form at the location of dryout Incipience, which marks the point of a substantial reduction in the heat transfer. Dryout Completion, on the other hand, where the film is fully consumed, is encountered farther downstream.

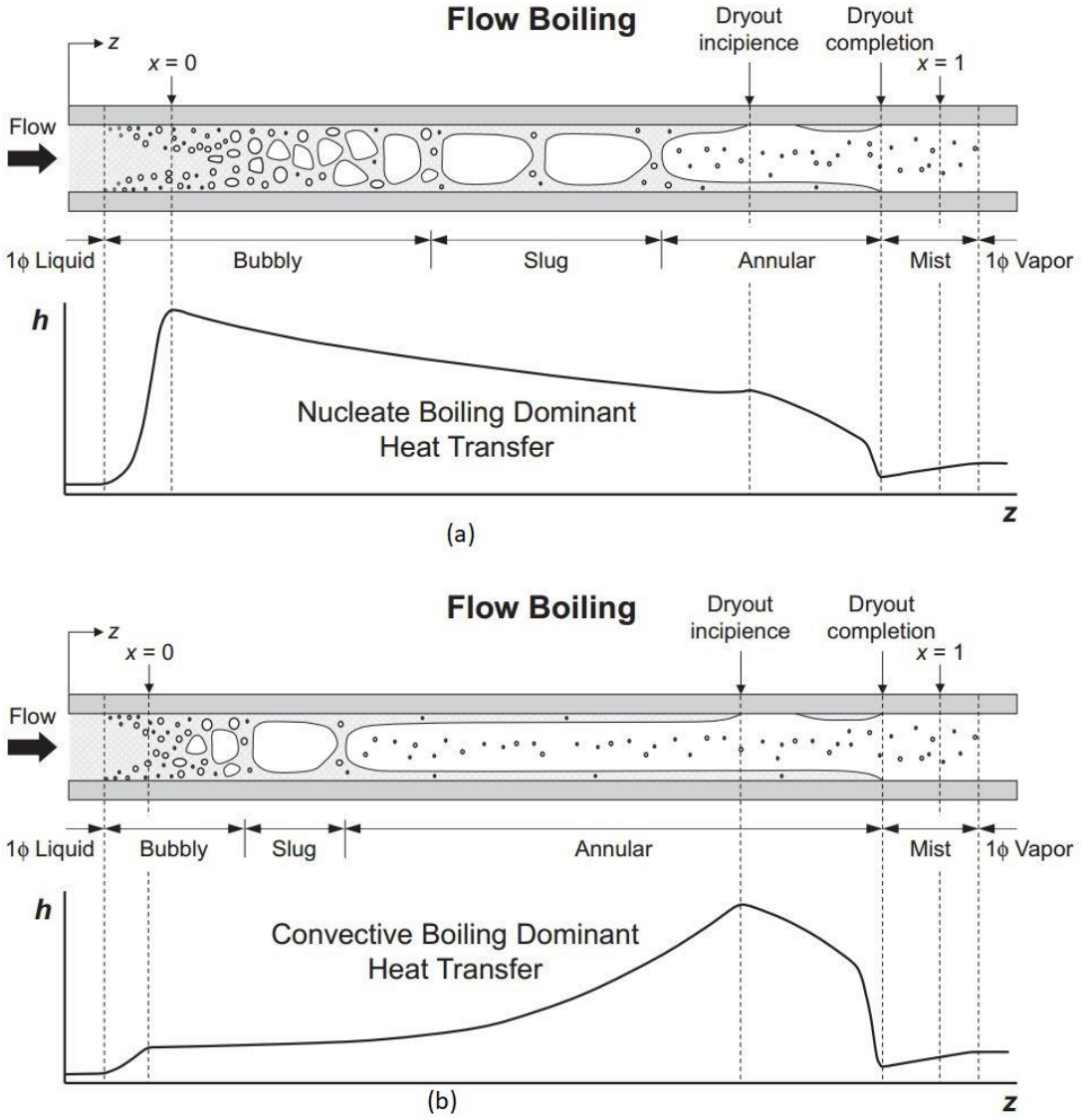

Fig. 1.3: Schematics of flow regimes, wall dryout and variation of heat transfer coefficient along uniformly heated channel for (a) nucleate boiling dominant heat transfer and (b) convective boiling dominant heat transfer (Kim and Mudawar, 2012)

Bigham and Moghaddam (2017) explained the physics of the microchannel flow boiling process. They conducted six benchmark experiments on bubbles at different growth stages to evaluate the assumptions of the existing microchannel flow boiling heat transfer models/hypothesis. The results (Figure 1.4) show that the bubble ebullition process

triggers a spike in the local surface heat flux due to the thin film evaporation and transient conduction heat transfer mechanisms. This enhancement in the surface heat flux is limited to a very small area at the bubble-surface contact region at the nucleation site limiting the overall heat transfer contribution of the bubble ebullition process. The contribution of these two mechanisms of heat transfer increases as the bubble-surface contact area becomes larger. As the bubbles length increases, the time period of activation of the microlayer evaporation mechanism substantially increases while that of the transient conduction mechanism remains relatively unchanged. When the microchannel is mostly occupied by bubbles, the thin film evaporation mechanism becomes the dominant heat transfer mode. The results clearly indicate that the single-phase heat transfer mechanism active at surface regions not covered by bubbles is governed by the laminar flow theory. In essence, a measurable enhancement effect in the liquid phase due to bubbles growth and flow has not been observed.

Baldassari and Marengo (2013) stated that it is very chancy to extrapolate macroscale two-phase flow boiling methods to microchannels, and, while the general trend of single-phase flow heat transfer in microscale seems to be reasonably well understood, this is not the case for boiling heat transfer.

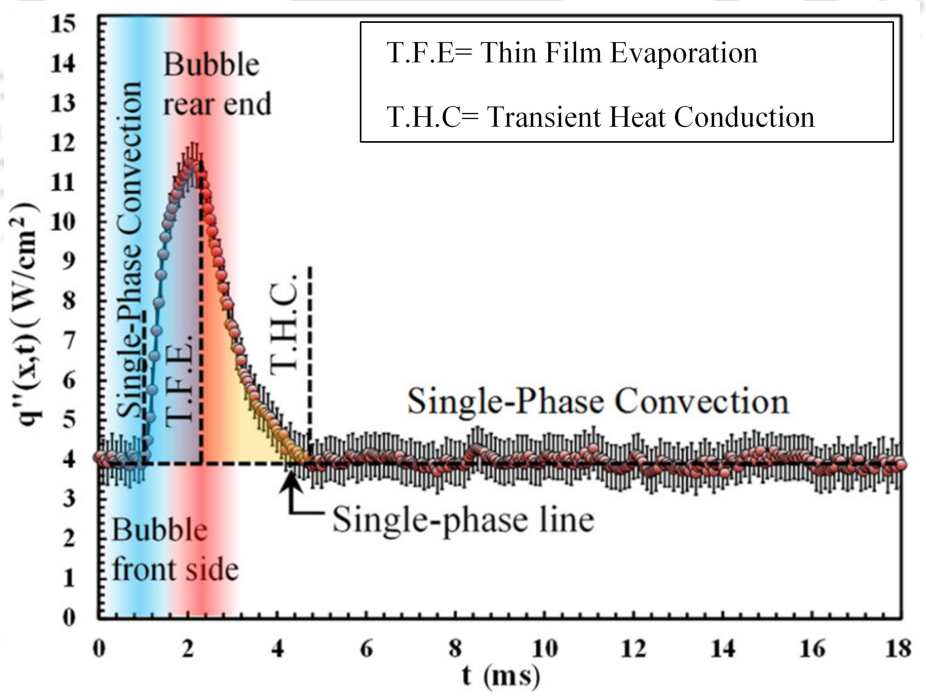

Fig. 1.4: Local heat flux data corresponding to a bubble with a passing time of 1.4 ms. Test is conducted at a mass flux of 68.4 kg/m^{2}s (Bigham and Moghaddam, 2017)

1.1.5 Flashing in Flow Boiling

Two-phase pressure drop in microchannels is relatively high as compared to conventional channels, due to their very small size and moderate mass fluxes. Due to the large pressure gradient, saturation temperature, and hence, the thermophysical properties along the length, vary, and the effect of flashing becomes significant. The phenomenon flashing in small tubes has been mentioned by several researchers ((Thome, 2004), Lin et al. (1991), Warrier et al. (2002)). A review on boiling in microchannels (Thome, 2004) has pointed out, "If the pressure drops are very large in the test sections, then the flashing effect on the enthalpy change has to be taken into account when determining and reporting the local vapor quality."

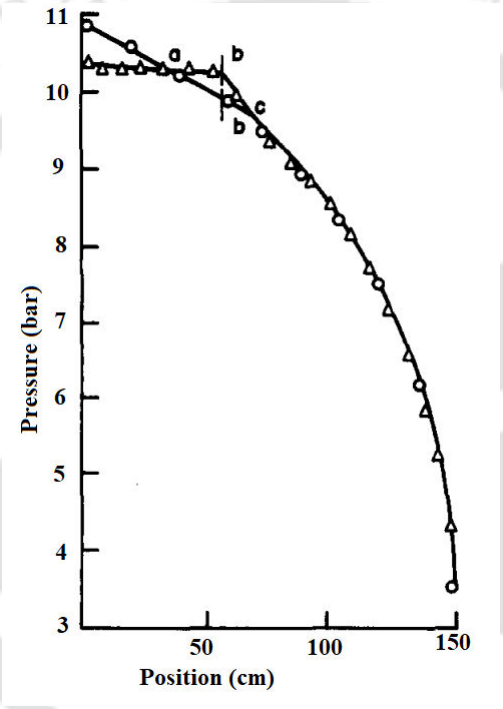

Fig. 1.5: Distributions of measured pressure, and the saturated pressure calculated from the corresponding temperature measured, along the capillary tube. Inlet pressure = 10.8 bar, inlet temperature = 316 K, back pressure = 3.0 bar, mass flux = 3975 kg/s (Lin et al., 1991)

Lin et al. (1991) explained the flashing phenomenon in the adiabatic flow of refrigerant in the capillary tube (Figure 1.5). Before vaporization of the refrigerant in the capillary tube, the measured temperature of the refrigerant is nearly constant. However, the measured pressure decreases linearly due to the friction losses. At the intersection point of the two pressure curves (a), the measured pressure is equal to the saturated pressure; therefore, the refrigerant is saturated at the intersection point. It can be seen that vaporization does not take place at the intersection. After point a, both the calculated saturated pressure (p_{sat}), and the measured pressure (p_{mes}), follow their original respective directions until

they reach section bb', as shown in figure 1.5. At point b, calculated saturated pressure suddenly drops–this is due to the temperature drop caused by absorption of the latent heat of vaporization of the refrigerant at this point. After point c, the two pressure curves join, indicating that $p_{mes} = p_{sat}$. This means that the thermodynamic equilibrium state is reached after point c (Lin et al., 1991).

Chapter 2

Literature Survey

Review is done on flow and heat transfer in microchannels and their predictive methods. The necessity of a more realistic predictive tool is underlined. Importance of flashing effect and difference between the boiling and adiabatic two-phase flows are discussed based on the literature. Single-phase pressure drop and heat transfer in microchannels are also discussed, and their importance in flow boiling modelling is highlighted.

2.1 Literature Survey

2.1.1 Single Phase Pressure Drop in Microchannels

Steinke and Kandlikar (2006) identified single-phase heat transfer enhancement techniques for use in microchannels and minichannels. They speculate that this increase in heat transfer performance from these techniques could place a single-phase liquid system in competition with a two-phase system; thus simplifying the overall complexity and reliability. However, they point out that the added pressure drop resulting from the techniques should be carefully evaluated. Therefore, it is important to evaluate the predictive methods for pressure drop occurring in a microchannel heat exchanger (MCHX). The design of supporting equipment such as the fluid pump and the secondary heat exchanger require an accurate estimate of the pressure drop in the MCHX. Flow characteristics of single-phase flow through microchannel is investigated by many researchers (Table 2.1) and these investigations can be categorized as the following groups.

- Effect of size and shape on pressure drop
- Effect of temperature dependent property
- Effect of roughness of the channel wall
- Effect of the entrance and exit losses in headers
- Flow behavior based on different conditions

Study of these categories are summarized in the table (Table: 2.1) where details of the experiments and numerical observations, flow condition, geometry and shape of the channels are listed. Single-phase pressure drop evaluation is an important part of total pressure drop calculation in microchannels since in practical use for a boiling heat removing device fluid enter at subcooled temperature.

Tab. 2.1: Literature survey on single phase pressure drop in microchannels

Authors (Year)	**Fluid**	**Shape**	$d_H(\mu\text{m})$	Re	**Key Findings**
Urbanek et al. (1993)	Isopropanol	T, Ti	5-25		Temperature variation affects the Poiseuille number (Po). As temperature deference increases, Po also increases.

Wang and Peng (1994)	Water, Methanol	R	311-745	80-3600	Considered the variation of thermophysical properties of the fluids. Earlier laminar to turbulent transition.
Peng and Peterson (1996)	Water	R	311	214-337	Fluid temperature, velocity have strong effects on flow transition.
Jiang et al. (1997)	Water	C, T	8-68	728	Flow resistance in non-circular microchannels is smaller than the conventional predictions.
Toh et al. (2002)	Water	R	84-105		As the temperature was increased, the friction factor decreased.
Park et al. (2003)	Water	R	73	4.2-19.1	PIV velocity measurement is used to investigate the flow characteristics. Thermal variation affects the velocity profiles in the microchannel.
Wu and Cheng (2003b)	Water	T, Ti	26-291	11.1-3060	Geometrical parameters have considerable influences on the apparent friction factor constant of the trapezoidal microchannels.
Qu and Mudawar (2003b)	Water	R	349	137-1670	Variation of pressure drop with respect to Re is depends on thermal variation of fluid viscosity and pressure losses at inlet and outlet sections.
Rathnasamy et al. (2005)	Water	R	1000, 655, 461	–	Analysis of friction factor versus Reynolds number relation shows a perceptible dependence on channel s
Shen et al. (2006)	Water	R	436	162-1257	Surface roughness has a considerable influence on the laminar flow. For high Reynolds number values, fRe is higher than the conventional theory predictions and increasing with growing Re.

M. et al. (2012)	Water	R	438-635	159-2303	When entrance effects, inlet and exit losses were considered, the results indicate that equations developed for conventional size channels are applicable for water flows in microchannels.
Sahara et al. (2017)	Water	R	100-1000	100-2000	The friction factor was found to decrease slightly with an increasing aspect ratio (AR) until AR $\approx$ 2, after which it increases continuously with AR. Thus, based on friction factor data only, an AR between 1 and 2 may be recommended for design to achieve low-pressure drop.

C=Circular; R=Rectangular; T=Trapezoidal; Ti: Triangular

2.1.2 Single Phase Heat Transfer in Microchannels

Single-phase heat transfer in microchannels was investigated and reported by several researchers. Some researchers claimed that the heat transfer coefficient in micro passages was different from that of macro passages; see Tuckerman and Pease (1981), Gao et al. (2002) and Silverio and Moreira (2008), whilst other researchers reported that conventional theory was still applicable for predicting the data for micro passages, e.g. Lelea et al. (2004) and Lee and Mudawar (2005). In contrast, Wang and Peng (1994) studied experimentally forced convective flow and heat transfer in rectangular stainless steel microchannels with hydraulic diameters ranging from 0.31 to 0.747 mm using water as the working fluid. They found that in turbulent flow, the trends of heat transfer coefficient could be predicted using Dittus-Boelter's correlation. In addition, they revealed that the laminar and transition heat transfer behavior in microchannels were unusual and complex and were strongly influenced by the liquid temperature, velocity and microchannel size.

The dependence of Nusselt number on the Reynolds number was found by Steinke and Kandlikar (2006). They investigated single-phase liquid heat transfer and pressure drop in various microchannel geometries. They used water as the working fluid, and the microchannels were made of a silicon substrate with D_H= 133.3 μm. They expressed the heat transfer performance in terms of thermal resistance. The thermal resistance depended on the Reynolds number for low mass fluxes but was independent of the Reynolds number for high mass fluxes. Similarly, Mishan et al. (2007), who studied experimentally the effect of developing thermal region on heat transfer performance of flow in microchannels made of aluminium with a hydraulic diameter of 440 μm, explained that the Nusselt number was not constant but increased with Reynolds number. Furthermore, the average Nusselt number increased from 5 to 7, with Reynolds numbers ranging from 40 to 560. A lower Nusselt number than conventional theory was found by Jiang et al. (2008). They elucidated that the Nusselt number remained constant when the flow rate was low, however, as the flow rate was increased, the Nusselt number significantly increased and exceeded the value of the Nusselt number for fully developed flow in conventional channels. Furthermore, the Nusselt number was affected by the heat flux when the mass flow rate was large. They stated that the Nusselt number of flows in microchannels was smaller than that in macrochannels at a flow rate of 1.8×10^{-5} m^3/s (1080 ml/min). The Nusselt number was constant at approximately two in the laminar regime for ΔT_{lm} ranging from 10 to 100. However, at a flow rate of 2.77×10^{-5} (1660 ml/min), the Nusselt number increased with ΔT_{lm} ranging from 10 to 60. In transition regimes, they found that the Nusselt number increased slightly, whilst in turbulent regimes, the Nusselt number increased sharply with the Reynolds number. A detailed review of the literature on Nusselt number prediction in microchannels is listed in Table 2.2.

Tab. 2.2: Literature survey on Nusselt number prediction in microchannel

Authors (Year)	**Fluid & Material**	**Shape**	$d_H(\mu\text{m})$	***Re***	**Key Findings**
Tuckerman and Pease (1981)	Water/Si	R	85-95	-	Nu is in the range of 3-9 and showing higher value
Wang and Peng (1994)	Water/SS	R	310-747	1000 -1500	Observed lover value of Nu w.r.t classical theory
Lelea et al. (2004)	Water/SS	C	100-500	10-800	Agreed with classical theory with Nu=4.36
Steinke and Kandlikar (2006)	Water/Si	R	133	61-364	Lower Nu observed.
Jiang et al. (2008)	Water/Cu	C, R	504	300-6000	Nu is lower for both the channels
Moharana et al. (2011)	Water/Cu	R	907	150-2500	Nu is smaller for minichannels
Duryodhan et al. (2015)	Water/Si	T	156	30-274	Agreed with their proposed correlation for diverging and converging microchannel
Sahara et al. (2017)	134a	R	409 & 461	200-2500	Experimental Nu is higher than that of their simulation
Wang et al. (2018)	HFE-7000	R	352	400-850	The local temperature along the centerline was always lower (indicating higher local heat transfer coefficient) than off the centerline due to vortex shedding and large-scale flow mixing

C=Circular; R=Rectangular; T=Trapezoidal; Ti: Triangular

2.1.3 Flow Boiling Pressure Drop in Microchannels

Dissipating high amount of heat flux is an important issue of modern thermal management with the ever-increasing demands for high performance and miniaturization. Flow boiling microchannel heat sinks have emerged as one of the most effective solutions for cooling high and ultrahigh heat flux devices such as high-performance computer chips, laser diodes (Kadam and Kumar, 2014). High heat flux removal miniature heat sinks are also used in the fusion reactor blanket design (Mudawar (2011)). Design of these miniature devices requires a proper estimation of two-phase heat transfer, which, in turn, necessitates accurate prediction of pressure drop in flow boiling. The total two-phase pressure drop of a fluid is the sum of the frictional pressure drop, the acceleration pressure drop, and the gravitational pressure drop. The frictional pressure drop can be determined by different two-phase models, and this has been an active research area for the last two decades. In order to calculate the two-phase pressure drop, extensive theoretical and experimental studies have been conducted. Since the mechanisms occurring in two-phase flow have not been effectively understood, a number of empirical correlations have been proposed instead (Xu and Fang, 2012).

Flow patterns exhibited during two-phase flow through microchannel also govern the two-phase pressure drop calculation. Collier and Thome (1994) have stated that the homogeneous model gives good predictions for bubbly and wispy-annular flow patterns, particularly at high velocities, whereas the separated flow model exhibits a good accuracy for slug flow and annular flow.

Two-phase pressure drop in microchannels is relatively high as compared to conventional channels, due to their very small size and moderate mass fluxes, the latter being so necessary to achieve reasonable heat transfer coefficients. Due to the large pressure gradient, saturation temperature, and hence, the thermophysical properties along the length, vary, and the effect of flashing becomes significant. It can be observed that pressure drop calculations in the literature are implicitly based on properties evaluated at the system pressure, neglecting the effect of flashing. The phenomenon of flashing in small tubes has been mentioned by several researchers. A review on boiling in microchannels (Thome, 2004) has pointed out, “If the pressure drops are very large in the test sections, then the flashing effect on the enthalpy change has to be taken into account when determining and reporting the local vapor quality.” Researchers have reported that flashing occurs in the flow of refrigerant in a small tube. The fluid pressure drops to the local saturation pressure at a certain axial location, flashing occurs at a point downstream, and the thermodynamic equilibrium state is resumed at a point further downstream (Mirmanto, 2014). Dário et al. (2016) incorporated the effect of flashing on thermodynamic quality, considering a linear pressure profile for heat transfer calculation. Mirmanto (2014, 2016) reported very informative observations by putting pressure sensors along the length of the microchannel. It

was observed that the pressure profile along the length was nonlinear, especially at higher heat flux, due to rapid bubble generation and non-uniform distribution of nucleation sites (Mirmanto, 2014). Pressure drop reported in the experiments was high (up to 75 kPa); therefore, existing modelling approach, based on system pressure, cannot predict these experimental data accurately. Park et al. (2012) also tried to validate the existing correlations for two-phase pressure drop with their experimental data considering properties at system pressure but ended up with significant deviation between the experimental result and the prediction. For vertical flow, using the homogenous model, Cioncolini and Thome (2017) considered the local pressure for evaluating thermophysical properties and calculated two-phase pressure drop. The evaporative channel was discretized into equal length subchannels, and the local pressure drop was computed using the local values of thermophysical properties. Then the pressure drops in the subchannels were added to get the total pressure drop. Experimental data from the literature show that depending upon the parameters (mass flux, heat flux, length, diameter), the two-phase pressure drop in the microchannel can reach up to nearly 100 kPa. For that range, if system pressure were considered then (for water as the working fluid), there would be an error (MAE) of 40% in v_g and 30% in h_f. As these two quantities (v_g and h_f) play an important role in the estimation of pressure drop and thermodynamic quality, they must be evaluated at the local pressure to get an accurate prediction of flow boiling pressure drop. The approaches used by different literature to predict flow boiling pressure drop is listed in Table 2.3.

Tab. 2.3: List of approaches used by different literature to predict flow boiling pressure drop

Authors (Year)	**Fluid/ Shape/ $d_H(\mu$m)**	**Model Used**	**Properties evaluated at / Flashing incorporated**	**Remarks**
Qu and Mudawar (2003b)	Water/ R/ 349	SFM	System Pressure / No	A new C-correlation is proposed which incorporates the effects of both channel size and G to improve pressure drop prediction

Lee and Mudawar (2005)	R134a / R/ 349	SFM	System Pressure / No	The new correlation incorporates the effects of liquid inertia, viscous force and surface tension on the two-phase pressure drop multiplier.
Huh and Kim (2007)	Water / R / 100	HEM, SFM	System Pressure / No	Existing approaches could not able predict the experimental two-phase frictional pressure gradient
Revellin and Thome (2007)	R134a, R245fa / C/ 509, 790	HEM	System Pressure / No	New prediction methods (f_{TP}) have been proposed here using the homogeneous model .
Lee and Garimella (2008)	Water / R / 162-570	SFM	System Pressure / No	A new pressure drop correlation based on the model of Mishima and Hibiki (1996) is developed.
Singh et al. (2009)	R134a / R /142	SFM	System Pressure / No	Qu and Mudawar (2003b) provides the best match with the experimental data.
Bhide et al. (2009)	Water / R / 45,65,70	SFM, HEM	System Pressure / No	All existing approaches over predicts the experimental data.
Ducoulombier et al. (2011a)	CO_2 / C / 529	HEM	System Pressure / No	respective pressure and fluid properties at the inlet pressure tap and outlet pressure tap was considered:
Li and Wu (2011)	R134a, R12 / R,C / 162-570	SFM, HEM	System Pressure / No	Surface-tension effects are considered with inclusion of the Bond number in the pressure drop calculation

Kim and Mudawar (2013b)	Water, R134a, R12, FC-72 / R,C / 349-3000	SFM, HEM	System Pressure / No	A new universal correlation for frictional pressure gradient is constructed.
Mahmoud et al. (2013)	R134a/ C / 1100	SFM, HEM	System Pressure / No	The test section heated length was found to have a significant effect on the measured pressure drop per metre length
Pike-Wilson and Karayiannis (2014)	R245fa / C / 1100	SFM, HEM	System Pressure / No	Importance of surface characteristics observed. The pressure drop correlations tested did not show good agreement with the experimental results
Dário et al. (2016)	R134a / R / 770	HEM	Linear Pressure profile / yes	The microscale correlations provide a better agreement with the experimental data than the macroscale ones.
Smpertegui-Tapia and Ribatski (2017)	R134a, R1234ze(E), R1234yf and R600a / C, R / 634-1100	SFM	Linear Pressure profile / No	Based on the broad database obtained, a new method for prediction of the two-phase frictional pressure drop was proposed.
Li and Hibiki (2017)	Water, R134a, R12, FC-72 / R,C / 100-3000	SFM, HEM	System Pressure / No	The C-correlation developed for 4 different conditions. (a) liquid-turbulent and gas-turbulent, (b) liquid turbulent and gas-laminar, (c) liquid-laminar and gas-laminar, and (d) liquid-laminar and gas-laminar.

Al-Zaidi et al. (2019)	HFE-7100 / R / 460	SFM, HEM	System Pressure / No	The flow boiling pressure drop data was predicted very well by the correlations ofMishima and Hibiki (1996) and Keepaiboon et al. (2016)
Markal et al. (2019)	water/ R / 100-250	SFM	System Pressure / No	Two new correlations are developed in order to predict flow boiling pressure drop in microchannels

C=Circular; R=Rectangular; T=Trapezoidal; Ti: Triangular

2.1.4 Difference of Boiling and Non-boiling flow behaviour

In microchannels, two-phase experiments have been reported in the literature for adiabatic as well as diabatic cases. In case of boiling, a significant effect of heat flux was observed for a smaller (190 μm) micro gap as compared to a larger gap (381 μm) (Alam et al., 2012). Kim and Mudawar (2013b) analyzed the fundamental differences in flow structure between boiling and non-boiling flows on the basis of existing literature (Kim and Mudawar, 2012). The difference was mainly due to the existence of entrained droplets in the vapor core for boiling flows and their absence from both condensing and adiabatic flows (Figure 2.1). For flow boiling in microchannels, bubbles coalesce very quickly in the upstream region of the channel, causing a rapid transition to annular flow, and liquid shattered from upstream forms small droplets that are entrained in the vapor core (Qu and Mudawar, 2004). However, in annular condensing flow in microchannels, no droplet entrainment in the vapor core has been observed (Kim and Mudawar, 2012). Thus, it can be inferred that there is a need for different predictive tools for pressure drop calculation in flow boiling as opposed to those for condensing and adiabatic flows. To account for these differences, Kim and Mudawar (2013b) modified the Chisholm parameter (C) for boiling as well as non-boiling cases.

2.1.5 Use of Dielectric Fluid for Flow Boiling in Microchannels

For the electronic cooling applications, dielectric fluids (FC-72 and FC-77) are suitable because they are thermally and chemically stable, compatible with sensitive materials, non-flammable, and practically nontoxic (Park et al., 2012; Jang et al., 2008). Condition under which microscale confinement effects are exhibited in flow boiling ($Bd^{0.5}Re = 160$) was given by Harirchian and Garimella (2010). Studies on flow boiling pressure drop of dielectric fluids in microchannels that fulfill the above mentioned condition are limited.

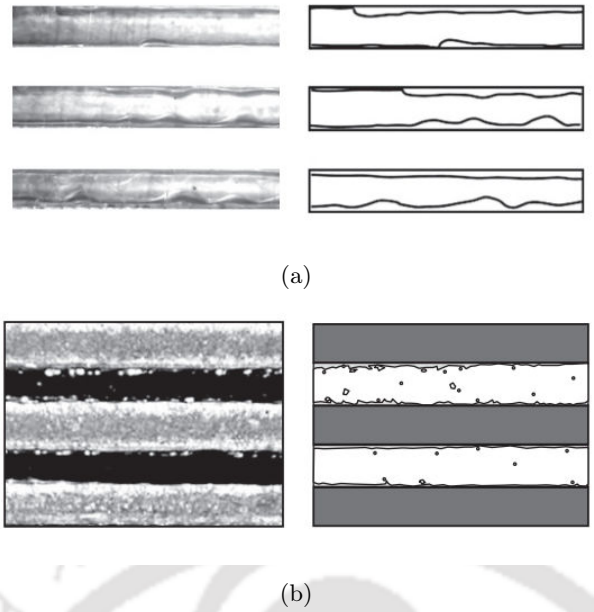

(a)

(b)

Fig. 2.1: Fundamental differences between (a) annular condensation (Kim and Mudawar, 2012) and (b) annular flow boiling in mini/micro-channels (Lee and Mudawar, 2005)

Flow boiling pressure drop characteristics and flow patterns of FC-77 in microchannels were studied by Harirchian and Garimella (2008, 2009b) and Chen and Garimella (2011). Jang et al. (2008) discussed the flow boiling pressure drop of FC-72 and modified existing pressure drop correlations by introducing the effective viscosity, including wall effects of the fluid in the small channel. Megahed and Hassan (2009) presented two-phase pressure drop data and flow visualization of FC-72 and observed that the frictional two-phase pressure drop increases with exit quality for a constant mass flux. Park et al. (2012) investigated the two-phase pressure drop of FC-72 and stated that pressure drop increased with increasing vapor quality and mass flux, and was nearly independent of heat flux for any given exit quality and mass flux. In view of the importance of dielectric fluids, further research on their flow boiling pressure drop characteristics and development of predictive tools for the design of microchannel heat sinks is the need of the hour.

2.1.6 Flow Boiling Heat Transfer in Microchannels

Most of the literature on flow boiling heat transfer in microchannels has focused on the mechanism of flow boiling. While the mechanism governs heat transfer trends, it is also important to develop accurate modelling approaches for evaluation of the local heat transfer coefficient ((h_{TP})) from the experimental data.Flow boiling local heat transfer coefficient (h_{TP}) can be calculated from Eq.(2.1). The measurement accuracy of heat flux and the wall temperature depends upon the power source reading considering heat loss calibration and thermocouples reading respectively and can be achieved with reasonable uncertainties.

$$h_{TP}(z) = \frac{q_{eff}}{T_w(z) - T_f(z)} \tag{2.1}$$

However, in microchannels, with direct contact method, local saturation temperature measurement in flow boiling is difficult due to space limitation (flow pattern disturbance) inside the channel. A limited number of studies were reported where local saturation pressure or temperature were measured and evaluated the local heat transfer coefficient. Using a large database compiled from multiple data sources, correlations for flow boiling heat transfer for microchannels were developed considering different flow conditions, hydraulic diameter, different fluids and aspect ratio. Along with these generalized correlations, some other correlations were developed using their own experimental data, which have a narrow range of parameters and may be useful for application within a similar range of parameters. In most of the correlations, during data reduction, local saturation temperature was evaluated by considering a linear pressure profile. And most importantly, thermophysical properties used in the correlations were evaluated at that pressure derived from linear pressure profile. All these assumptions will be valid if the pressure drop is low. For high-pressure drop, Mirmanto (2014) had observed experimentally that pressure profile for flow boiling in the microchannel is nonlinear, especially at higher heat flux, due to rapid bubble generation and non-uniform distribution of nucleation sites.

The trend of local heat transfer coefficients basically depends on the local saturation pressure (or saturation temperature) inside the channel and the wall temperature. Meanwhile, there was no accurate correlation to predict the local saturation pressures (temperatures) along the channel. Therefore, some authors considered the saturation pressure distribution decreases linearly in the two-phase region. The local saturation temperature depends on the prediction of local saturation pressures. The values of the local saturation temperature are greatly influenced by the assumption of the local pressure distribution. In general, experimental flow boiling pressure drops reported in the literature were obtained from the inlet and outlet pressure measurements, while the local pressure distribution usually was not reported. But many correlations for flow boiling pressure drop have been developed. Mirmanto (2014) also discussed that applying this pressure correlation to calculate the local pressure distribution as well as local heat transfer coefficient along the channel was not simple and even becoming more complicated when all components of the pressure drop such as accelerational and frictional pressure drops were included therefore Mirmanto considered linear pressure profile to evaluate local heat transfer coefficient Mirmanto (2014).

Contradictory experimental results were observed in the microchannel studies, and different interpretations on heat transfer trends and mechanisms were given. Some researchers, concluded that nucleate boiling was the dominant mechanism, whereas some others, reported that convective boiling dominated the heat transfer mechanism in mi-

crochannels. Several attempts have been made by different researchers to unify experimental data from different studies, but none of the models has been able to capture various trends observed in the experiments accurately.

Lin et al. (2001) performed a systematic experimental study of flow boiling with refrigerant R141b in circular tubes of diameter 1.8, 2.8, 3.6 mm and one square tube of 2 × 2 mm cross-section. They observed that the local heat transfer coefficient is a strong function of heat flux, a weak function of mass flux and depends on vapour quality. They concluded that both nucleate boiling and convective boiling occur during boiling in smaller channels. They also concluded that transition from nucleate boiling to convective boiling at high flux occurs at higher quality for smaller channels. The mean heat transfer coefficient was found to vary only slightly with channel dimension and was a function of mainly heat flux.

Tab. 2.4: List of approaches used by different literature to predict flow boiling heat transfer

Authors (Year)	**Fluid/ Shape**	**Range of $d_H(\mu$m)**	**Pressure profile/Consider Flashing**
Lazarek and Black (1982)	R134a/ C	3150	Linear / No
Shah (1982)	Water, R12, R22 / C	3150-25400	Linear / No
Warrier et al. (2002)	FC-84/ R	750	Non-Linear / Yes
Bertsch et al. (2009)	Water, FC-72/ R, C	160-2920	Linear / No
Li and Wu (2010)	Water, FC-77/ R, C	160-3100	Linear / No
Ducoulombier et al. (2011b)	CO_2 /C	529	Linear / No
Oh and Son (2011)	R134, R22 /C	1770, 3360, 5350	Linear / No
Kim and Mudawar (2013a)	Water, R134a, FC-77 / R,C	190-6500	Linear / No
Fang et al. (2015)	Water/ R,C	190-6500	Linear / No
Fayyadh et al. (2017)	R134a/ R	420	Linear / No
Korniliou et al. (2019)	FC 72/ R	190	Non-Linear / No
Jayaramu et al. (2019)	water/ R	324.3	Linear / No

C=Circular; R=Rectangular; T=Trapezoidal; Ti: Triangular

Qu and Mudawar (2003b, 2004) studied flow boiling heat transfer, pressure drop, flow patterns and instabilities in 21 parallel microchannels of 231 μm width and 721 μm depth using water as working fluid. They fabricated their test sections in oxygen-free copper block and used a transparent polycarbonate cover plate to enable high-speed visualisation while pressure drop and wall temperature (at four places) were also measured simultaneously. Qu and Mudawar (2003a) discussed heat transfer behavior and evaluated eleven existing heat transfer correlations with findings from their experiment. They found that the saturated flow boiling heat transfer coefficient is a strong function of mass flux and a weak function of heat flux. They also observed that annular flow as the dominant flow pattern at moderate to high heat fluxes. Hence, they hypothesized that dominant heat transfer mechanism for flow boiling in the microchannel is forced convection not nucleate boiling. They observed that unlike conventional channels, heat transfer coefficient decreases with increasing thermodynamic equilibrium quality. They found significant deviation in overall heat transfer trends even though correlations developed for smaller channels yield less mean error (Figure 2.2)

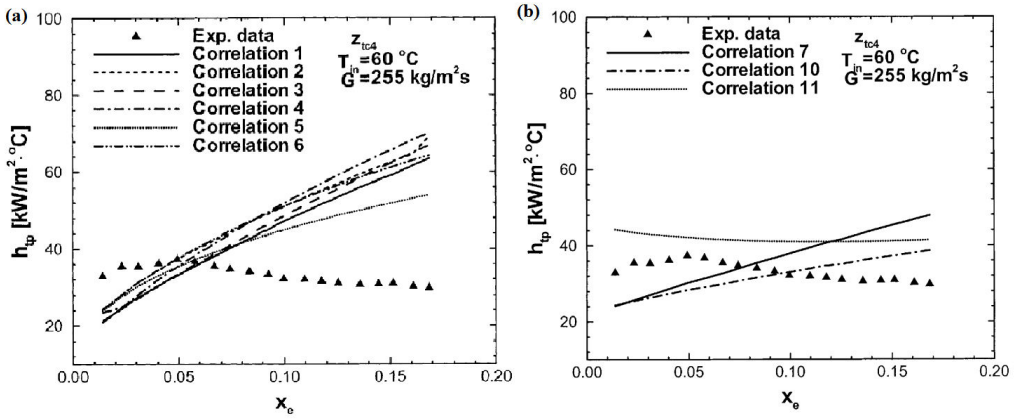

Fig. 2.2: (a) Comparison of saturated flow boiling heat transfer coefficient data with (a) macro scale and (b) mini/micro-channel correlation predictions (Qu and Mudawar, 2003a)

Steinke and Kandlikar (2004) performed an experimental investigation of flow boiling using water in six parallel, horizontal microchannels with a hydraulic diameter of 207 μm. They performed flow visualisation and measured pressure drop and heat transfer coefficient for a range of system parameters. They observed a decreasing trend of heat transfer coefficient with quality and concluded that nucleate boiling is the dominant mode of heat transfer.

Liu and Garimella (2006) carried out an experimental study of flow boiling heat transfer in microchannels of dimensions 275 μm $\times$ 636 μm and 406 μm $\times$ 1063 μm using DI water as a coolant. They identified two boiling regions, subcooled boiling and saturated boiling and tested some heat transfer correlations available in the literature for these regions. They

commented that Shah correlation (Shah and London, 1978) gave a reasonable prediction of heat transfer in the subcooled boiling region and developed a new correlation for saturated flow boiling regions based on Chen correlation (Chen, 1966). They found good agreement between prediction from the developed model and experimental data. They observed that amount of inlet subcooling and mass flux effect onset of nucleate boiling (ONB) but have little effect after ONB occurs.

(Harirchian and Garimella, 2008, 2009b) studied flow boiling of FC-77 through parallel rectangular microchannels of various sizes (width ranging from 100 μm to 5850 μm and depth of 400 μm). They fabricated their test pieces in the silicon wafer and measured wall temperature distribution with 5×5 array of temperature sensing diodes and also pressure drop across the channels. (Harirchian and Garimella, 2008) discussed the effect of channel size on flow boiling heat transfer and pressure drop. They found that for a fixed channel size, boiling curves and heat transfer coefficient is independent of mass flux in nucleate boiling dominant low heat fluxes. For microchannels of a size larger than 400 μm, the boiling curve also becomes independent of the channel width. Heat transfer coefficient increased with heat flux. They also tested pre-existing heat transfer correlations and found that Cooper correlation is able to predict the data with high accuracy. They commented that nucleate boiling is dominant for channels larger channels while convective boiling becomes important for smaller channels at low mass flux and hence concluded that convective boiling becomes more important as channel size and mass flux decrease. Mode of flow boiling heat transfer in different literature is listed in Table 2.5.

(Bertsch et al., 2009) studied flow boiling heat transfer with the refrigerants R-134a and R-245fa in copper microchannel arrays of hydraulic diameter 1.09 and 0.54 mm with an aspect ratio of 2.5. They found that the flow boiling heat transfer coefficient strongly increases with increasing heat flux and is dominated by nucleate boiling. They developed a correlation for flow boiling heat transfer considering different source of data from the literature.

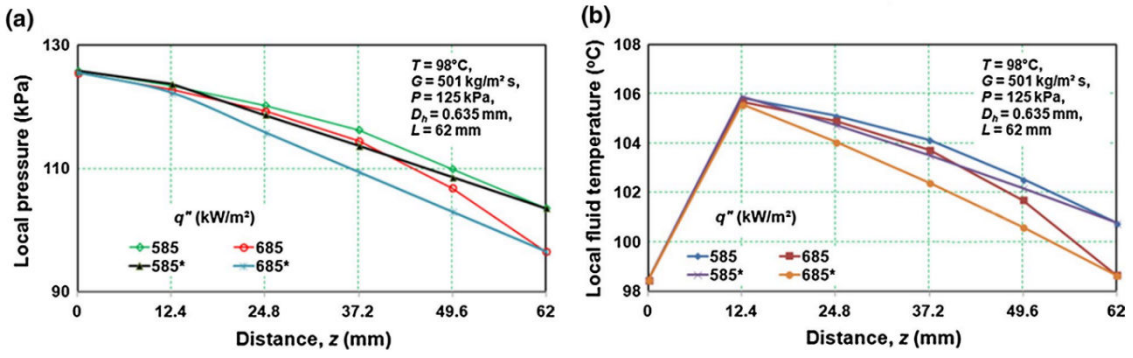

Fig. 2.3: Comparison between linear pressure gradient and actual variation (Mirmanto, 2016)

Mirmanto (2014, 2016) performed an experimental study of flow boiling of water

through rectangular copper microchannels with the hydraulic diameter of 0.438, 0.561 and 0.635 mm. Local pressure distribution was measured using four pressure tapings in axial direction while, wall temperature was also estimated for each of those locations using thermocouples inserted into the test section. The pressure drop across the channel was also measured. The author assumed a linear distribution of pressure in the axial direction to calculate saturation properties based on that pressure and compared that with calculations from actual pressure calculations. It was found that effect of heat flux on heat transfer was significant for bigger channels, and heat transfer coefficient increased with heat flux. For small channels, the effect decreases. It was found that a linear pressure gradient assumption was not accurate and introduced significant error in calculating the heat transfer coefficient (Figure 2.3). List of approaches used by different literature to predict flow boiling heat transfer is presented in Table 2.4.

Xu et al. (2016) investigated flow boiling of R-134a in circular tubes of diameters 1.002, 2.168 and 4.065 mm covering a mass flux range of 185-935 kg/m^2 s, a heat flux range of 18.0-35.5 kW/m^2, a saturation pressure range of 0.578-0.82 MPa, and a vapour quality range of 0.03-1.0. They found that heat transfer increases with increasing saturation pressure. For the smallest tube, heat transfer increased with quality, remaining constant in moderate quality values and then deceased. Using both their experimental data and database collected from literature, they evaluated 28 heat transfer correlations from literature including previously mentioned Fang correlations (Fang et al., 2015) and Bertsch (Bertsch et al., 2009) correlation. They found that Fang correlation developed for R-134a performs the best amongst the correlations tested collected from the literature.

Korniliou et al. (2019) studied the two-phase flow boiling heat transfer in a high-aspect ratio microchannel using FC-72 liquid. The hydrodynamic and flow boiling characteristics of the microchannel were monitored using high frequency and high spatial resolution infrared thermography, with heat transfer coefficients obtained as a function of axial position, lateral position and time and at the inlet, middle and outlet sections of the microchannel. The results suggest that the two-phase heat transfer coefficient does not increase monotonically with the heat flux, and actually decreases under certain conditions. This work identifies that the heat transfer coefficient depends on the range of the heat flux and is correlated with vapour-liquid dynamics and liquid film thinning resulting in suspected dryout, observed simultaneously with the temperature measurements.

Tab. 2.5: Mode of flow boiling heat transfer in different literature

Authors (Year)	**Fluid/ Shape/ $d_H(\mu$m)**	**Parameter Range**	**Dominant mode of Heat Transfer**
Lin et al. (2001)	Water/ C/ 1800 -3600	$G = 50 - 3500$ kg/m^{2}s $q_{eff} = 1 - 300$ kW/m^2	Both convective and nucleate
Qu and Mudawar (2003b)	Water/ C/ 349	$G = 255$ kg/m^{2}s $q_{eff} = 50 - 200$ W/cm^2	Forced convective boiling
Huo et al. (2004)	-/ C/ 4260	$G = 100 - 500$ kg/m^{2}s $q_{eff} = 50 - 200$ W/cm^2	Forced convective boiling
D. and V. (2006)	Water/ R / 400-700	$G = 221 - 1283$ kg/m^{2}s $q_{eff} = 1290$ kW/m^2	Nucleate boiling
Chen and Garimella (2007)	FC-72/ R / 1500	$m = 30 - 50$ ml/min	Contribution from convective boiling increases with mass flux
Ong and Thome (2009)	R134a, R236a/ C/ 1003	$G = 200 - 1600$ kg/m^{2}s $q_{eff} = 2.3 - 259$ kW/m^2	Nucleate boiling for low quality, convective boiling for high quality
Bertsch et al. (2009)	R134a/ R / 1009	$G = 20 - 350$ kg/m^{2}s $q_{eff} = 0 - 200$ kW/m^2	Nucleate boiling
Chen and Garimella (2011)	FC-72/ R / 160	$G = 253 - 1015$ kg/m^{2}s	5 different boiling regimes
Bertsch et al. (2009)	R134a/ R / 1009	$G = 20 - 350$ kg/m^{2}s $q_{eff} = 0 - 200$ kW/m^2	Nucleate boiling
Galvis and Culham (2012)	Water/ R / 120, 400	$G = 340 - 1296$ kg/m^{2}s $q_{eff} = 2197$ kW/m^2	Nucleate boiling
Mahmoud et al. (2013)	R134a/ C / 1100	$G = 100 - 500$ kg/m^{2}s $q_{eff} = 25 - 78$ kW/m^2	Nucleate boiling
Mirmanto (2014, 2016)	Water/ R / 438, 635, 561	$G = 200 - 800$ kg/m^{2}s $q_{eff} = 17 - 685$ kW/m^2	Nucleate boiling
Fayyadh et al. (2017)	R134a/ R / 420	$G = 50 - 300$ kg/m^{2}s $q_{eff} = 11.46 - 403.1$ kW/m^2	Nucleate boiling

Korniliou et al. (2019)	FC 72/ R / 190	$G = 7.37$ kg/m^{2}s $q_{eff} = 3.34 - 61.95$ kW/m^2	Both convective and nucleate boiling
Jayaramu et al. (2019)	water/ R / 324.3	$G = 1000 - 2220$ kg/m^{2}s $q_{eff} = 400 - 1200$ kW/m^2	Nucleate boiling

C=Circular; R=Rectangular; T=Trapezoidal; Ti: Triangular

2.2 Literature Closure

A detailed review of the existing literature is carried out for single-phase and two-phase flow in miniature channels. The main focus of the present review is on the methodologies used in the prediction of flow boiling pressure drop and heat transfer in microchannels. It can be concluded from the literature that the axial pressure profile for flow boiling is not the same for small and large pressure drop cases. Single-phase pressure drop or heat transfer prediction are also needed to predict the overall estimation of pressure drop and heat transfer of the evaporative system. Therefore, literature related to single-phase pressure drop and heat transfer is also reviewed. The summary of the review is listed below.

1. Experimental data from the literature show that, depending upon the parameters, the two-phase pressure drop in microchannels can reach up to nearly 100 kPa. For that range, if the system pressure were considered then (for water as the working fluid), there would be an error (MAE) of 40% in v_g and 30% in h_f. As these two quantities play an important role in the estimation of pressure drop and thermodynamic quality, they must be evaluated at the local pressure to get an accurate prediction of flow boiling pressure drop. Due to the axial variation of thermophysical properties, the effect of flashing become significant.

2. To develop the pressure drop modelling approach, most of the studies considered system pressure for evaluating the thermodynamic quantity and neglected the effect of flashing. Mirmanto (2014) observed that for large pressure drop cases, no pressure drop models predict the experimental data with good accuracy. Hence, there is a need for an accurate approach for pressure drop modelling for all ranges of pressure drop cases

3. To formulate flow boiling heat transfer correlations, estimation of local saturation temperature is important, and it requires an accurate axial pressure profile. In most of the correlation development methods, linear pressure profile was assumed to evaluate the local saturation temperature. This assumption is valid if the pressure drop is small. For large pressure drop case, axial pressure profile is non-linear, especially at

high heat flux (Mirmanto, 2014). Therefore a proper modelling approach is required to formulate heat transfer correlations.

4. Experimental flow boiling pressure drop and heat transfer data with large pressure drop is limited in the literature. Therefore the validation of these cases requires large pressure drop experiments in microchannels with deferent fluids.

5. In single-phase pressure drop study, there is no correlation of fRe for heated trapezoidal microchannel. Flow-through heated microchannels experience property variations along the length especially the effect of variation of viscosity near the wall.

2.3 Objectives

Although a large number of investigations have been carried out involving flow and heat transfer in microchannels, there is scope and need for the development of prediction methods in single-phase flow as well as in boiling. Therefore, the following objectives were identified.

1. To evaluate the effectiveness of the existing predictive approach for flow boiling pressure drop and heat transfer for small as well as large pressure drop cases and to investigate the causes of errors in the predictions.

2. To develop a predictive approach for flow boiling pressure drop and heat transfer in a microchannel for all ranges of pressure drop cases, by incorporating the significant phenomena, e.g., the effect of local thermophysical properties and flashing.

3. To generalize the predictive methodology for flow boiling pressure drop and heat transfer in a microchannel for fluids exhibiting non-ideal gas behavior of vapor phase.

4. To validate the new predictive approach for flow boiling pressure drop by conducting experiments with the variation of mass flux, heat flux and thermodynamic quality for different fluids

5. To illustrate the new modelling approach for flow boiling heat transfer, by developing a sample correlation using experimental data from the literature and validating it with own experiments.

6. To study single-phase pressure drop and heat transfer in a trapezoidal microchannel and to develop a one-dimensional mathematical model for liquid pressure drop in a heated microchannel incorporating variable properties.

The main approach to achieve the above objectives is to relax some of the assumptions made in the existing predictive method and to propose a new methodology to predict pressure drop and heat transfer for flow boiling in microchannels.

2.4 Outline of the thesis

In chapter 1, the need for this study, motivation to work on the topic and basic flow and heat transfer mechanism are discussed.

In chapter 2, work done by other researchers are put forth. The physics related to flow and heat transfer in microchannels for single-phase as well as flow boiling is discussed based on the literature review.

In chapter 3, existing approaches and correlations for evaluation of pressure drop and heat transfer in microchannels are verified. The results are analyzed to identify phenomena that need to be modelled accurately, especially for large pressure drop cases.

In chapter 4, two new predictive approaches for evaluating flow boiling pressure drop and heat transfer for large pressure drop are presented and validated with experimental data from the literature.

In chapter 5, the fabrication process of the test section, selection of the equipment and assembling and the flow loop are described.

In chapter 6, single-phase flow and heat transfer through a microchannel for heated and unheated cases are discussed. A correlation of friction factor considering two working fluids (water and FC-72) for a heated trapezoidal microchannel is developed from the present experimental data.

In chapter 7, flow boiling pressure drop in a microchannel is investigated for water as well as FC-72. Effects of parameters (heat flux, mass flux and thermodynamic quality) on flow boiling pressure drop are examined experimentally. The data obtained are used to validate the new pressure drop modelling approaches developed in Chapter 4.

In chapter 8, flow boiling heat transfer in a trapezoidal microchannel is experimentally investigated for water as well as FC-72. Effects of parameters on flow boiling heat transfer are studied. Using the new pressure drop predictive approach, a new methodology is devised and illustrated by developing and validating a sample correlation for flow boiling heat transfer.

In chapter 9, finally, the conclusions of the work done in all the chapters are summarized, and future extensions of the present work are discussed.

Chapter 3

Assessment of Existing Approaches

In this chapter, existing approaches for the evaluation of flow boiling pressure drop and heat transfer are discussed. Experimental data are extracted from the literature, and different correlations for flow boiling pressure drop and heat transfer are examined. Existing approaches for pressure drop show good predictions for small pressure drop, but they suffer from significant deviations in predicting relatively large pressure drop data. For the prediction of flow boiling heat transfer, the existing methods use linear pressure profile to evaluate local saturation temperature and thermophysical properties. This is a reasonable assumption if the pressure drop is small but causes a significant error in prediction if the pressure drop is large.

3.1 Existing Approach for Flow Boiling Pressure Drop

The two-phase pressure drop in steady-state can be expressed as the sum of frictional, gravitational and acceleration components. In two-phase flow through microchannels, commonly observed flow patterns in the literature were slug flow and annular flow (Qu and Mudawar, 2004). Researchers have observed different flow patterns in microchannels, but for very small hydraulic diameter (around 100 μm) bubbly flow gets suppressed(Kawahara et al. (2002) and Wang et al. (2007)). The homogeneous equilibrium model of two-phase flow assumes no slip between the phases and hence, cannot accurately model these flow patterns (Collier and Thome, 1994). Therefore, most of the literature used the separated flow model to obtain good agreement with experimental data because of its applicability with observed flow patterns (slug and annular flow) (Mishima and Hibiki, 1996; Lee and Lee, 2001; Qu and Mudawar, 2003b; Lee and Mudawar, 2005; Li and Wu, 2011; Kim and Mudawar, 2013b; Li and Hibiki, 2017). The frictional pressure drop component evaluated from the separated flow model was expressed by Equation (3.1), and the acceleration pressure drop was given by Equation (3.2). The thermodynamic equilibrium quality (x) was determined from the energy balance considering Figure 3.1, without the effect of flashing and given by Equation (3.3). The exit quality (x_o) was found by putting $z = L$.

$$(\Delta p_{_{tp}})_{fric} = \int_0^{x_o} \left[\frac{2G^2 v_f}{D_H} (1 - x_o)^2 \phi_f^2 \right] dx \tag{3.1}$$

$$(\Delta p_{tp})_{acc} = G^2 v_f \left[\frac{x_o^2 v_g}{\alpha_o v_f} + \frac{(1 - x_o)^2}{1 - \alpha_o} - 1 \right] \tag{3.2}$$

$$x = \frac{q_{eff} P_h}{G A h_f g} (z - L_{sp}) \tag{3.3}$$

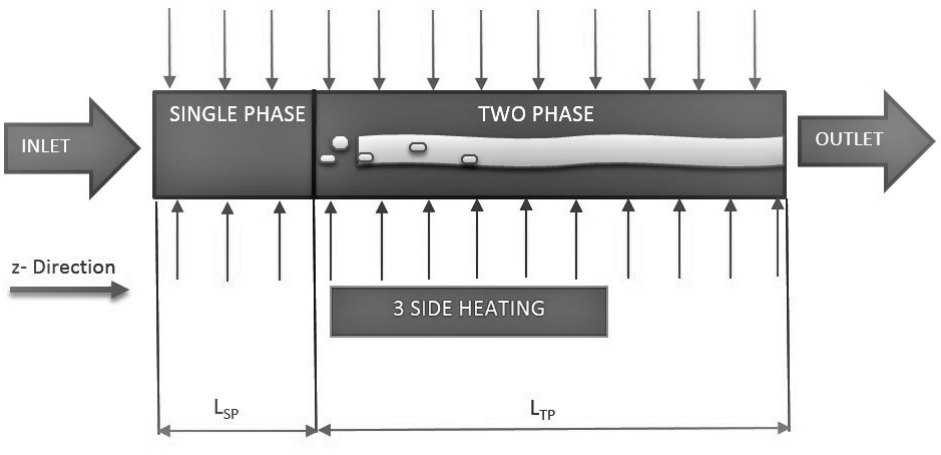

Fig. 3.1: Process flow of the Fabrication Technique

In the frictional pressure drop, the two-phase multiplier ϕ_f^2 and the Martinelli parameter (X_{vv}) (Collier and Thome, 1994) for laminar vapor and laminar liquid were expressed by Equation (3.4) and Equation (3.5), respectively. All experimental data used in the thesis (Qu and Mudawar, 2003b; Mirmanto, 2014) falls into the laminar vapor and laminar liquid region.

$$\phi_f^2 = 1 + \frac{c}{X_{vv}} + \frac{1}{X_{vv}^2} \tag{3.4}$$

$$X_{vv} = \left(\frac{\mu_f}{\mu_g}\right)^{0.5} \left(\frac{v_f}{v_g}\right)^{0.5} \left(\frac{1-x}{x}\right)^{0.5} \tag{3.5}$$

Evaluation of the accelerational pressure drop requires a relation for void fraction. In most of the literature related to miniature channels (Mishima and Hibiki, 1996; Lee and Lee, 2001; Qu and Mudawar, 2003b; Lee and Mudawar, 2005), Zivi's void fraction correlation, given by Equation (3.6), has been used.

$$\alpha_o = \frac{1}{\left(1 + \left(\frac{1-x_o}{x_o}\right)\left(\frac{v_g}{v_f}\right)^{(2/3)}\right)} \tag{3.6}$$

In the existing approach to pressure drop modelling, the Chisholm parameter (C) was modified to predict the pressure drop. All the modified expressions for the Chisholm parameter (C) are listed in Table 3.1 In Figure 3.2, pressure drops predicted with the existing approach using different correlations (Mishima and Hibiki, 1996; Lee and Lee, 2001; Qu and Mudawar, 2003b; Lee and Mudawar, 2005; Li and Wu, 2011; Kim and Mudawar, 2013b; Li and Hibiki, 2017) are compared with experimental data from the literature (Qu and Mudawar, 2003b) where the pressure drop was small. It is observed that almost all the correlations are able to predict the data with reasonably good accuracy.

In Figure 3.3, the predictions of the same correlations (listed in Table 3.1) with the existing modelling approach are compared with experimental data from the literature (Mirmanto, 2014) where the pressure drop was relatively high. It is observed that the existing approach, with any of the correlations, exhibits poor prediction of the experimental data for these cases, the percentage deviation being larger for higher pressure drop. The existing approach neglects the effect of local properties and the effect of flashing - assumptions valid for low-pressure drop cases only. MAE (%) for each model is listed in Table 3.1 and given by Equation (3.7).

$$\text{MAE } (\%) = \frac{1}{N} \sum \frac{|\Delta p_{pred} - \Delta p_{exp}|}{\Delta p_{exp}} \times 100 \tag{3.7}$$

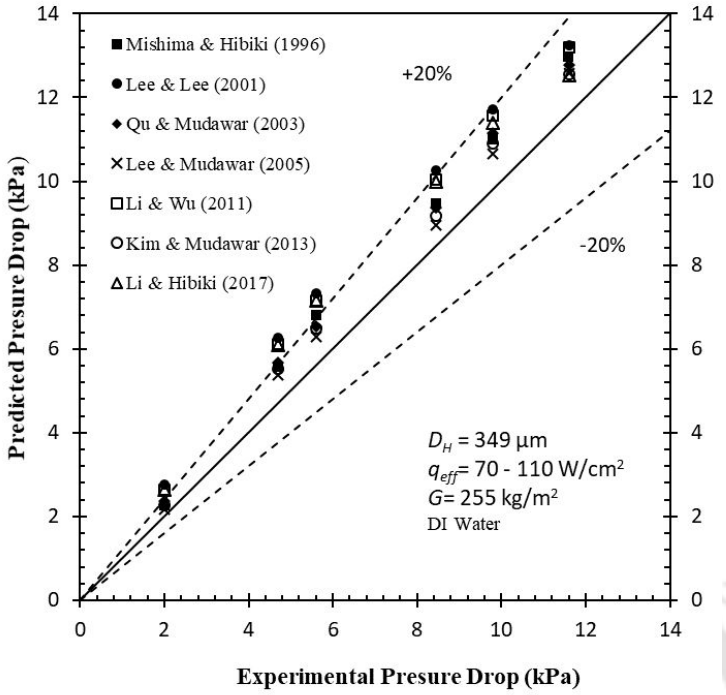

Fig. 3.2: Comparison of the existing correlation for small pressure drop case with experimental data from (Qu and Mudawar, 2003b); Water, $D_H = 349$ μm and G=255 kg/m^{2}s

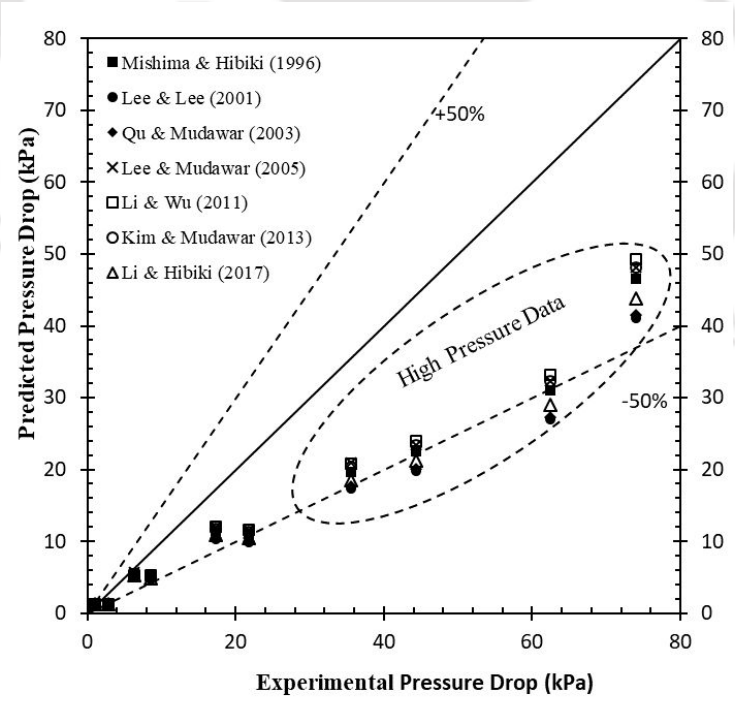

Fig. 3.3: Comparison of the existing correlation for large pressure drop case with experimental data from (Mirmanto, 2014), water, $D_H = 438$ μm and G=805 kg/m^{2}s

The causes for this high margin of errors in the calculation of two-phase pressure drop in microchannels, in case of high-pressure drop, are the following.

1. For relatively high-pressure drop cases, assumption of system pressure instead of local pressure to evaluate the thermophysical properties contributes a part of total error.

2. Effect of flashing, i.e., the effect of pressure drop in the calculation of the thermodynamic quality was not considered in the existing approach. Hence, the vapor quality is underpredicted, which results in an underestimation of the pressure drop.

3. Estimation of two-phase frictional pressure drop for boiling channels requires a different approach as opposed to non-boiling channels. This effect was incorporated in C by (Kim and Mudawar, 2013b), thus resulting in the lowest MAE among all models listed in Table 3.1.

Tab. 3.1: List of modified Chisholm parameter from literature

Authors [References]	Equations for Chisholm Parameter (Liquid Laminar and Gas Laminar)	MAE (%) LPD	MAE (%) SPD
Mishima and Hibiki (1996)	$C = 21(1 - e^{319D_H})$	43.73	17.35
Lee and Lee (2001)	$C = 6.185 \times 10^{-2} Re_{fo}^{0.726}$	42.24	16.13
Qu and Mudawar (2003b)	$C = 21(1 - e^{319D_H}) \times (0.00418G + 0.06613)$	41.67	12.15
Lee and Mudawar (2005)	$C = 2.16 Re_{fo}^{0.047} We_{fo}^{0.60}$	40.12	11.95
Li and Wu (2011)	$C = 5.6 Bd^{0.28}$ for $Bd < 0.1$	43.35	15.25
Kim and Mudawar (2013b)	$C_{boil} = 3.5 \times 10^{-5} Re_{fo}^{0.44} Su_{go}^{0.5} (\rho_f/\rho_g)^{0.48} \times \left[1 + 530 We_{fo}^{0.52} (Bo(P_H/P_F))\right]$	37.79	10.73
Li and Hibiki (2017)	$C = 41.7 Nu_{\mu_{TP}}^{0.66} Re_{TP}^{0.42} x^{0.21}$ $Nu_{TP} = \mu_{TP} / \left(\rho_{TP} \sigma \sqrt{\sigma / g \Delta\rho}\right)^{0.5}$ $1/\mu_{TP} = (1-x)/\mu_f + x/\mu_g$ $\rho_{TP} = (1-x)/\rho_f + x\rho_g$	40.05	11.36

LPD = Large Pressure Drop; SPD= Small Pressure Drop

3.2 Existing Approach for Flow Boiling Heat Transfer

Although, flow boiling mechanism governs the trend of heat transfer, accurate approach to evaluate local heat transfer coefficient (h_{TP}) from the experimental data is the matter of discussion. Flow boiling local heat transfer coefficient (h_{TP}) can be calculated from Equation (3.8). The measurement accuracy of heat flux and the wall temperature depends upon the power source reading considering heat loss calibration and thermocouples reading respectively and can be achieved with reasonable uncertainties.

$$h_{TP}(z) = \frac{q_{eff}}{T_w(z) - T_f(z)} \tag{3.8}$$

However, in microchannels, with direct contact method, local saturation temperature measurement in flow boiling is difficult to obtain due to space limitation (flow pattern disturbance) inside the channel. A limited number of studies were reported where local saturation pressure or temperature were measured and evaluated the local heat transfer coefficient. For proper estimation of saturation temperature at that local point ($T_f(z)$), proper estimation of local saturation pressure ($p_{sat}(z)$) is required. In most of the literature, to evaluate $T_f(z)$, a linear pressure profile was assumed and was given by Equation (3.9)

$$p_{sat}(z) = p_o + \frac{L - z}{L - L_{sub}} \left(p_{sat}(z_{sub} - p_o)\right) \tag{3.9}$$

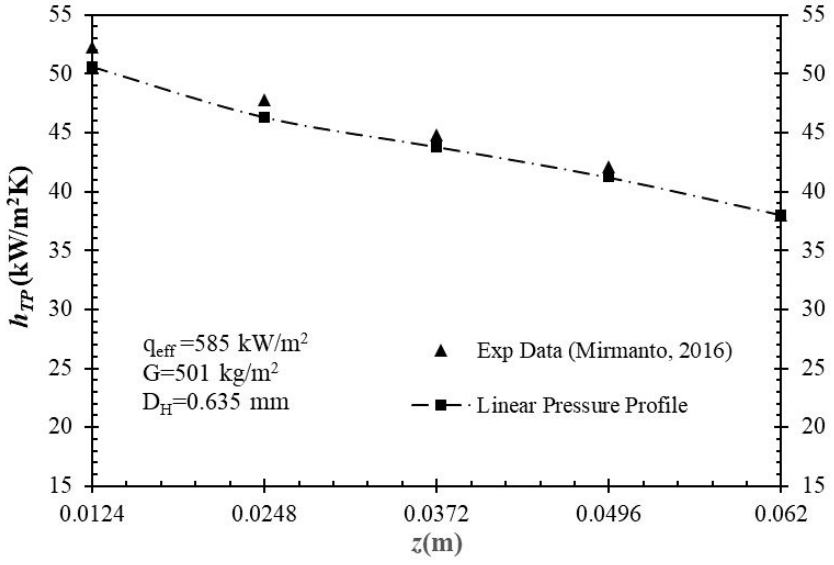

Fig. 3.4: Local two phase heat transfer coefficient considering linear pressure profile was compared with experimental data for small pressure drop case; Mirmanto (2016), water, $D_H = 635$ μm and G=501 kg/m^{2}s

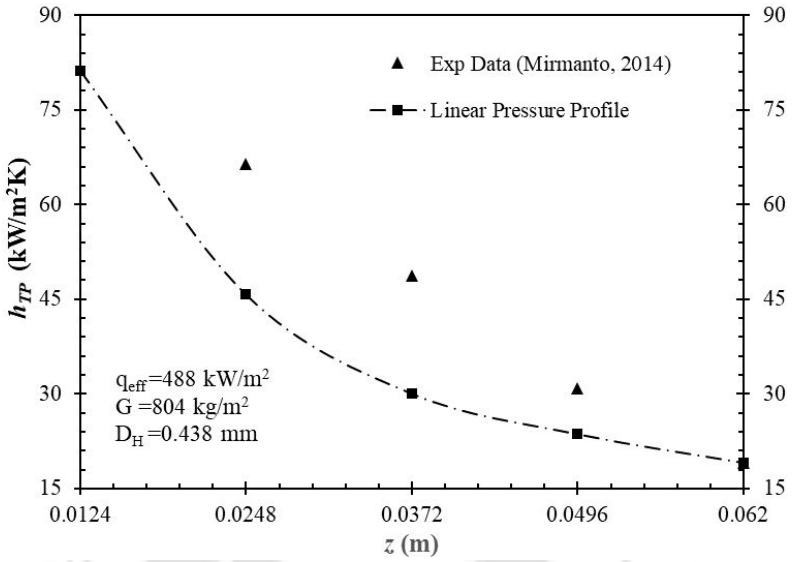

Fig. 3.5: Local two phase heat transfer coefficient considering linear pressure profile was compared with experimental data for large pressure drop case; Mirmanto (2014), water, $D_H = 438$ μm and G=805 kg/m^{2}s

Mirmanto (2014, 2016) reported very informative observations by putting pressure sensors along with the length of the microchannel. It was observed that the pressure profile along the length was nonlinear, especially at higher heat flux, due to the rapid bubble generation and non-uniform distribution of nucleation sites (Mirmanto, 2014). Pressure drop reported in the experiments was high (up to 75 kPa); therefore, existing modelling approach, based on system pressure, cannot predict these experimental data accurately. Mirmanto (2014, 2016) had the actual value of $T_f(z)$ at five different locations (vertically aligned with the location ($T_w(z)$) along the axis, therefore, the comparison of experimental h_{TP} draws a clear view of the applicability of linear pressure profile assumption.

In Figures 3.4 and 3.5, local two-phase heat transfer coefficient considering the linear pressure profile was compared with experimental data from Mirmanto (2014, 2016). In Figure 3.4 prediction of h_{TP} shows a good agreement with the experimental h_{TP}. Whereas, in Figure 3.5, a significant deviation of predicted h_{TP} with experimental data is observed. Evaluation of local saturation temperature for flow boiling where pressure drop is large play a significant role in the heat transfer coefficient evaluation. Therefore for large pressure drop case, to evaluate local saturation temperature following points to be considered.

1. For relatively high-pressure drop cases, assumption of system pressure instead of local pressure to evaluate the thermophysical properties contributes a part of total error.

2. Effect of flashing, i.e., the effect of pressure drop in the calculation of the thermodynamic quality was not considered in the linear pressure profile case. Hence, the vapor quality is under predicted, which results in an underestimation of the local

saturation pressure or temperature.

3. Estimation of two-phase frictional pressure drop for boiling channels requires a different approach as opposed to non-boiling channels. This point also is in keep in mind for local saturation temperature evaluation in case of flow boiling.

3.3 Correlations for Flow Boiling Heat Transfer

Existing heat transfer correlations are unable to accurately predict the flow boiling heat transfer coefficient in small channels over a wide range of operating parameters as the heat transfer mechanisms are not fully understood. For heat transfer in microchannel dedicated flow boiling correlations are limited. All these correlations were formulated and validated with the experimental heat transfer coefficient data where the pressure drop is small. Kim and Mudawar (2013a) formulated their correlation using 10,805 data points, including both and large and low-pressure drop data and suggested a correlation with MAE of 20.3%. Beforehand, they observed that most of the high pressure data were underpredicted by the Shah (1982) and Liu and Winterton (1991) and over predicted by Lazarek and Black (1982), Warrier et al. (2002) and Agostini and Bontemps (2005). In the present study, based on the literature survey, some the heat transfer coefficient correlations were examined with a new set of data points from the literature (Mirmanto, 2014, 2016). These heat transfer coefficient data points were chosen where pressure drops are significant (> 10 kPa). The correlations listed in Table 3.2 were specially developed for flow boiling in mini/microchannels except for the Cooper (1984) correlation which was developed for the pool boiling but a recent review (Kim and Mudawar, 2013a) showed that the correlation outperforms dedicated flow boiling correlations when applied to a large database of results from different research groups for channels of hydraulic diameters smaller than 2 mm. The correlation listed in table 3.2 was developed considering different fluid (water, refrigerate, di-electric fluids), different shape and size of the channels. Most of the correlations tested here (Steinke and Kandlikar (2004), Bertsch et al. (2009),Li and Wu (2010), Kim and Mudawar (2013a), Fang et al. (2015), Lim et al (2015), Markel et al (2017), Shah (2017)), used water as one of the fluids in their formulation. Therefore, experimental data for water are used for testing these correlations. Other correlations (Lazarek and Black (1982),Kew and Cornwell (1997), Ducoulombier et al. (2011), Karayiannis and Mahmoud (2013), Thiangtham et al. (2016))did not consider water during formulation, but those are widely used for miniature channels. The experimental data used in the study are from Mirmanto (2014, 2016) where the local heat transfer coefficient was calculated using local measurements of wall temperature as well as saturation temperature by putting pressure ports along the length. These experimental data were not used in the formulation of any of the existing correlations, and thus, it gives an independent mode of validation.

Tab. 3.2: List of correlation for two phase heat transfer coefficient from literature

Authors [References]	Equations for Flow Boiling Heat Transfer Coefficient	MAE (%)	Φ (%)
Lazarek and Black (1982)	$h_{TP} = 30 Re_{lo}^{0.857} Bo^{0.714} \left(\frac{k_f}{D_H}\right)$	31.5	56.6
Cooper (1984)	$h_{TP} = 55 P_R^{0.12-0.4343 \ln R_p} \times (-0.4343 \ln R_p)^{-0.55} M^{-0.55} q_{eff}^{0.67}$	35.72	41.10
Kew and Cornwell (1997)	$h_{TP} = 30 Re_{lo}^{0.857} Bo^{0.714} \left(\frac{k_f}{D_H}\right) (1-x)^{0.143}$	32.1	62.66
Steinke and Kandlikar (2004)	$h_{TP} = 0.6683 Co^{-0.2} (1-x)^{0.8} h_{lo} + 1058.0 Bo^{0.7} (1-x)^{0.8} h_{lo}$ $Co = \left(\frac{\rho_g}{\rho_f}\right)^{0.5} \left(\frac{(1-x)}{x}\right)^{0.8}$ $Bo = \frac{q_{eff}}{G h_{fg}}$	134	0.5
Bertsch et al. (2009)	$h_{TP} = h_{NB} \times S + h_{CB} \times F$ $S = 1 - x$ $F = 1 + 80(x^2 - x^6) e^{-0.6Co}$ $h_{NB} = 55 P_R^{0.12-0.4343 \ln R_p} \times (-0.4343 \ln R_p)^{-0.55} M^{-0.55} q_{eff}^{0.67}$ $h_{CB} = h_{sp,fo}(1-x) + h_{sp_go} x$ $h_{sp,fo} = \left(3.66 + \frac{\left(0.0668 \frac{D_H}{L} Re_{fo} Pr\right)}{1 + 0.04 \left(\frac{D_H}{L} Re_{fo} Pr\right)^{2/3}} \frac{k_f}{D_H}\right)$ $h_{sp,go} = \left(3.66 + \frac{k_g}{D_H} \frac{\left(0.0668 \frac{D_H}{L} Re_{go} Pr\right)}{1 + 0.04 \left(\frac{D_H}{L} Re_{go} Pr\right)^{2/3}}\right)$	27.26	58.66
Li and Wu (2010)	$h_{TP} = 334 Bo^{0.3} (Bd Re_f^{0.36})^{0.4} \frac{k_f}{D_H}$	50.69	6.71

Ducoulombier et al. (2011b)	$h_{TP} = max(h_{NB}, h_{CB})$ $h_{NB} = 131 P_R^{-0.0063} (-logP_R)^{-0.55} M^{-0.5} q_{eff}^{0.58}$ $if Bo > 1.1 \times 10^{-4}$ $h_{CB} = \left[1.46 \times 10^4 Bo + 0.93 \left(\frac{1}{X_{tt}}\right)^{2/3}\right] \times \left(0.023 Re_{fo}^{0.8} P_r^{1/3} \frac{k_f}{D_H}\right)$ $if Bo < 1.1 \times 10^{-4}$ $h_{CB} = \left[1 + 1.80 \left(\frac{1}{X_{tt}}\right)^{0.986}\right] \times \left(0.023 Re_f^{0.8} P_r^{0.4} \frac{k_f}{D_H}\right)$	289	0.5
Kim and Mudawar (2013a)	$h_{NB} = \left[2345 \left(Bo \frac{P_H}{P_F}\right)^{0.7} P_R^{0.38} (1-x)^{0.51}\right] \times \left(0.023 Re_f^{0.8} P_r^{0.4} \frac{k_f}{D_H}\right)$ $h_{CB} = \left(0.023 Re_f^{0.8} P_r^{0.4} \frac{k_f}{D_H}\right) \left[5.2 \left(Bo \frac{P_H}{P_F}\right)^{0.08} \times We_{fo}^{-0.54} + 3.5 \left(\frac{1}{X_{tt}}\right)^{0.94} \left(\frac{\rho_g}{\rho_f}\right)^{0.25}\right]$ $h_{TP} = \left(h_{NB}^2 + h_{CB}^2\right)^{0.5}$	72.12	28.41
Mahmoud and Karayiannis (2013a)	$h_{TP} = S_{new} h_{copper} + F_{new} h_f$ $h_f = 4.36 \frac{k_f}{D_H} for Re_f < 2000$ $h_f = 0.023 Re_{fo}^{0.8} P_r^{0.4} \frac{k_f}{D_H}$ $F_{new} = (1 + A/X)^{0.644}$ $A = 2.812 Co^{-0.408}$ $S_{new} = \frac{1}{1 + 2.56 \times 10^{-6} (Re_f F_{new}^{1.25})^{1.17}}$	20.5	76.66
Fang et al. (2015)	$h_{TP} = Nu \frac{k_f}{D_H}$ $Nu = 0.00061 (S + F) Re_f Fa^{0.11} Pr_f^{0.4} / \ln U$ $S = 142.5 Bo^{0.9} M^{0.55} \left(\frac{\rho_f}{\rho_g}\right)^{0.33}$ $F = x \left(\frac{x}{1-x}\right)^{0.9} \left(\frac{\rho_f}{\rho_g}\right)^{0.35}$ $U = 1.02 \left(\frac{\mu_{f,w}}{\mu_{l,w}}\right)$	75.46	1.66

Lim et al. (2015)	$h_{TP} = \frac{Re^{0.196} k_f}{Bo^{0.177} C_{FR}^{0.42} D_H}$ $C_{FR} = 0.4905 + Fr(1 - x^{3.134})$ $Fr = \frac{G^2}{\rho_f^2 g D_H}$	51.92	2.72
Thiangtham et al. (2016)	$h_{TP} = \frac{10^{16.7} Bo^{0.3} We^{2.7} k_f}{Re_{4.95} (\rho_f/\rho_g)^{0.9} D_H}$	83.86	2.2
Markal (2017)	$h_{TP} = \frac{0.054 Re_L^{0.214} \beta^{0.552} Bo^{0.913} \left(\frac{1-x}{x}\right)^{0.7} \left(\frac{k_f}{D_H}\right)^{1.959}}{We_{fo}^{0.094} Pr_f^{0.333}}$	84.4	0.0
Shah (2017)	$h_{TP} = F h_{Shah(1982)}$ $F = 2.1 - 0.008 We_g - 110 Bo$ If $F < 1$, then $F = 1$ For fully heated channel $D_H = D_{HP}$ For pertially heated channel, use D_H in We_g and Fr and D_{HP} in other expression	103.3	21.72

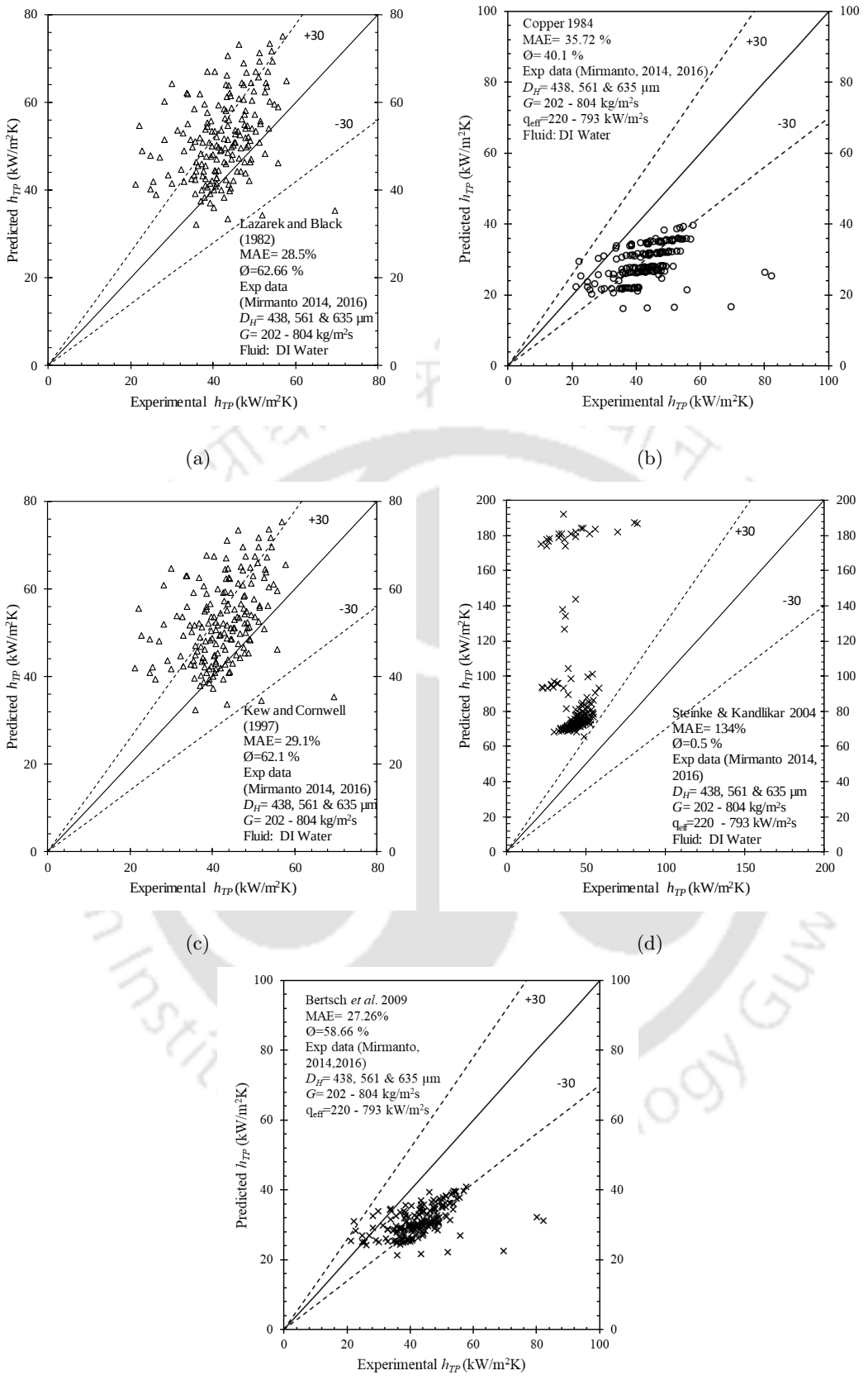

Fig. 3.6: Comparison of different correlation of boiling heat transfer from the literature, with the experimental data from Mirmanto (2014, 2016) where pressure drop is large. Correlation tested (a)Lazarek and Black (1982) (b)Cooper (1984) (c)Kew and Cornwell (1997) (d) Steinke and Kandlikar (2004) (e) Bertsch et al. (2009)

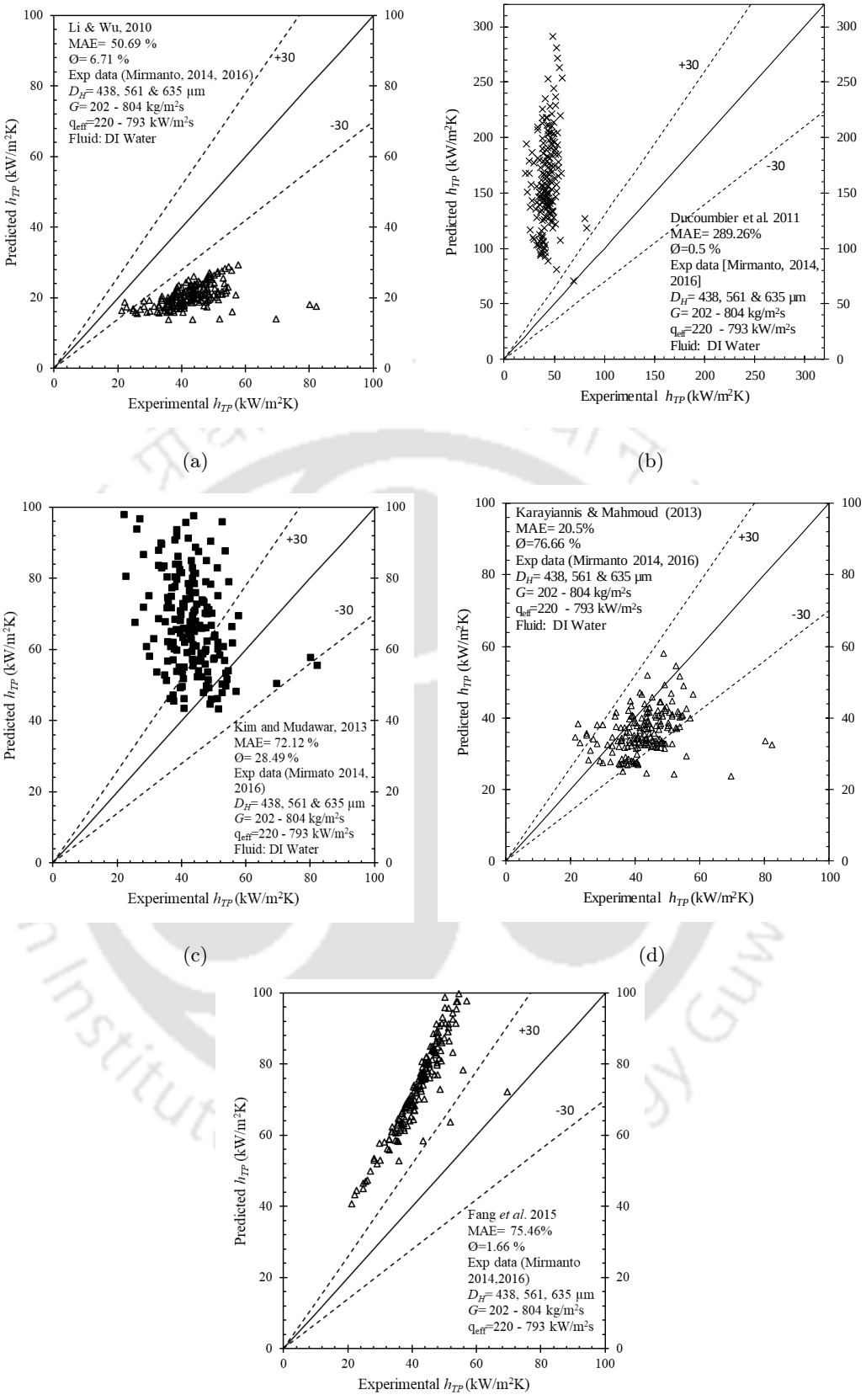

Fig. 3.7: Comparison of different correlation of boiling heat transfer from the literature, with the experimental data from Mirmanto (2014, 2016) where pressure drop is large. Correlation tested (a)Li and Wu (2010) (b)Ducoulombier et al (2011) (c)Kim and Mudawar (2013a) (d) Karayiannis and Mahmoud (2013) (e) Fang et al. (2015)

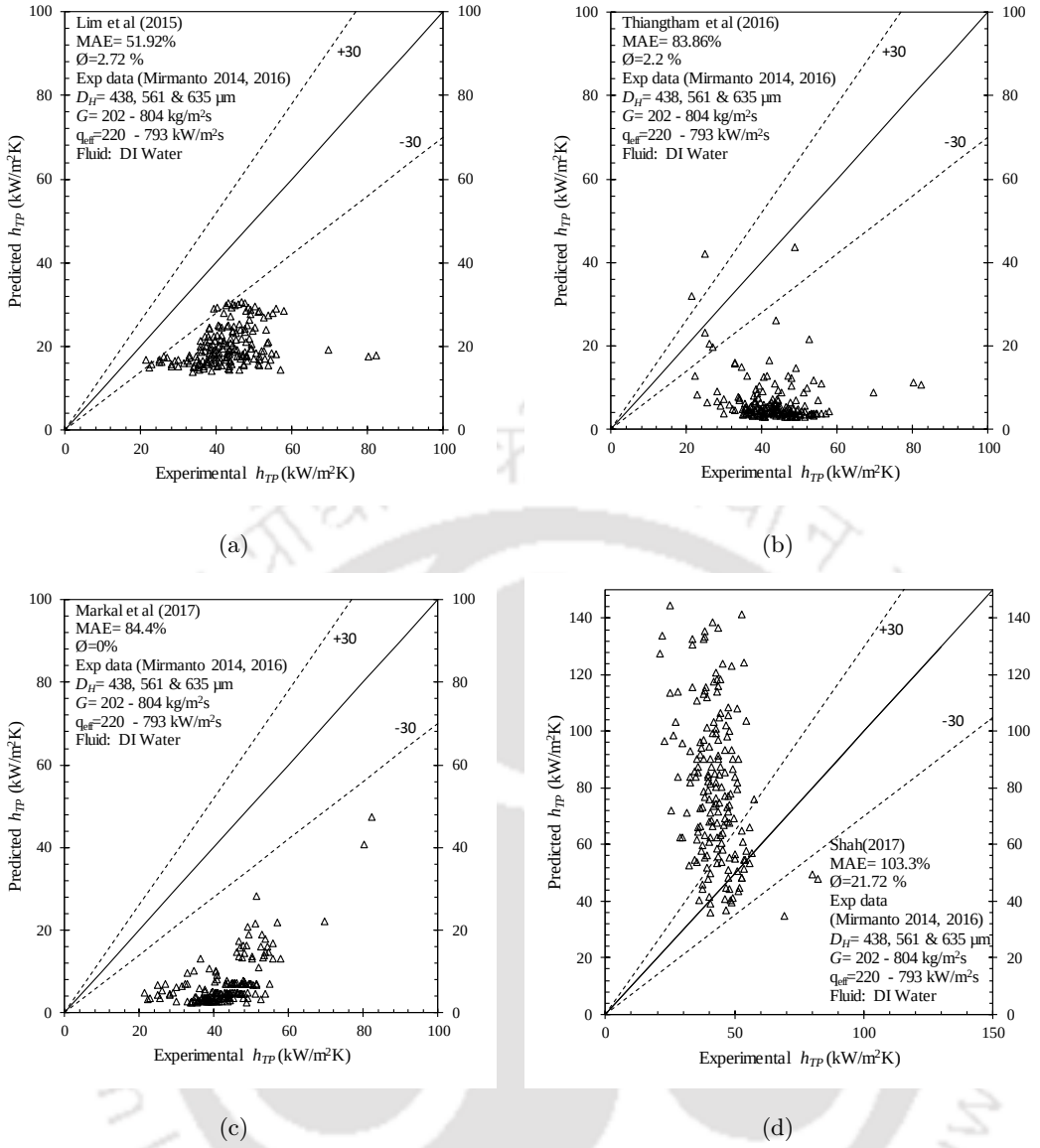

Fig. 3.8: Comparison of different correlation of boiling heat transfer from the literature, with the experimental data from Mirmanto (2014, 2016) where pressure drop is large.Correlation tested (a)Lim et al (2016) (b)Thiangtham et al (2016) (c) Markel et al (2017) (d) Shah (2017)

From Table 3.2 and the Figures 3.6,3.7 and 3.8 it is observed that most of the existing correlations predicted the local flow boiling heat transfer coefficient for microchannel, with a significant error. In the present study, along with MAE, a number of data points under ± 30% error band (ϕ) are also shown. All the correlations predicted less percentage of data points which fall under ± 30% error band. The correlation given by Mahmoud and Karayiannis (2013b) performs best with 20.5% of MAE only with 75.66 % data points in ± 30% error band. Similarly, Bertsch et al. (2009) shows good prediction with MAE 27.26 % and ϕ=58.66. Another correlation(Fang et al. (2015)) predicts the data not accurately (MAE= 75.46 and ϕ=1.66%) but able to predicts the trend successfully. All the correlations (listed in Table 3.2) used linear profile pressure assumption during the evaluation of local saturation pressure (or temperature) and did not consider effect of flashing in the thermodynamic quality. Therefore, these two assumptions can be relaxed, and a new and more realistic approach can be developed. Using the new approach, any correlation can be modified to an improved version.

During the evaluation, the sources of errors in the above correlations (listed in table 3.2) are not only due to linear pressure assumption and flashing effect, other factors like heat transfer mechanism, surface characteristics (Pike-Wilson and Karayiannis (2014)), aspect ratio (Singh et al. (2008)), fluid properties also influence the predictions. A good data reduction method which can accurately extract local experimental heat transfer data, predict the variable associated with heat transfer correlations along with sound physical significance surely improve the prediction (significance of the improvement may be more or less).

3.4 Summary

The assessment of the existing correlations for flow boiling pressure drop and heat transfer are summarized as follows

- It was observed that for small pressure drop cases the prediction of the existing correlations for flow boiling pressure drop was good, but for the large pressure drop cases, the same correlations showed significant error in the prediction.

- For relatively high-pressure drop cases, assumption of system pressure instead of local pressure to evaluate the thermophysical properties contributes a part of total error. The effect of flashing (significant for large pressure drop) was also not considered in the calculation of the thermodynamic quality.

- During local heat transfer calculation, local saturation temperature (or pressure) is evaluated by considering a linear pressure profile and this assumption is valid for small

pressure drop. For large pressure drop cases, it gave a significant error (compared with experimental data from Mirmanto (2014)).

- The effect flashing was not considered in x, which is an important parameter in the correlation development.
- The existing h_{TP} correlations tested against large pressure drop data showed significant error except the correlations given by Mahmoud and Karayiannis (2013b) and Bertsch et al. (2009).

Chapter 4

New Modelling Approaches for Microchannels

The preceding chapter indicated the need for improvements in predictive approaches for flow boiling pressure drop and heat transfer, especially for large pressure drop. This chapter proposes simple but accurate approaches to model the complex interplay between the various thermophysical phenomena occurring in flow boiling. The idea is to incorporate the effect of local thermophysical properties and flashing on the pressure gradient and the effect of heat flux on the two-phase multiplier. Using published experimental data, it is observed that these effects are significant in case of a large pressure drop. The pressure drop modelling is done by employing different correlations from the literature in the separated flow model. To generalize the approach, a modified form of the Clausius-Clapeyron equation is derived to characterize the saturation line on the P-T plane for fluids whose the vapour phase has nearly constant compressibility factor in the range of operation. The axial pressure profile is estimated, and the saturation temperature is evaluated locally. Hence, the variables associated with heat transfer correlations are calculated accurately, using local thermophysical properties and the thermodynamic quality accounting for flashing. The effectiveness of the modelling approach is established by comparing with the experimental local heat transfer coefficient from the literature and shows a significant improvement over the existing approach.

4.1 A new approach to predict flow boiling pressure drop

As it has been observed, the predictions of the existing approach are good for low-pressure drop cases but poor for relatively higher pressure drop cases. Therefore, in this study, a new approach is proposed to accurately predict flow boiling pressure drop in microchannels, especially when the pressure drop is large. In most of the experiments, it was assumed that coolant enters the heat sink in subcooled condition and maintains a single-phase liquid state until it reaches zero thermodynamic equilibrium quality ($x = 0$). Microchannels can be divided into two regions, single-phase and two-phase regions, as shown in Figure 4.1.

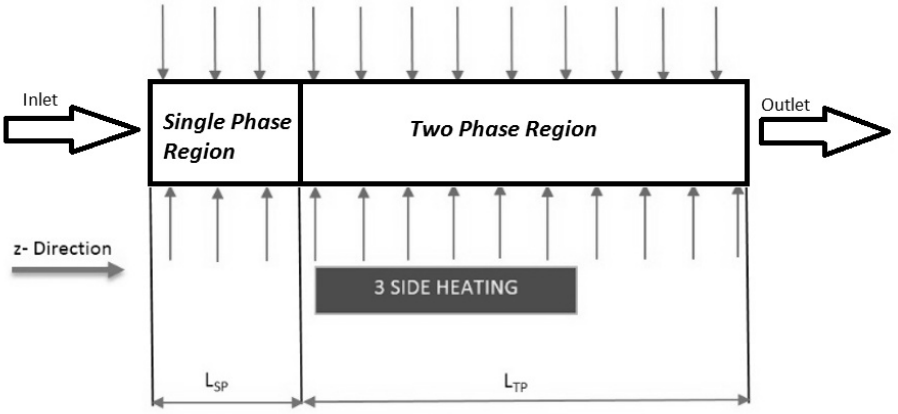

Fig. 4.1: Process flow of the fabrication technique

4.1.1 Single-phase pressure drop

In diabatic flow, the single-phase pressure drop is significantly influenced by the variation of viscosity with temperature. For water, it is given by Equation (4.1) (Al-Shemmeri, 2012)

$$\mu(T_{SP}) = 2.414 \times 10^{-5} \times 10^{\frac{247.8}{T_{SP}-140}} \tag{4.1}$$

For a rectangular channel, fully-developed friction factor f_{SP} is a function of the channel aspect ratio β given by given by Equation (4.2) (Shah and London, 1978). Re_{SP} is given by the (4.3)

$$Re_{SP} f_{SP} = \left(1 - 1.3553\beta + 1.9475\beta^2 - 1.7012\beta^3 + 0.95564\beta^4 - 0.2537\beta^5\right) \tag{4.2}$$

$$Re_{SP} = \frac{GD_H}{\mu(T)} \tag{4.3}$$

From energy balance, the axial temperature profile can be expressed by Equation (4.4)

$$T = \frac{q_{eff} P_H}{GAc_p} z + T_{in} \tag{4.4}$$

The pressure drop in single phase region is evaluated by Equation (4.5)

$$\Delta p = \int_0^{L_{SP}} \frac{f_H G^2}{D_H \rho_f} dz \tag{4.5}$$

where L_{SP} is the length from the inlet to the saturation point and is given by Equation (4.6)

$$L_{SP} = \frac{GAC_p\,(T_{sat} - T_{in})}{P_H q_{eff}} \tag{4.6}$$

4.1.2 Flow boiling pressure drop

In the two-phase region, the pressure and hence the saturation temperature decreases along the length, thus causing axial variation of thermophysical properties along the axial direction. If the pressure drop is low, then thermophysical properties can be evaluated at the system pressure, if the pressure drop is high, then a variation of these properties plays a significant role in the evaluation of the pressure drop. To evaluate these thermophysical properties, the local saturation temperature is evaluated from the local pressure by using the Clausius-Clapeyron relation, which is given by Equation (4.7), where p_{ref} and T_{ref} are the reference pressure and temperature, respectively. Thermophysical properties h_f and v_g vary significantly with local pressure. For the evaluation of v_g, the vapor phase was considered as an ideal gas, which is a fair approximation for low-pressure case (for compressibility factor near unity). Change of v_g, and h_f, with respect to the pressure, is given by Equations (4.11) and (4.14). Detailed derivations of the quantities dh_f/dp and dv_g/dp are given equations (4.7 – 4.14).

Clausius-Clapeyron relation given by Equation (4.7)

$$T = \left[\frac{1}{T_{ref}} - \frac{R}{h_{fg}} ln\left(\frac{p}{p_{ref}}\right)\right] \tag{4.7}$$

Differentiation of the Equation (4.7) with respect to p we will have Equation (4.8)

$$\frac{dT}{dp} = \frac{RT^2}{p h_{fg}} \tag{4.8}$$

Considering the vapor phase as an ideal gas v_g can be expressed by Equation (4.9)

$$v_g = \frac{RT}{p} \tag{4.9}$$

Differentiation of the Equation (4.9) with respect to p we will have Equation (4.10)

$$\frac{dv_g}{dp} = \frac{R}{p}\frac{dT}{dp} - \frac{RT}{p^2} \tag{4.10}$$

From Equations (4.9) & (4.10) we will get $\frac{dv_g}{dp}$ given by Equation (4.11)

$$\frac{dv_g}{dp} = \frac{RT}{p^2}\left[\frac{RT}{h_{fg}} - 1\right] \tag{4.11}$$

Liquid saturated enthalpy can be expressed by Equation (4.14) using Equations (4.12 and 4.13)

$$h_f - h_{ref} = C_{v,f}(T - T_{ref}) + v_f(p - p_{ref}) \tag{4.12}$$

$$\frac{dh_f}{dp} = C_{v,f}\frac{dT}{dp} + v_f \tag{4.13}$$

$$\frac{dh_f}{dp} = C_{v,f}\frac{RT^2}{ph_{fg}} + v_f \tag{4.14}$$

In the boiling region, $(L_{SP} - L)$, boiling causes vapor generation, resulting in a large pressure drop as compared to purely liquid flow. Consider the channel shown in Figure 4.1. From energy balance, the thermodynamic vapor quality x can be expressed by Equation (4.15), which accounts for axial changes in quality due to heat input as well as flashing that results from enthalpy changes with pressure.

$$\frac{dx}{dz} = \frac{1}{h_{fg}}\left[\frac{q_{eff}P_H}{GA} - \frac{dh_f}{dp}\frac{dp}{dz}\right] \tag{4.15}$$

The term $\frac{1}{h_{fg}}\left(\frac{dh_f}{dp}\frac{dp}{dz}\right)$ takes account of the increment in the thermodynamic quality due to flashing. When pressure drop is significant, enthalpy change due to pressure drop contributes to the vapor quality evaluation. Flashing is a consequence of pressure drop and also influences pressure drop. When the local pressure drops to the saturation pressure, liquid flashes into vapor to maintain thermal equilibrium (Lin et al., 1991), this results in a higher vapor quality than that estimated by neglecting pressure drop (Thome, 2004). This, in turn, causes a larger pressure drop than that estimated without flashing. In addition, lower local pressure results in a higher specific volume of the vapor phase, which causes a higher pressure drop than that estimated by neglecting the effect of local properties. These effects are modelled by coupled Equations (4.15) and (4.16) and validated, as shown in Figure 4.2. Here, thermodynamic equilibrium is assumed throughout the channel length. There is scope for development of an even more realistic modelling approach by considering the effect of thermodynamic non-equilibrium in the metastable region (Saurel et al., 2008) that may occur over a short distance. Considering the properties (h_f and v_g) within the saturated region as functions of the local pressure, the pressure gradient is expressed by Equation (4.16).

$$-\frac{dp}{dz} = \frac{\left[\frac{2f_{fo}G^2v_f}{D_H}\phi_{fo}^2 + G^2\frac{dx}{dz}\left(\frac{2xv_g}{\alpha} - \frac{2(1-x)v_f}{1-\alpha}\right)\left(\frac{\delta\alpha}{\delta p}\right)_p\left(\frac{(1-x)^2v_f}{(1-\alpha)^2} - \frac{x^2v_g}{\alpha^2}\right)\right]}{\left[1 + G^2\left[\frac{x^2}{\alpha}\left(\frac{dv_g}{dp}\right) + \left(\frac{\delta\alpha}{\delta p}\right)_x\left(\frac{(1-x)^2v_f}{(1-\alpha)^2} - \frac{x^2v_g}{\alpha^2}\right)\right]\right]} \tag{4.16}$$

Zivi's void fraction correlation (Equation 4.17) is used to determine the void fraction. Equations (4.15) and Equation (4.16), which are coupled, were solved using 4th order Runge-Kutta method (ode45 function of MATLAB). Detailed derivations of $\left(\frac{\delta\alpha}{\delta x}\right)_p$ and $\left(\frac{\delta\alpha}{\delta p}\right)_x$ are given by equations (4.17 – 4.19)

To get the final expression $\left(\frac{\delta\alpha}{\delta x}\right)_p$, differentiate Equation (4.17) w.r.t. x, keeping p or the properties dependent on p constant. Final form of $\left(\frac{\delta\alpha}{\delta x}\right)_p$ is given by Equation (4.18).

$$\alpha = 1\Big/\left(1 + \frac{1-x}{x}\left(\frac{v_g}{v_f}\right)^{2/3}\right) \tag{4.17}$$

$$\left(\frac{\delta\alpha}{\delta x}\right)_p = \frac{\left(\frac{v_g}{v_f}\right)^{2/3}}{\left(x + \left(\frac{v_g}{v_f}\right)^{2/3} - x\left(\frac{v_g}{v_f}\right)^{2/3}\right)} \tag{4.18}$$

To get the final expression $\left(\frac{\delta\alpha}{\delta p}\right)_x$, differentiate Equation (4.17) w.r.t. p, keeping x and v_f constant w.r.t. p. Final form of $\left(\frac{\delta\alpha}{\delta p}\right)_x$ is given by Equation (4.19) where $\frac{dv_g}{dp}$ is evaluated by Equation (4.11).

$$\left(\frac{\delta\alpha}{\delta p}\right)_x = \left[\frac{6v_f^2v_g\left(\frac{1-x}{x}\right)}{\left(v_f^2\left(\frac{1-x}{x}\right) + 3v_g\right)^2}\right]\frac{dv_g}{dp} \tag{4.19}$$

4.1.3 Results and discussion of the new modelling approach

Table 4.1 shows a list of pressure drop correlations based on the separated flow model. The existing modelling approach with different C-correlations from the literature evaluates pressure drop using the thermophysical properties evaluated at the system pressure (and the saturation temperature corresponding to it). The same correlations were used with the new modelling approach by incorporating the effect of the thermophysical properties at the local pressure and the effect of flashing on thermodynamic quality. These modified models (Table 4.1) were compared with the experimental data of Mirmanto (2014, 2016). From Figure 4.2, it is observed that incorporation of the effect of local properties and flashing improved the prediction of the correlations to a great extent as compared to the existing approach. In Table 4.1, comparison of MAE (%) of all the models reveals that model M6 shows lowest MAE (%). This model uses the correlation of Kim and Mudawar

(2013b) for the Chisholm parameter C, which incorporated the effect of heat flux on C. In a heated microchannel with the liquid-vapor mixture flow, bubble nucleation and coalescence occurs very quickly in the upstream region of the channel, which causes a rapid transition to annular flow (Qu and Mudawar, 2004). At lower thermodynamic quality, the frictional pressure drop in the presence of heat flux is higher than that in an unheated channel (Collier and Thome, 1994). Therefore, a further modification is required on the other models (M1–M5, M7), in order to improve their predictions. Tarasova et al. (1966) (as cited by Collier and Thome (1994)), gave an empirical Equation (4.20) relating the value of ϕ_{fo}^2 in heated and unheated tubes for the steam-water system. This correlation is combined with these models (M1-M5, M7). Then the results of these modified models are compared with the experimental data of Mirmanto (2014, 2016). From Figure 4.3 and Table 4.1, it is observed that the effect of heat flux on ϕ_{fo}^2 improves the predictions of the models. Equation (4.20) is not incorporated in model M6, whose Chisholm parameter already contains the heat flux effect. Improvement of the new modelling approach (local thermophysical properties and flashing) with the incorporation of heating effect on ϕ_{fo}^2 for large pressure drop case is shown in Appendix B (Figure B.1).

$$\left[\phi_{fo}^2\right]_{heatedtube} = \left[\phi_{fo}^2\right]_{unheatedtube} \left[1 + 4.4 \times 10^{-3} \left(\frac{q_{eff}}{G}\right)^{0.7}\right] \tag{4.20}$$

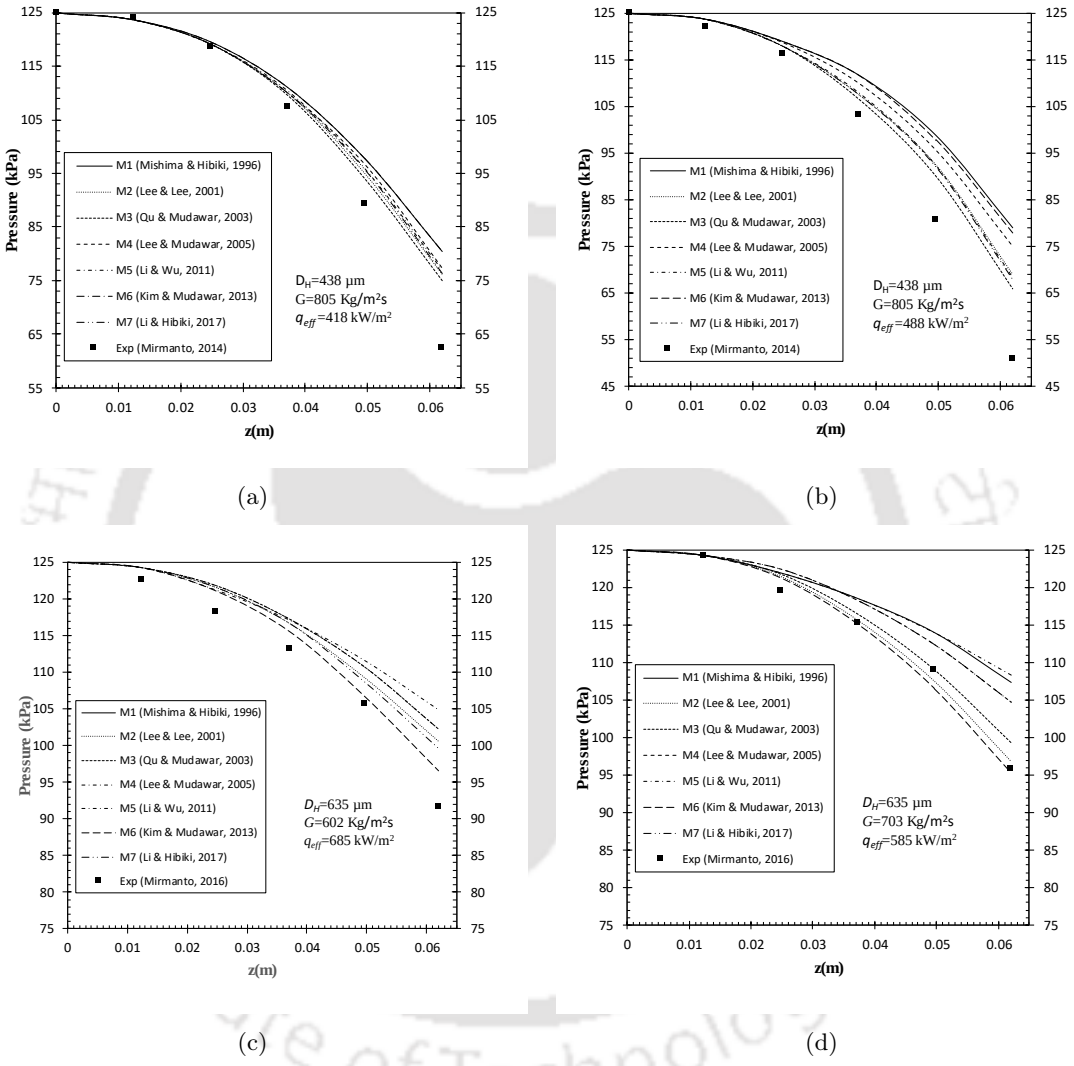

Fig. 4.2: Predictions of models from the literature, with local properties and flashing effect, compared with experimental data from (a,b) Mirmanto (2016) (c,d) Mirmanto (2014) for large pressure drop case. Fluid: DI water

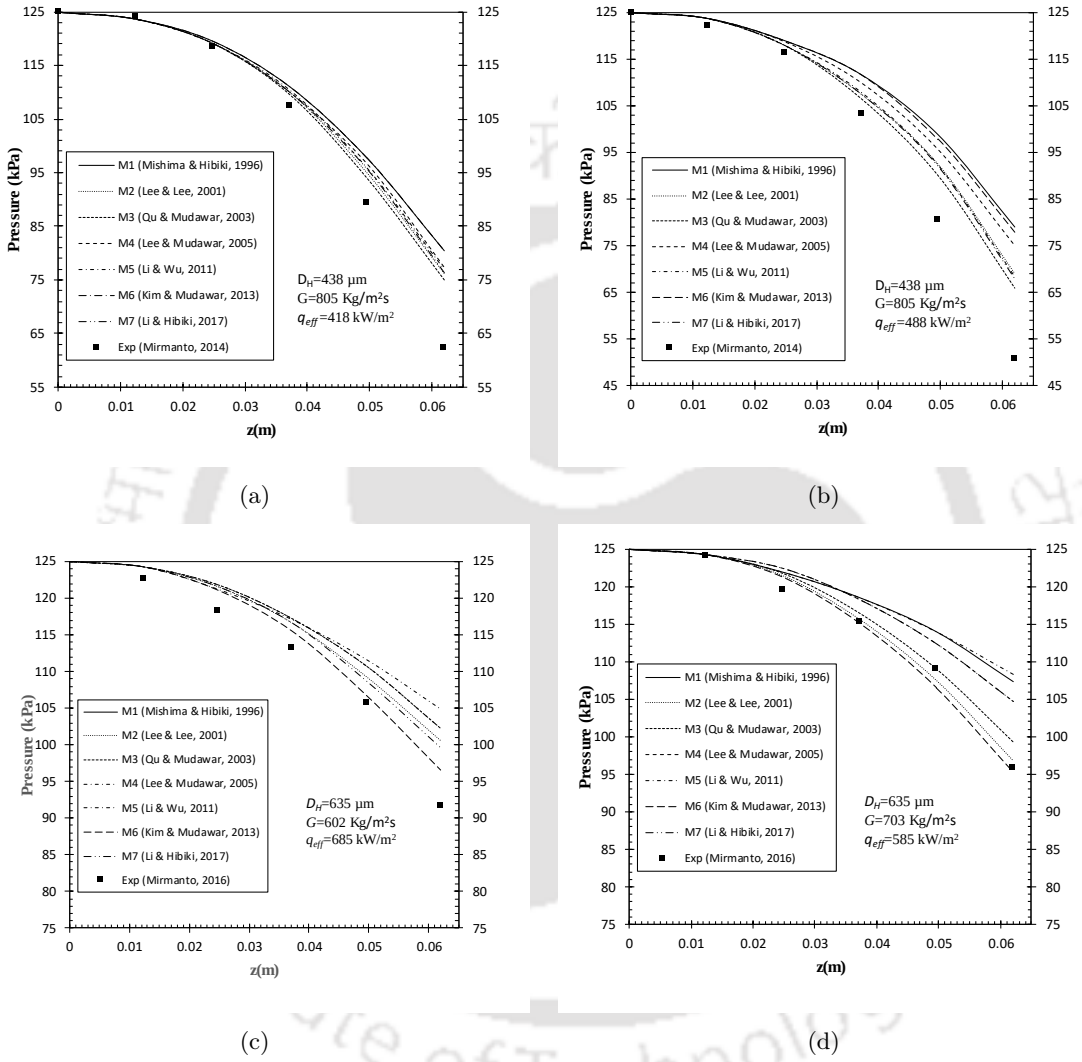

Fig. 4.3: Predictions of models from the literature , with local properties, flashing effect and heating effect in ϕ_{fo}^2 compared with experimental data from (a,b) Mirmanto (2016) (c,d) Mirmanto (2014) for large pressure drop case. Fluid: DI water

Tab. 4.1: List of MAE in pressure drop calculation for different C-correlations with existing and new approaches

Model nomenclature [References]	Equations for Chisholm Parameter (Liquid Laminar and Gas Laminar)	MAE (%) SYP	MAE (%) LOP	MAE (%) LOPH
M1 (Mishima and Hibiki, 1996)	$C = 21(1 - e^{319D_H})$	44.24	26.96	20.89
M2 (Lee and Lee, 2001)	$C = 6.185 \times 10^{-2} Re_{fo}^{0.726}$	41.68	23.63	15.15
M3 (Qu and Mudawar, 2003b)	$C = 21(1 - e^{319D_H}) \times (0.00418G + 0.06613)$	42.63	26.98	15.17
M4 (Lee and Mudawar, 2005)	$C = 2.16 Re_{fo}^{0.047} We_{fo}^{0.60}$	40.57	25.62	10.50
M5 (Li and Wu, 2011)	$C = 5.6 Bd^{0.28}$ for $Bd < 0.1$	44.54	23.24	20.02
M6 (Kim and Mudawar, 2013b)	$C_{boil} = 3.5 \times 10^{-5} Re_{fo}^{0.44} Su_{go}^{0.5} (\rho_f/\rho_g)^{0.48} \times \left[1 + 530 We_{fo}^{0.52} \left(Bo \frac{P_H}{P_F}\right)\right]$	38.37	18.35	18.35
M7 (Li and Hibiki, 2017)	$C = 41.7 Nu_{\mu_{TP}}^{0.66} Re_{TP}^{0.42} x^{0.21}$ $Nu_{TP} = \mu_{TP} / \left(\rho_{TP} \sigma \sqrt{\sigma / g \Delta\rho}\right)^{0.5}$ $1/\mu_{TP} = (1-x)/\mu_f + x/\mu_g$ $\rho_{TP} = (1-x)/\rho_f + x\rho_g$	40.12	24.72	11. 67

SYP = System Pressure; LOP= Local Pressure; LOPH = Local Pressure with Heat

4.2 Generalization of the new modelling approach

This approach described above for predicting flow boiling pressure drop is limited to the fluids where the vapor phase of the fluid satisfies ideal gas assumption i.e. compressibility factor is close to unity. For a non-ideal gas condition, a modified form of Clausius-Clapeyron relation is derived. For the evaluation of v_g, modified ideal gas equation ($pv_g = ZRT$) is considered. Here Z is considered as constant since the variation along the length is not significant (2-3%). Let p and T be the saturation vapor pressure and saturation temperature, respectively. The Clausius-Clapeyron relation for the equilibrium between liquid and vapor is given by equation (4.21)

$$\frac{dp}{dT} = \frac{h_{fg}}{T(v_g - v_f)} \tag{4.21}$$

Since $v_g >> v_f$, therefore Clausius-Clapeyron relation reduces to equation (4.22)

$$\frac{dp}{dT} = \frac{h_{fg}}{Tv_g} \tag{4.22}$$

Now v_g can be evaluated with equation (4.23), which account the compressibility factor in the ideal gas equation

$$v_g = \frac{ZRT}{p} \tag{4.23}$$

$$\frac{dp}{dT} = \frac{ph_{fg}}{ZRT^2} \tag{4.24}$$

Equation (4.24) is the modified form of Clausius-Clapeyron equation and using this modified form of the equations (4.25–4.27) can be achieved for the non-ideal case.

To evaluate these thermophysical properties, the local saturation temperature is evaluated from the local pressure by using the Clausius-Clapeyron relation which considers the ideal gas approximation for the vapor phase. For a non-ideal gas condition, a modified form of Clausius-Clapeyron relation is derived, considering the compressibility factor (Z) (Equation 4.25), where p_{ref} and T_{ref} are the reference pressure and temperature, respectively.The thermophysical properties h_f and v_g vary significantly with local pressure. For the evaluation of v_g, the modified ideal gas equation ($pv_g = ZRT$) is considered. Here Z is considered as constant since the variation along the length is not significant (2-3%). Change of v_g and h_f with respect to the pressure is given by Equations (4.26) and (4.27).

$$T = \left[\frac{1}{T_{ref}} - \frac{ZR}{h_{fg}} ln\left(\frac{p}{p_{ref}}\right)\right] \tag{4.25}$$

$$\frac{dv_g}{dp} = \frac{ZRT}{p^2}\left[\frac{ZRT}{h_{fg}} - 1\right] \tag{4.26}$$

$$\frac{dh_f}{dp} = C_{v,f}\frac{ZRT^2}{ph_{fg}} + v_f \tag{4.27}$$

Detailed derivations of the expressions for $\frac{dv_g}{dp}$, $\frac{dh_f}{dp}$ are given by Equations (4.28–4.33). Considering the vapor phase as an ideal gas, v_g can be expressed by Equation (4.28). After differentiating Equation (4.28) we get Equation (4.29)

$$v_g = \frac{ZRT}{p} \tag{4.28}$$

$$\frac{dv_g}{dp} = \frac{ZR}{p}\frac{dT}{dp} - \frac{RT}{p^2} \tag{4.29}$$

From Equations (4.28) and (4.29) we will get $\frac{dv_g}{dp}$ given by Equation (4.30)

$$\frac{dv_g}{dp} = \frac{Z^2RT}{p^2}\left[\frac{RT}{h_{fg}} - 1\right] \tag{4.30}$$

Again the liquid saturated enthalpy can be expressed by Equation (4.27) and $\frac{dh_f}{dp}$ will be given by Equation (4.33).

$$h_f - h_{ref} = C_{v,f}(T - T_{ref}) + v_f(p - p_{ref}) \tag{4.31}$$

$$\frac{dh_f}{dp} = C_{v,f}\frac{dT}{dp} + v_f \tag{4.32}$$

$$\frac{dh_f}{dp} = C_{v,f}\frac{ZRT^2}{ph_{fg}} + v_f \tag{4.33}$$

To show the importance of generalization, in Appendix B (Figure B.3), comparison of generalized model with the ideal-gas flow based model is shown for a the fluid whose vapour phase does not behave like ideal gas.

4.3 New methods for the formulation of heat transfer correlation

From Chapter 3, it is evident that to formulate accurate flow boiling heat transfer correlations for microchannels with large pressure drops, a new modelling approach is necessary. The following steps are proposed.

- Selection of the form of the correlation considering the physics associated with flow boiling heat transfer in microchannels.
- Correct reduction of heat transfer coefficient data from experiments, since in most of the microchannel experiments, local saturation temperatures were not measured.
- Correct estimation of variables used in the heat transfer coefficient correlation. For example, the effect of flashing is significant in the thermodynamic equilibrium quality estimation in case of a large pressure drop.

To formulate a heat transfer correlation, correct reduction of heat transfer coefficient from the experimentally measured quantities is important. As per the Equation (4.34), to evaluate local heat transfer, there is a need for accurate estimation of the heat flux, local wall temperature and local saturation temperature (at local pressure).

$$h_{TP}(z) = \frac{q_{eff}}{T_w(z) - T_f(z)} \tag{4.34}$$

In most cases of flow boiling in microchannels, it was observed that local measurements of saturation pressure were not reported. Instead, an axial pressure profile was assumed. For simplicity, a linear pressure profile (Equation 4.35) had been used in most of the cases. From figure 4.4 (a) and (b) it is observed that for large pressure drop cases, linear pressure

profile gives a significant error (MAE= 320 %) in prediction whereas the present modelling approach (MAE= 21%) for pressure drop evaluation shows a significant improvement.

$$p_{sat}(z) = p_o + \frac{L - z}{L - L_{sub}} \left(p_{sat}(z_{sub} - p_o)\right) \tag{4.35}$$

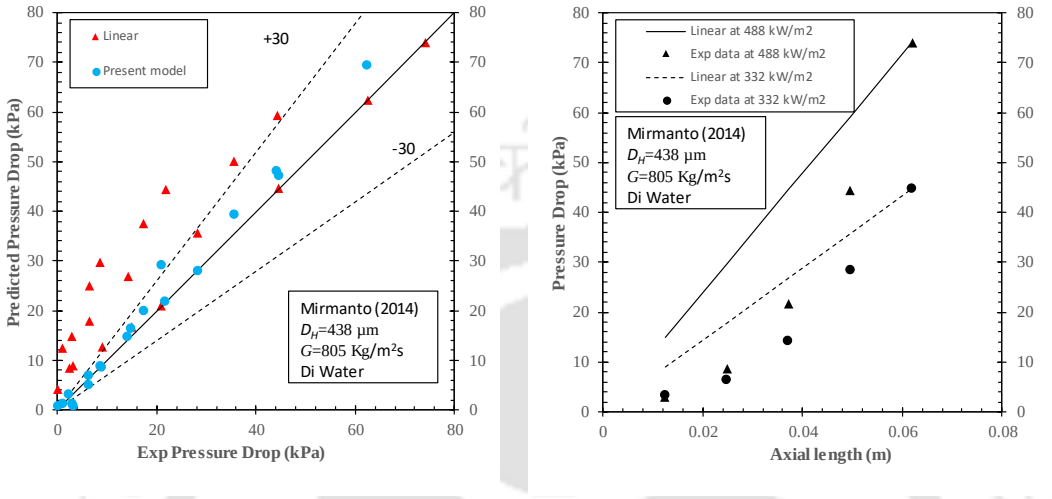

(a) (b)

Fig. 4.4: (a) Comparison of linear pressure drop with experimental data (Mirmanto (2014)) for large pressure drop case (b) axial variation of linear pressure drop compared with experimental data (Mirmanto (2014))

This necessitates an accurate predictive approach for two-phase pressure drop. For large pressure drop cases, the effect of local thermophysical properties and effect of flashing in thermodynamic equilibrium quality are significant. Considering these effects, in the above section, a new methodology is developed for the flow boiling pressure drop in a microchannel. Prediction of pressure drop in flow boiling requires estimation of the Chisholm parameter, for which many correlations have been proposed by different researchers. Kim and Mudawar (2013b) developed a Chisholm Parameter correlation (Equation 4.36) from a large database of 2378 data points, which was amassed from 16 sources, especially for flow boiling in microchannels. In the present study, the axial pressure profile is estimated using the present modelling approach with the Chisholm parameter correlation of Kim and Mudawar (2013b).

$$C_{boil} = 3.5 \times 10^{-5}\ Re_{fo}^{0.44}\ Su_{go}^{0.5}\ (\rho_f/\rho_g)^{0.48} \times \left[1 + 530 We_{fo}^{0.52} \left(Bo \frac{P_H}{P_F}\right)\right] \tag{4.36}$$

Where, $Su_{go} = \frac{\rho_g \sigma D_H}{\mu_g^2}$; $We_{fo} = \frac{G^2 D_H}{\rho_f \sigma}$; $Bo = \frac{q_{eff}}{G h_{fg}}$

To evaluate thermophysical properties, the local saturation temperature can be evaluated from the local pressure by using the Clausius-Clapeyron relation, which considers the

ideal gas approximation for the vapour phase. For a non-ideal gas condition, a modified form of Clausius-Clapeyron relation (Equation (4.25)) developed by considering the compressibility factor (Z). Since the thermophysical properties v_g and h_f vary significantly with local pressure, their rates of change with pressure are given by Equations (4.29) and (4.33). Accordingly, the pressure gradient can be expressed by Equation (4.16). The local thermodynamic vapor quality x is given by Equation (4.14), which incorporates the effect of flashing in the second term on the right-hand side. The void fraction can be estimated from Zivi's correlation (Equation (4.20)).

From the linear conduction equation (Equation (4.37)), T_w is obtained and effective heat flux is calculated by heat loss calibration.

$$T_w(z) = T_{tc}(z) - \frac{q_{eff}t}{k_s} \tag{4.37}$$

4.3.1 Results of the new methodology

In Figures 4.5 and 4.6, two modelling approaches for heat transfer coefficient evaluation are tested for the small and large pressure drop cases, respectively. In both the methods, the wall temperature and the heat flux are evaluated in a similar manner, but the saturation temperature is estimated differently. In the experimental data (Mirmanto, 2014, 2016), $T_{sat}(z)$ was measured directly, putting pressure ports along the length of the microchannel. In Figure 4.5, it is observed that, for a small pressure drop, both the methods predict the experimental data with good accuracy. This implies that the existing methodology is applicable for a small pressure drop. For the large pressure drop case (Figure 4.6), the linear pressure profile assumption underpredicts the experimental data measurably, while the present modelling approaches achieve significant improvement in the prediction accuracy.

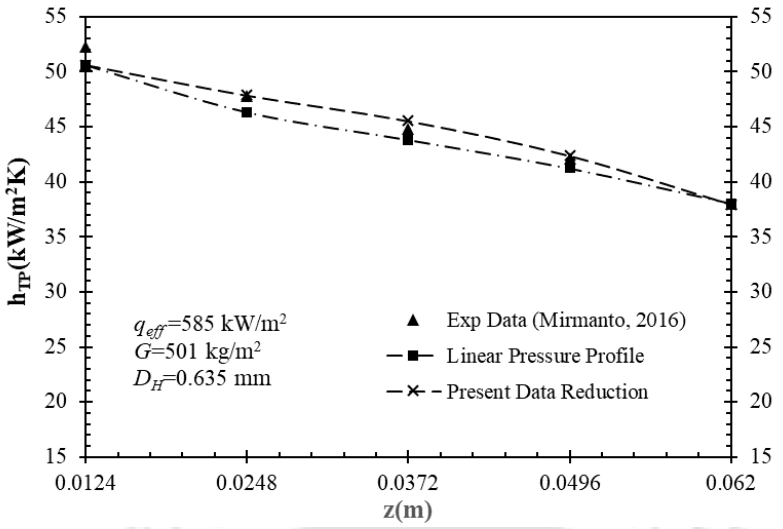

Fig. 4.5: Comparison of experimental heat transfer coefficient from literature with linear pressure assumption and the new approach for small pressure drop (Mirmanto, 2016)

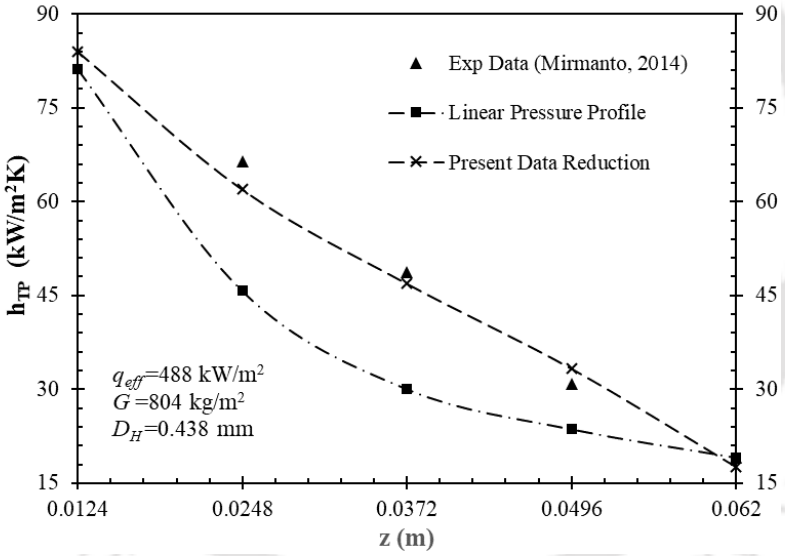

Fig. 4.6: Comparison of experimental heat transfer coefficient from literature with linear pressure assumption and the new approach

4.4 Summary

This chapter proposes simple but accurate approaches to model the complex interplay between the various thermophysical phenomena occurring in flow boiling. The findings are summarised as follows.

- The pressure drop modelling is done by employing different correlations from the literature in the separated flow model. This new modelling approach incorporates

the effect of local thermophysical properties and flashing on the pressure gradient and the effect of heat flux on the two-phase multiplier.

- To generalize the approach, a modified form of the Clausius-Clapeyron equation is derived to characterize the saturation line on the P-T plane for fluids whose vapour phase has nearly constant compressibility factor in the range of operation.
- The axial pressure profile is estimated with the new pressure drop modelling approach, and the saturation temperature is evaluated locally. The variables associated with heat transfer correlations are calculated accurately, using local thermophysical properties and the thermodynamic quality accounting for flashing.
- The effectiveness of the modelling approach is established by comparing with the experimental local heat transfer coefficient from the literature and shows a significant improvement over the existing approach for the large pressure drop cases.

Chapter 5

Test Section Fabrication and Experimental Facility

To access the effectiveness of the methodologies discussed in Chapter 4, flow boiling pressure drop and heat transfer experiments in a microchannel were planned. In this chapter, the detailed fabrication process of silicon microchannel test section is discussed. It includes a chemical etching process to fabricate microchannel of desired size and shape and the deposition of an integrated microheater on the backside of the channel. Heat loss calibration and uncertainty analysis are done to ensure the correctness of the measurements.

5.1 Test Section Fabrication

5.1.1 Microchannel Heat Sink Fabrication Steps

The test section was fabricated at Centre for Excellence in Nanotechnology, IIT Bombay. The basic process consists of Photolithography, Etching, Heater Deposition and Bonding. Double-sided polished, (100) p-type, 2-inch silicon wafer with resistivity 4–7 Ω-cm was used for fabrication. Microchannel was etched using the chemical etching process, and a trapezoidal cross-section was obtained. Based on an etch rate of 1.067 μm/min, the etched depth got was of the order of 90 μm. This is confirmed either with a Profilometer (non-destructive testing) or using a Scanning Electron Microscope (destructive testing). An integrated microheater of approximately 50 nm thickness was deposited on the backside of the wafer. Topside of the microchannel then bonded with quartz plate with PDMS bonding. The fabrication process used here is based on the process given by Singh et al. (2009). This process is illustrated in Figure 5.1 and its details are described as follows.

Material Selection and Initial Work:

- Get Silicon wafer (p-type): 2 inch both side polished having <100> orientations and 275 ± 25 μm thickness, 5-10 Ω-cm resistivity.
- Give it for RCA cleaning.
- Give it for oxidation: oxide layer thickness should be between 700-1000 nm.

First Level Photolithography

- Wafer dehydration: heat the wafer at 95°C for 5–10 minutes.
- On wafer backside (the side which will not be exposed to UV light): put PPR (positive photoresist) solution and spin at 3000 rpm for 45 seconds.
- Heat, the PPR, coated wafer 95°C for 3 minutes or 90°C for 3 minutes or 70°C for 15 minutes.
- Repeat the above two processes for the front side of the wafer.
- On Karl Suss Mask Aligner MJB4: expose wafer front side for 8 seconds at 13.8 doses under UV light.
- Put it in MF319 (PPR developer) for 30 seconds. Use Petridis for this purpose.
- Clean the wafer with DI water.
- Post bakes (if required): again heat the wafer at 95°C for 5–10 minutes.

TMAH (Tetra-methyl-ammonium hydroxide Solution) Wet-etch

- Use Buffered Oxide Etch, 5:1 (BHF) to etch the silicon oxide layer by putting the wafer in BHF and vibrating the Petridis. This takes 3–5 minutes depending upon the oxide layer thickness. (For 275 nm oxide thickness it took around 4 minutes. Clean the wafer with DI water.
- Now remove the PPR layer using Acetone (CH_3COCH_3).
- Again clean the wafer with DI water.
- Now put the wafer in TMAH in between 70 and 80°C. Fixed time depending upon the depth required.

Second Level Photolithography

- Use Buffered Oxide Etch, 5:1 (BHF) to etch (remove) the silicon oxide layer by putting the wafer in BHF and vibrating the Petridis. This takes 3–5 minutes depending upon the oxide layer thickness.
- Clean the wafer with DI water.
- Heat the wafer at 95°C for 5–10 minutes. This is called dehydration.
- On wafer backside (the side was heater will be deposited): put PPR (positive photoresist) solution and spin at 3000 rpm for 30 seconds.
- Heat the PPR coated wafer at 95°C for 3 minutes or 90°C for 3 minutes or 75°C for 15 minutes.
- On Double-Sided Aligner (DSA): expose wafer backside for 8 seconds at 13.8 doses under UV light.
- Put it in MF319 (PPR developer) for 30 seconds. Use Petridis for this purpose.
- Clean the wafer with DI water.

Heater Deposition

- Deposit 20 nm (Thick) Titanium (Ti) and 50 nm of Platinum (Pt) over Ti.
- Remove the PPR using Acetone.
- Finally clean the wafer with DI water.

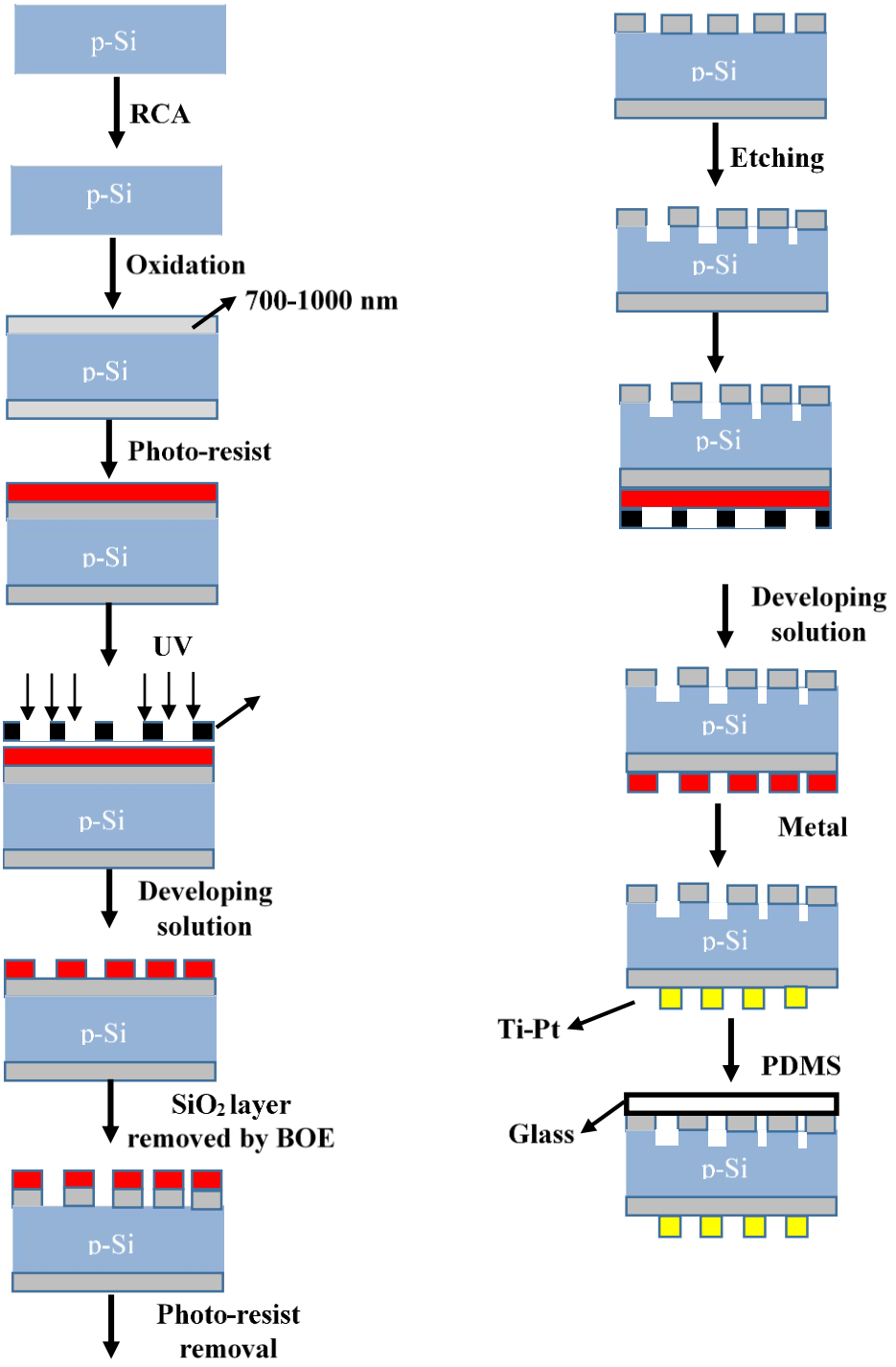

Fig. 5.1: Process flow of the fabrication technique

5.2 Microchannel Size Shape and Dimensions

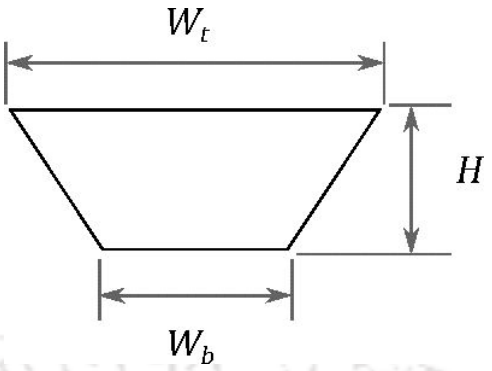

Fig. 5.2: Shape of the cross section of the silicon microchannel

The shape of the cross-section of the microchannel is trapezoidal as shown in Fig. 5.2. Details of the dimensions of the channel are given in Table 5.1. The shape and the roughness of the surface are measured with an XP2 Stylus-based Surface Profilometer at CEN IIT Bombay.

Tab. 5.1: Dimensions of the channel

L (mm)	W_t (μm)	W_b (μm)	H (μm)	D_H (μm)	R_a (nm)	No of channels
20	245	115	92	111	45	1

The channel shape is trapezoidal and, therefore heat transfer area for the 3-side heated walls is given by Equation (5.1)

$$A_{ht} = \left[2\sqrt{((W_t - W_b)/2)^2 + H^2} + W_b\right] \times L \tag{5.1}$$

5.3 Experimental Facility

Photograph of the experimental setup, microchannel test section, microheater is shown in Figure 5.3. All the devices are connected in series using silicone tubing. The setup is consists of a syringe pump (to regulate the mass flux) a differential pressure transducer (pressure drop measurement), a DC power supply (to provide heat to the microheater and to excite the pressure transducer), thermocouples(measure fluid and wall temperatures),a data acquisition system and computer to store the data. An SLR camera with a microlens is also used to visualize the flow through the microchannel. List of equipment with photograph is given in Table 5.2.

The inlet and outlet connectors were permanently attached to the plenums with Omega make temperature resistant epoxy adhesive (OMEBOND OB-100). OB-100 can withstand temperature up to 130 °C and it bond well with glass and plastic surfaces. The epoxy acts as a sealant to prevent leakages from joints with was one of the major problems faced during experiments.

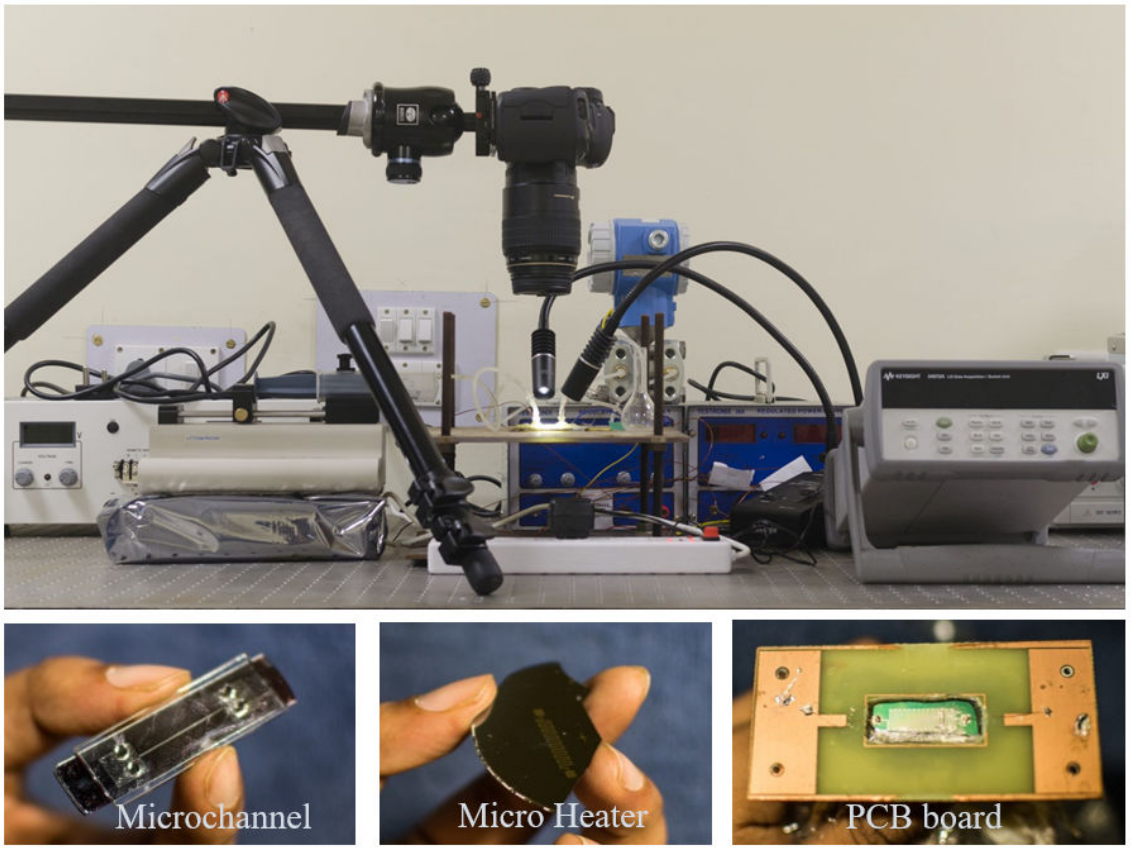

Fig. 5.3: Photograph of the experimental set up, Microchannel, Micro heater and PCB board for the connection

Tab. 5.2: List of equipment

Sl No	Name of the equipment	Specifications
1	Syringe Pump	Flow rate: 0 to 6 ml/min Pressure: 3 bar Input voltage: 220 V
2	Differential pressure transducer	Range: 0 to 0.50 bar Resolution: 0.001 kPa Output: 4-20 mA Excitation Required: 24 V DC
3	DC power supply	Voltage range: 0 to 130 V Resolution: 0.01 V
4	SLR camera with microlens	Canon EOS 5D Mark III 100 mm Micro Lens
5	K-type Thermocouple	Bead Size: 0.8 mm Accuracy: ±0.5°C Maximum Temperature: 500°C
6	Data Accusation System	Single channel reading rates to I/O: 500 readings/sec; Directly measure the temperature for k-type thermocouples

5.4 Test procedure

Schematic of the experimental setup employed in the measurements is shown in figure 5.4 (a). The setup consists of a syringe pump, a differential pressure gauge, a test section, a DC power supply, and a data logger to record inlet/outlet temperatures of water and surface. All devices were connected using silicone tubing (Master Flex). A pre-calibrated syringe pump (Cole Parmer) was used for metering and controlling the mass flow rate of water. A pre-calibrated digital pressure gauge (Deltabar PMD75) was used to measure the pressure drop across the microchannel. A contact probe was used to make electric contact between microheater and DC power supply. K-type thermocouples (Cole-Parmer) of 1 mm bead size were placed inside the inlet and outlet reservoirs. Another K-type thermocouple was placed on the bottom surface (microheater side) of the microchannel to measure the wall temperature. All the thermocouples were connected to a data logger which logs the temperature. The test sections were fabricated using microfabrication facility available at CEN, IIT Bombay. Double-sided polished (100) p-type, 2-inch silicon wafer with resistivity

4–7 Ω-cm was used for fabrication. Microchannel was etched using a chemical etching process, and a trapezoidal cross-section was obtained. It was then bonded to the quartz cover plate. The fabrication process was the same as that used by Singh et al. (2009). The detailed geometrical specifications of the microchannel employed in the experiment are given in Table 5.3. The following procedure was adopted while performing the experiments. The fluid was vigorously boiled for 30 min to remove dissolved air and then cooled to the ambient temperature. The flow was started, and then an input electric power was provided by supplying a fixed voltage and current using a DC power supply. Continuous monitoring of the inlet and outlet temperatures and pressure drop were undertaken to check for steady-state. Once steady-state condition was achieved, all relevant parameters such as pressure drop, inlet-outlet temperatures, the power supplied and flow rate were recorded. The above procedure was repeated for other values of flow rates and heat fluxes.

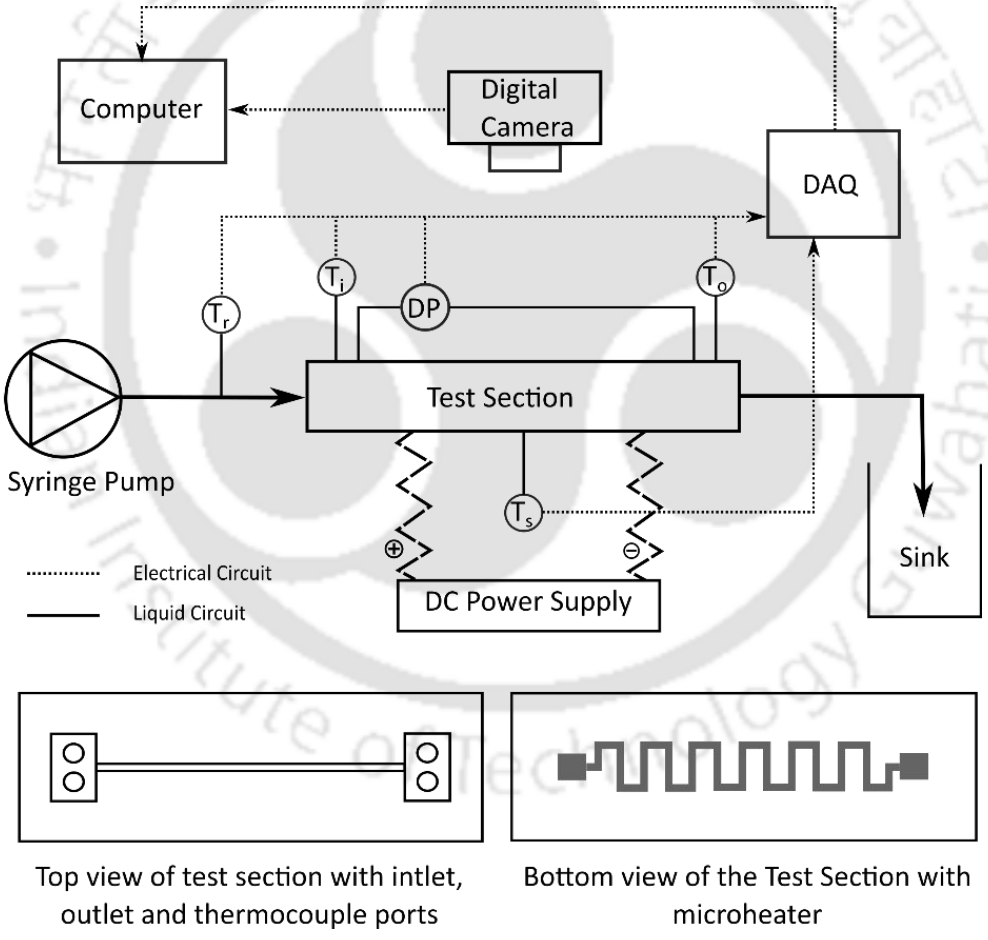

Fig. 5.4: Schematic of experimental flow loop and test section of microchannel heat array.

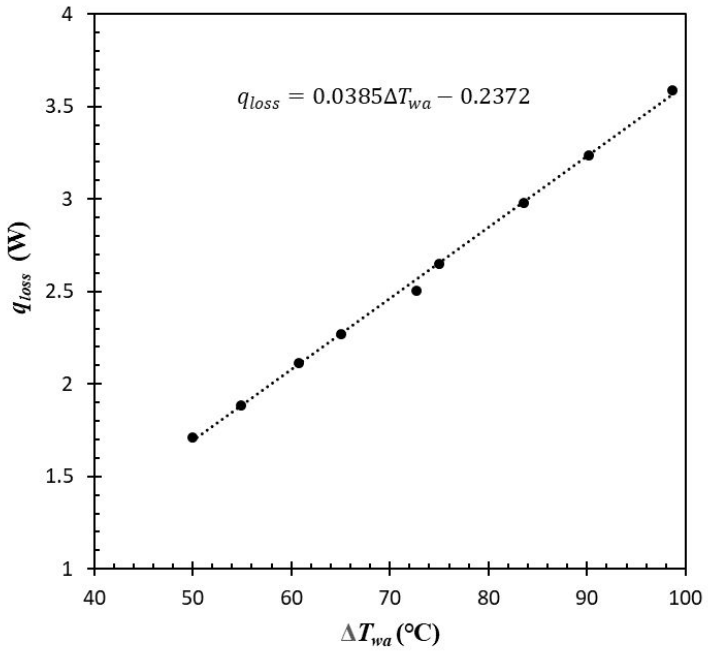

Fig. 5.5: Schematic of experimental flow loop and test section of microchannel heat array.

5.5 Heat loss calibration

To estimate the heat loss, a constant power was applied to the microheater, resulting in an increase of the temperature of the test section. After the steady state was reached, the wall temperatures on the test section together with that of the ambient were recorded and correlated with the power input to the microheater. This procedure was repeated for several input powers, as shown in Figure 5.5. A linear relation $q_{loss} = 0.0385\Delta T_{wa} - 0.2372$ was fitted to the data points. Here, ΔT_{wa} is the average wall-to-ambient temperature difference $\Delta T_{wa} = T_w - T_{amb}$. This method is the same as that used by Lee and Garimella (2008). Downstream of the syringe pump, the fluid gets heated in the inlet header before entering the microchannel. The heat utilized to heat the fluid inside the header is given by equation (5.2).

$$q_{header} = GAC_p(T_{in} - T_{syringe}) \tag{5.2}$$

The effective heat flux was assumed to be uniform along the microchannel length and is given by equation (5.3) (Here q_{input} is the electric power supplied to the microheater).

$$q_{eff} = \frac{q_{input} - q_{header} - q_{loss}}{A_{ht}} \tag{5.3}$$

5.6 Uncertainty analysis

Uncertainty can be defined as an estimate of the interval or range that contains an error in the experimental measurement or result. The total error in a measurement is the difference between the measured value and the true value, which is the sum of the systematic or bias errors and the random or precision errors.

For an experimental result r, defined by Eq. (5.4) which is a function of j measured variables X_i, the propagated error can be calculated using Eq. (5.5) (Coleman and Steele (2009)).

$$r = r\left(X_1, X_2, ..., X_j\right) \tag{5.4}$$

$$U_r = \sqrt{\left(\frac{\delta r}{\delta X_1}\right)^2 U_{X_1}^2 + \left(\frac{\delta r}{\delta X_2}\right)^2 U_{X_2}^2 + ... + \left(\frac{\delta r}{\delta X_j}\right)^2 U_{X_j}^2} \tag{5.5}$$

Equation (5.5) gives the absolute uncertainty, Ur, in the result. It can also be written in the dimensionless form shown in Eq. (5.6), to give the relative uncertainty, Ur/r of the result, as follows

$$\frac{U_r}{r} = \sqrt{\left(\frac{\delta r}{\delta X_1}\frac{X_1}{r}\right)^2 \left(\frac{U_{X_1}}{X_1}\right)^2 + \left(\frac{\delta r}{\delta X_2}\frac{X_2}{r}\right)^2 \left(\frac{U_{X_2}}{X_2}\right)^2 + ... + \left(\frac{\delta r}{\delta X_j}\frac{X_j}{r}\right)^2 \left(\frac{U_{X_j}}{X_j}\right)^2} \tag{5.6}$$

The above approach was used to carry out the propagated uncertainty analysis for all parameters. The uncertainties of measuring instruments and derived quantities are summarized in Table. 5.2. For example, uncertainty analysis of some important parameters are given below

- The cross-sectional area of the trapezoidal section is calculated using Eq. (5.7), where the top width, W_t, bottom width, W_b and height, H, are measured quantities as given in Table 5.2. The propagated uncertainty in the area (A) is obtained from Eq. (5.8) and the relative uncertainty can be evaluated from equation (5.9).

$$A = \left(\frac{W_b + W_t}{2}\right) H = W_{Avg} H \tag{5.7}$$

$$U_A = \sqrt{\left(\frac{\delta A}{\delta W_{Avg}}\right)^2 U_{W_{Avg}}^2 + \left(\frac{\delta A}{\delta H}\right)^2 U_H^2} \tag{5.8}$$

$$\frac{U_A}{A} = \sqrt{\left(\frac{1}{W_{Avg}}\right)^2 U_{W_{Avg}}^2 + \left(\frac{1}{H}\right)^2 U_H^2} \tag{5.9}$$

- Hydraulic diameter for the trapezoidal cross-section is assumed as given by the equation Eq. (5.10). The propagated uncertainty in hydraulic diameter is obtained from Eq. (5.11) and the relative uncertainty can be evaluated from equation (5.12).

$$D_H = \frac{2W_{Avg}H}{W_{Avg}+H} \tag{5.10}$$

$$U_{D_H} = \sqrt{\left(\frac{\delta D_H}{\delta W_{Avg}}\right)^2 U_{W_{Avg}}^2 + \left(\frac{\delta D_H}{\delta H}\right)^2 U_H^2} \tag{5.11}$$

$$\frac{U_{D_H}}{D_H} = \sqrt{\left(\frac{H}{W_{Avg}+H}\frac{U_{W_{avg}}}{W_{avg}}\right)^2 + \left(\frac{W_{Avg}}{W_{Avg}+H}\frac{U_H}{H}\right)^2} \tag{5.12}$$

- Mass flux is given by the equation Eq. (5.13). The uncertainty of A is known; therefore, the relative uncertainty of G can be evaluated from equation (5.14).

$$G = \frac{\dot{m}}{A} \tag{5.13}$$

$$\frac{U_G}{G} = \sqrt{\left[\frac{U_{\dot{m}}}{\dot{m}}\right]^2 + \left[\frac{U_A}{A}\right]^2} \tag{5.14}$$

- Heat flux is given by the equation Eq. (5.15). Where V and I are input voltage and current to the heater. The uncertainty of A is known; therefore, the relative uncertainty of q_{eff} can be evaluated from equation (5.16).

$$q_{eff} = \frac{VI - Q_{loss}}{A} = \frac{0.87VI}{A} \tag{5.15}$$

$$\frac{U_{q_{eff}}}{q_{eff}} = \sqrt{\left[\frac{U_V}{V}\right]^2 + \left[\frac{U_I}{I}\right]^2 + \left[\frac{U_A}{A}\right]^2} \tag{5.16}$$

- Reynolds number is given by the equation Eq. (5.17). Where the relative uncertainty of G and D_H are known. The uncertainty of Re can be evaluated from equation (5.18).

$$Re = \frac{GD_H}{\mu} \tag{5.17}$$

$$\frac{U_{Re}}{Re} = \sqrt{\left[\frac{U_{D_H}}{D_H}\right]^2 + \left[\frac{U_G}{G}\right]^2} \tag{5.18}$$

- Local flow boiling heat transfer coefficient is the ratio of effective heat flux (q_{eff}) to the temperature difference between wall and the bulk fluid and is given by the Eq. (5.19). Where the relative uncertainty of q_{eff} is known. The uncertainty of h can be evaluated from Eq. (5.20).

$$h = \frac{q_{eff}}{(T_w - T_f)} \tag{5.19}$$

$$\frac{U_h}{h} = \sqrt{\left[\frac{U_{q_{eff}}}{q_{eff}}\right]^2 + \left[\frac{U_{T_w}}{(T_w - T_f)}\right]^2} \tag{5.20}$$

- The pressure drop in the subcooled flow boiling region is given by Eq. (5.21). Considering friction factor equal to Constant$(K_1)/Re$, the relative uncertainty of Δp can be evaluated from Eq. (5.22). The relative uncertainty of G, Re and D_H are known.

$$\Delta p = \frac{K_1 G^2 L v_f}{Re D_H} \tag{5.21}$$

$$\frac{U_{\Delta p}}{\Delta p} = \sqrt{\left[\frac{U_G}{G}\right]^2 + \left[\frac{U_L}{L}\right]^2 + \left[\frac{U_{Re}}{Re}\right]^2 + \left[\frac{U_{D_H}}{D_H}\right]^2} \tag{5.22}$$

- The two-phase pressure drop is defined by subtracting the single-phase pressure drop from the total channel pressure drop (Δp_{CP}), and the relative uncertainty in the two-phase pressure drop is expressed by Eq. (5.23)

$$\frac{U_{\Delta p_{TP}}}{p_{TP}} = \sqrt{\left[\frac{U_{\Delta p_{CP}}}{\Delta p_{CP} - \Delta p_{SP}}\right]^2 + \left[\frac{U_{\Delta p_{SP}}}{\Delta p_{CP} - \Delta p_{SP}}\right]^2} \tag{5.23}$$

Tab. 5.3: Estimation of uncertainties in various parameters measured and derived.

Parameter	**Value**	**Uncertainty (%)**
Top width (W_i)	245 μm	$\pm$ 0.43
Bottom width (W_b)	115 μm	$\pm$ 0.85
Height (H)	90 μm	$\pm$ 1.11
Length (L)	20 mm	$\pm$ 0.50
Diameter (D_H)	111 μm	$\pm$ 1.48
Heat Area (A_{ht})	6.74×10^{-7} m^2	$\pm$ 3.33
Heat Flux (q_{eff})	4–19.5 W/cm^2	$\pm$ (2.03 – 5.01)
Mass Flux (G)	205–690 kg/m^{2}s	$\pm$ (2.52 – 5.32)
Reynolds number (Re)	65–125	$\pm$ (2.92 – 5.22)
Pressure Drop (Δp)	10–45 kPa	$\pm$ (2.67 – 7.02)
Heat transfer coefficient (h_{TP})	7.5–37 kW/m^{2}K	$\pm$ (4.21 – 7.82)

5.7 Summary

The present study is focused on a large pressure drop, which results in significant effects of variable thermophysical properties and flashing. To generate large pressure drop, a microchannel with a hydraulic diameter around 100 μm was aimed, and a channel of D_H =111 μm successfully fabricated on silicon. The fabrication process made the shape trapezoidal, but it served our purpose to obtain large pressure drop. The fabrication of the microchannel and the integrated microheater were done using microfabrication facility available at CEN, IIT Bombay (As per steps stated in Singh et al. (2009)). The assembling of the test section (installation of the cover plate, inserting thermocouples) was done in Microfluidics Lab, IIT Bombay. Heat loss calibration and uncertainty analysis were done to ensure the correctness of the measurements.

Chapter 6

Experiments on Single Phase Flow

Single phase pressure drop and heat transfer experiments are conducted for water and FC-72 to validate the previous correlations for trapezoidal microchannel. For adiabatic condition, the existing friction factor for trapezoidal microchannel is validated with a good prediction of present experimental data. A sample correlation of friction factor for the trapezoidal microchannel with the non-adiabatic condition is developed (For FC-72). It incorporates the variation of viscosity with temperature. For heat transfer, a correlation from the literature gives good agreement with the present experimental data.

6.1 Single-phase Pressure Drop

Adiabatic single-phase experiments were conducted on the same test section and setup described in Chapter 4. DI water and FC-72 were used as working fluids to validate the existing correlation for microchannel with a trapezoidal cross-section. For adiabatic flow, Wu and Cheng (2003b) had given the most popular friction factor correlation (Equation 6.1) for trapezoidal microchannel. It was developed based on the experimental data with different W_b/W_t ratio. Experiments were done on the test section. The fluid was passed through the test section, and the pressure difference between the inlet and outlet was recorded. Experimental friction factor was calculated from the experimental pressure drop and compared with the correlation Wu and Cheng (2003b) specially developed for the trapezoidal cross-section.

$$fRe = 11.43 + 0.80e^{\left(\frac{2.67W_b}{W_t}\right)} \tag{6.1}$$

In Figure 6.1 and Figure 6.2, comparison of friction factor correlation (Wu and Cheng, 2003b) with experimental data for adiabatic flow are shown for water and FC-72 respectively, and it is observed that the correlation predicts the experimental data for both the fluids with good accuracy. Therefore, this friction factor correlation (Wu and Cheng, 2003b) can be used for further study on diabatic single-phase flow pressure drop with required modification.

In diabatic flow, the single-phase pressure drop is significantly influenced by the variation of viscosity with temperature, considering only the axial variation of temperature, Equation (6.2) and equation (6.3) are used for water (Al-Shemmeri, 2012) and for FC-72 (a linear fit to property data). Here, T is in Kelvin.

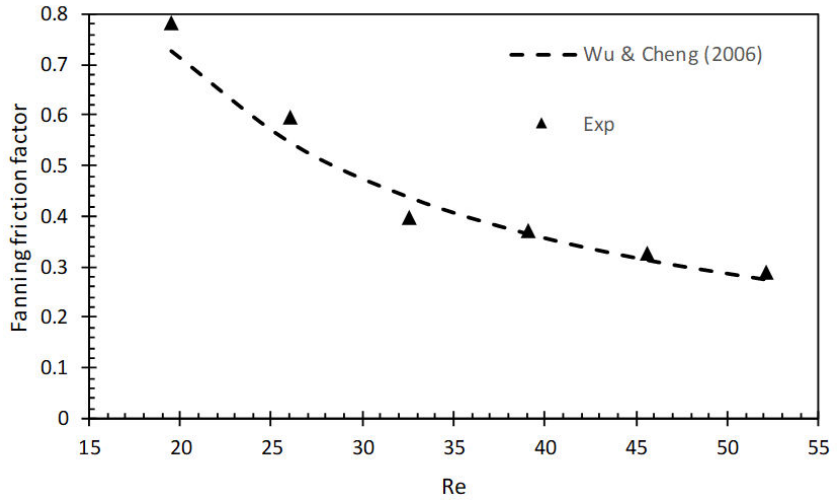

Fig. 6.1: Comparison of friction factor correlation (Wu and Cheng, 2003b) with experimental data at no heat condition. $D_H = 111$ μm. Fluid: DI Water

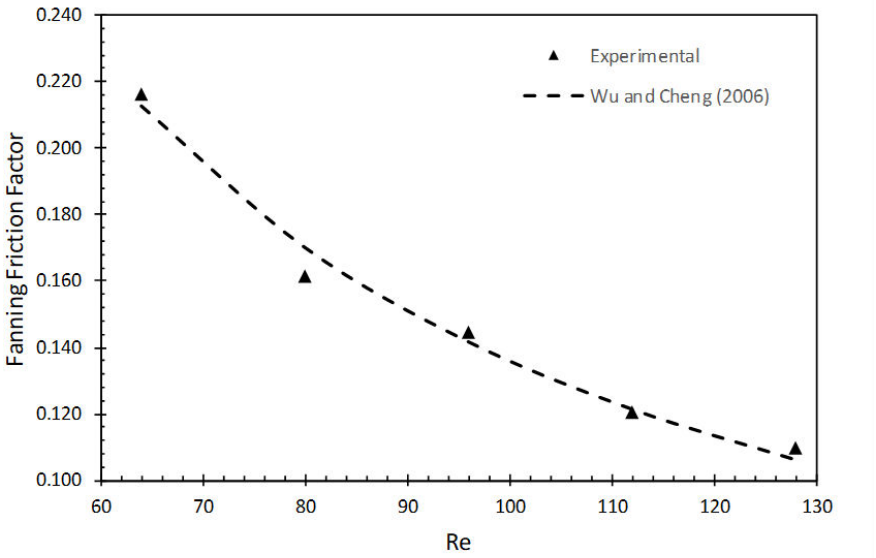

Fig. 6.2: Comparison of friction factor correlation (Wu and Cheng, 2003b) with experimental data at no heat condition. $D_H = 111$ μm. Fluid: FC-72

$$\mu(T) = 2.414 \times 10^{-5} \times 10^{247.8/(T-140)} \tag{6.2}$$

$$\nu(T) = 1.135 \times 10^{-6} - 2.5872 \times 10^{-9} T \tag{6.3}$$

For rectangular channel fully-developed friction constant f_{SP} is a function of the channel aspect ratio β given by equation (6.4) of Shah and London (1978) For the trapezoidal cross section, Equation (6.1) is used to evaluate friction factor.

$$Re_{SP} f_{SP} = 24\left(1 - 1.3553\beta + 1.945\beta^2 - 1.7012\beta^3 + 0.9564\beta^4 - 0.2537\beta^5\right) \tag{6.4}$$

where, Equation (6.5) gives Re_{SP}

$$Re_{SP} = \frac{GD_H}{\mu(T)} \tag{6.5}$$

From energy balance, the axial temperature profile can be expressed by Equation (6.6)

$$T = \frac{q_{eff} P_H}{GAc_p} z + T_{in} \tag{6.6}$$

The pressure drop in the single-phase region is evaluated by equation (6.7) where f_H denotes the friction factor for heated case.

$$\Delta p = \int_0^{L_{SP}} \frac{f_H G^2}{D_H \rho_f} dz \tag{6.7}$$

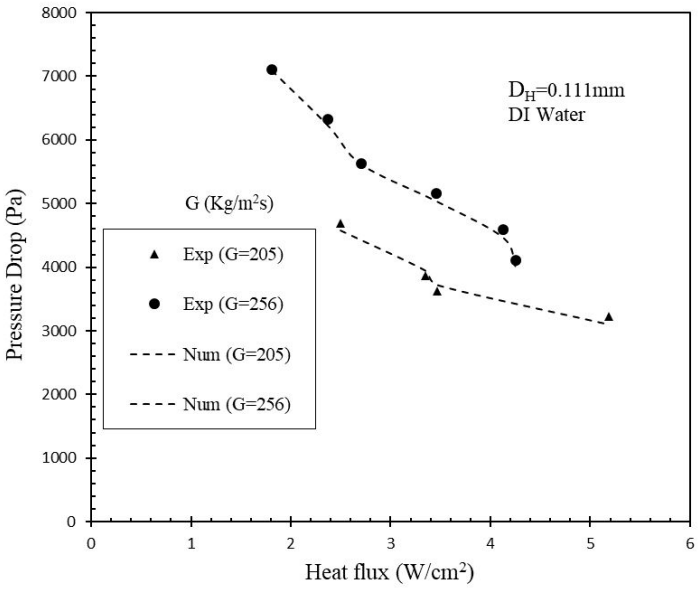

Fig. 6.3: Experimental single pressure drop compared with present 1 D model for heating condition water

where L_{SP} is the length from the inlet to the saturation point or boiling boundary and is given by equation (6.8)

$$L_{SP} = \frac{GAC_p(T_{sat} - T_{in})}{P_H q_{eff}} \tag{6.8}$$

This methodology to evaluate single-phase pressure drop for the non-adiabatic case is compared with the experimental data in Figure 6.3. It is observed that the prediction of this one-dimensional model is good when compared with different heat flux and mass fluxes.

Single-phase pressure drop experiments are conducted for different mass flux and heat flux conditions and are shown in Figure 6.4. This parametric study was done experimentally to find the key parameters affecting the friction factor for the heated case apart from the effects present in the unheated case. In case of unheated case Wu and Cheng (2003b), correlate fanning friction factor to (W_b/W_t). It was observed that in case of heated microchannel for a constant cross-sectional aspect ratio, friction factor increases with mass flux and decreases with heat flux.

$$f_H Re_H = f_{UH} Re_{UH} \left[2.88 \left(\frac{q_{eff}}{q_{ref}} \right)^{0.22} \left(\frac{G_{eff}}{G_{ref}} \right)^{0.48} \right] \tag{6.9}$$

The parametric study was done experimentally to find the key parameters affecting the friction factor for the heated case in addition to the effects present in the unheated case. It

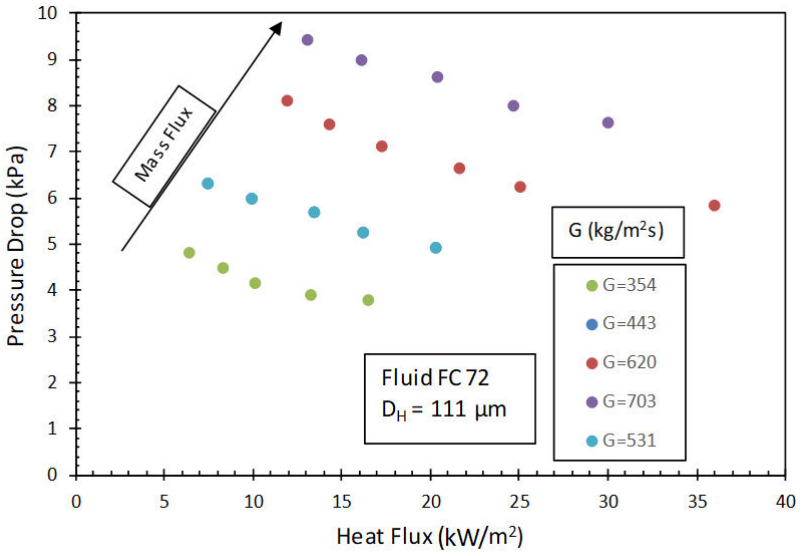

Fig. 6.4: Experimental single pressure drop for different mass flux and heat flux. Fluid: FC-72

was observed that, for a constant cross-sectional aspect ratio, the friction factor increases with the mass flux and decreases with the heat flux. Considering the experimental data, through regression analysis, a sample correlation was developed to predict the friction factor for trapezoidal microchannel. The new sample correlation is given by equation (6.9).where G_{ref} is the reference mass flux (500 kg/m^2) and q_{ref} is the reference heat flux (10 W/cm^2).

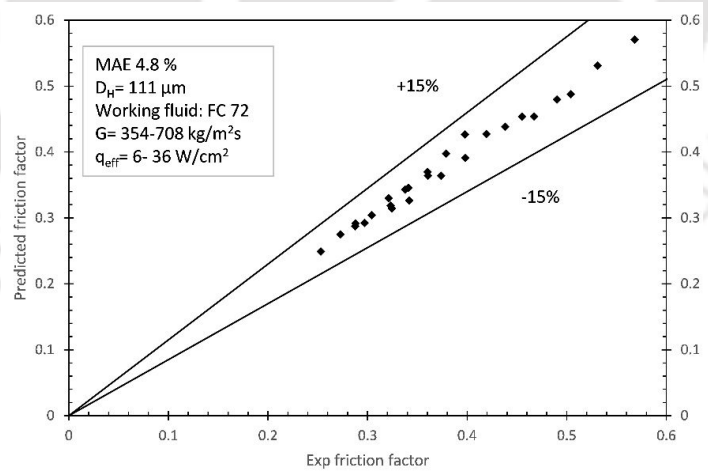

Fig. 6.5: Predicted friction factor versus experimental friction factor at middle of the test section.

Figure 6.5 shows the predicted friction factor using equation (6.9) versus experimental friction factor data at the middle of the test section, and it shows good agreement with the experimental data.The data set used for the validation was for axial length 10 mm from the inlet, and it shows the effectiveness of the regression analysis. The new sample correlation

contains the effect of heat flux and mass flux. Since for heated case, change of viscosity plays a critical role in shear stress determination; therefore, new correlation predicts the heated data points more accurately. The predictions of the proposed equation are plotted along with the experimental data to show the effectiveness of the regression analysis. Further experiments with more data points are required to develop a new correlation for the heated trapezoidal microchannels.

6.2 Single-phase Heat Transfer

Single-phase heat transfer experiments for trapezoidal microchannel for water as well as FC-72 were carried out considering different mass fluxes and heat fluxes. In Figure 6.6 and figure 6.7, a parametric study of the local heat transfer coefficient is presented for different heat flux and mass flux. The experimental results show that the Nusselt number increases with the Reynolds number linearly for both the fluids. For some cases, at constant mass flux, the local heat transfer coefficient increases with increasing heat flux. It is because, for the present experimental condition, the flow is not thermally fully developed, therefore for laminar flow Nusselt number is not constant.

$$h_{SP}(z) = \frac{q_{eff}}{T_w(z) - T_f(z)} \tag{6.10}$$

$$T_w(z) = T_{tc}(z) - \frac{q_{eff}t}{k_s} \tag{6.11}$$

$$T = \frac{q_{eff}P_H}{GAc_p}z + T_{in} \tag{6.12}$$

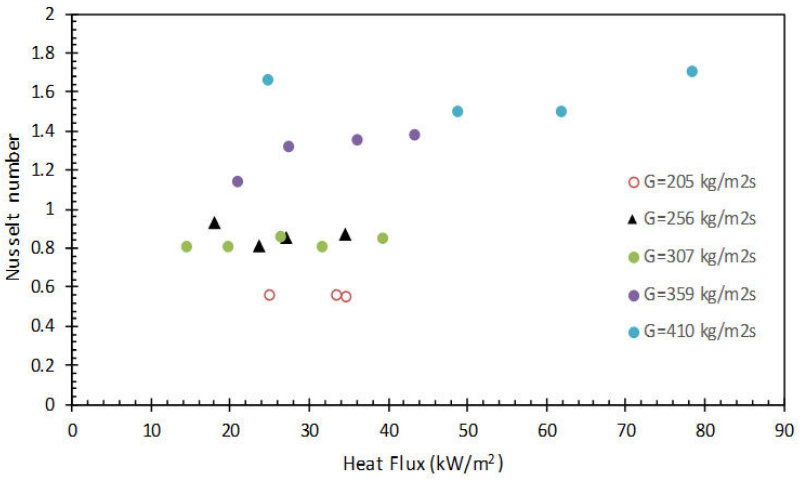

Fig. 6.6: Single phase heat transfer coefficient against heat flux for different mass flux Fluid: DI water; $D_H = 111$ μm, mass fluxes= 205–410 kg/m^{2}s

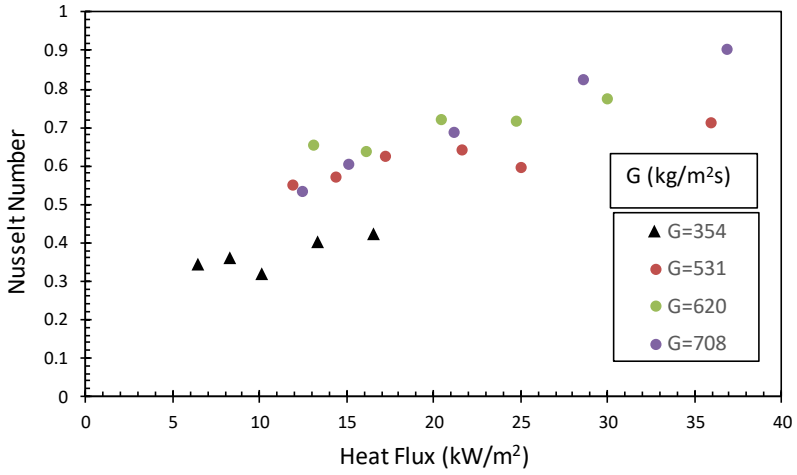

Fig. 6.7: Single phase heat transfer coefficient against heat flux for different mass flux Fluid: FC-72; $D_H = 111$ μm, mass fluxes= 345–708 kg/m^{2}s

Experimental Nusselt number was compared with the correlation from the literature (Wu and Cheng, 2003a), specifically developed for trapezoidal microchannel. It was observed that prediction was good for all the cases and this correlation can be used further for the evaluation of two-phase heat transfer coefficient for trapezoidal channel. Single phase heat transfer coefficient is evaluated by equations (6.10–6.12).

6.2.1 Correlation for single phase heat transfer coefficient

Wu and Cheng (2003a) performed an experimental investigation on the laminar convective heat transfer and pressure drop of water for 13 different trapezoidal silicon microchannels. It is found that the values of Nusselt number and apparent friction constant depend greatly on different geometric parameters. The laminar Nusselt number and apparent friction constant increase with the increase of surface roughness and surface hydrophilic property. These increases become more obvious at larger Reynolds numbers. The experimental results also show that the Nusselt number increases almost linearly with the Reynolds number at low Reynolds numbers ($Re < 100$), but increases slowly at a Reynolds number greater than 100. Based on 168 experimental data points, dimensionless correlations for the Nusselt number and the apparent friction constant are obtained for the flow of water in trapezoidal microchannels having different geometric parameters, surface roughnesses and hydrophilic surface properties.

Correlation proposed by Wu and Cheng (2003a) is given by equations (6.13) and equation (6.14) depending upon the Reynolds Number range. For $10 < Re < 100$, equation (6.13) is used and for $100 < Re < 1500$ equation (6.14) is used.

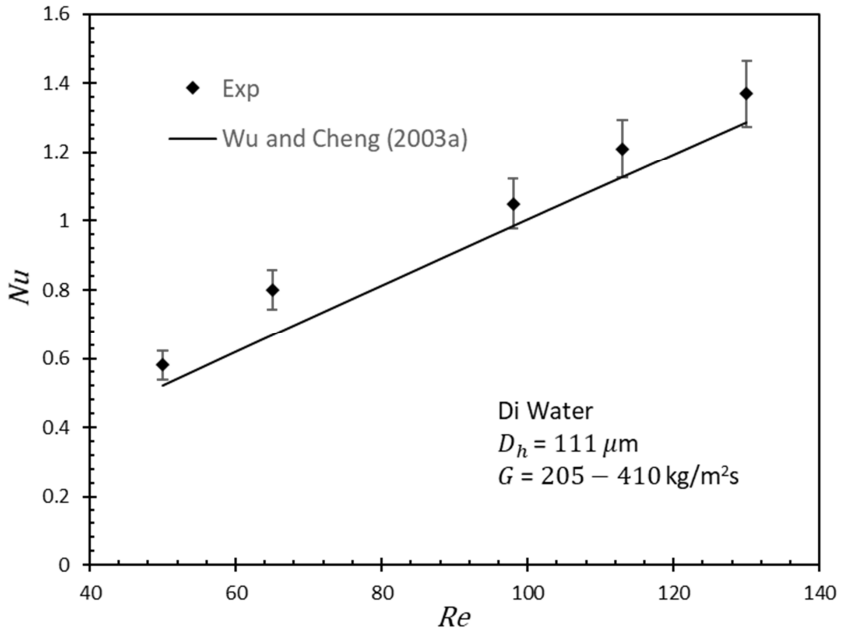

Fig. 6.8: Nusselt Number (Wu and Cheng, 2003a) vs Raynolds Number for water

$$Nu = C_1 Re^{0.946} Pr^{0.488} \left(1 - \frac{W_b}{W_t}\right)^{3.547} \left(\frac{W_t}{H}\right)^{3.577} \left(\frac{k_f}{D_H}\right)^{0.041} \left(\frac{D_H}{L}\right)^{1.369} \tag{6.13}$$

$$Nu = C_2 Re^{0.148} Pr^{0.488} \left(1 - \frac{W_b}{W_t}\right)^{0.908} \left(\frac{W_t}{H}\right)^{1.001} \left(\frac{k_f}{D_H}\right)^{0.033} \left(\frac{D_H}{L}\right)^{0.798} \tag{6.14}$$

In Figure 6.8 and Figure 6.9, Nusselt Number (Wu and Cheng, 2003a) vs Raynolds Number is compared for Water and FC-72 respectively. It is observed that for both the fluid, the correlation gives very good agreement for different mass flux condition.

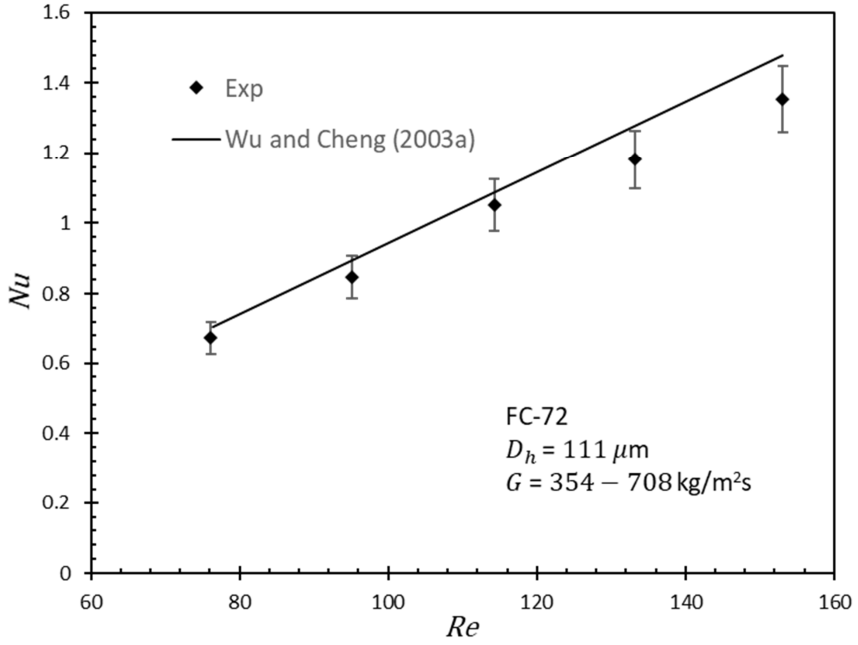

Fig. 6.9: Nusselt Number (Wu and Cheng, 2003a) vs Raynolds Number for FC-72

6.3 Summary

Single-phase pressure drop and heat transfer experiments are conducted for deionized water and FC-72 to validate the previous correlations for trapezoidal microchannel. For the non-adiabatic case, the existing friction factor (Wu and Cheng (2003b)) correlation for the trapezoidal microchannels was validated with the present experimental data and showed a good agreement. A sample correlation of friction factor for the trapezoidal microchannel with the non-adiabatic condition was developed for FC-72 by incorporating the effect of variable viscosity. The correlation was validated with the same experimental data to see the effectiveness of the regression analysis. Further experiments with more data points are required to develop a new correlation for the heated trapezoidal microchannels.

Chapter 7

Validation of New Methodologies for Pressure Drop

Flow boiling experiments are performed using two working fluids (water and FC-72) with mass flux 205–690 kg/m^{2}s and heat flux 4.5–19.5 kW/m^2. It is observed that the pressure drops are large for both the fluids, facilitating validation of the new modelling approaches. The vapour phase of water can be considered ideal gas at present operating pressure, and the new modelling approach is validated with the flow boiling pressure drop data for water. On the other hand, the vapour phase of FC-72 does not behave like an ideal gas, but the compressibility factor remains constant for the operating conditions used. The pressure drop data of FC-72 is used to validate the generalized modelling approach. It is observed that both the new methodologies improve the predictions over the existing approach.

7.1 Flow Boiling Pressure Drop in a microchannel

Flow boiling pressure drop in a microchannel is investigated for water as well as FC-72. Effect of heat flux, mass flux and thermodynamic quality on flow boiling pressure drop are examined experimentally. In Figure 7.1, for two mass flux, at different heat flux pressure drop is reported. Water as a working fluid enters to the microchannels at subcool condition. Once heat flux increases, at first pressure drop decreases. It is because this region is single phase and due to a decrease in viscosity pressure drop decreases since increment of heat flux at constant mass flux leads to an increase in fluid temperature. After the onset of nucleate boiling (at x=0), pressure started to increase with increase in heat flux for constant mass flux. After that pressure drop increases rapidly as heat flux increases, this region is flow boiling region. Here, due to increases in void fraction, increases the accelerational as well as two-phase frictional pressure drop are observed.

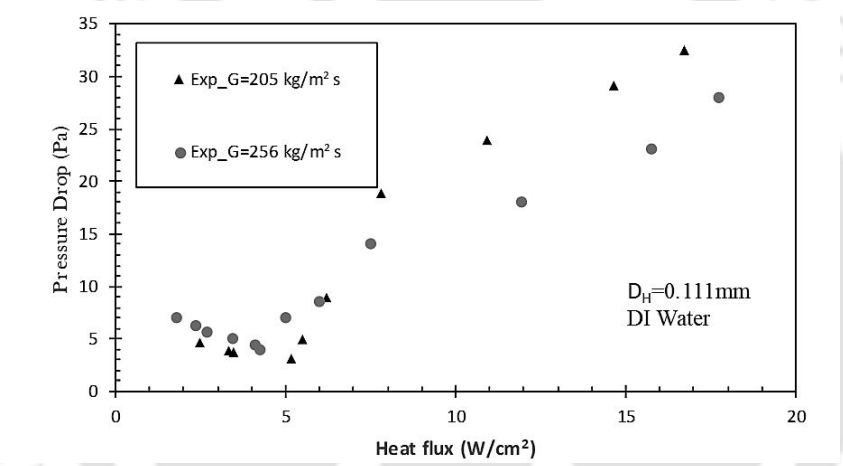

Fig. 7.1: Experimental Pressure drop vs heat flux at different mass flux condition.

Figures 7.2 and 7.3 show the variation of total pressure drop with the wall heat flux and the exit vapor quality, respectively. Here, the exit vapor quality is chosen as the total pressure drop is the pressure difference between the inlet and outlet headers. As seen from Figures 7.2 and 7.3, total pressure drop increases with an increase in the heat flux or with the exit vapor quality for all the mass flux values. Here, the exit vapor quality was calculated considering the flashing effect. Apart from the increase in the pressure drop due to acceleration and friction with increase with outlet quality, there is another effect in very small channels, as explained by Markal et al. (2016). Due to increase in the heat flux, evaporation momentum force increases, which results in the fact that extended bubble toward the inlet of the channel begins to apply more force, and consequently, flow resistance increases. The force opposed to evaporation force is due to the inertia of the liquid, and it increases with increasing mass flux. Markal et al. (2016) also stated that for very low flow rates (between 2.0 and 3.63 ml/min) and very small channel dimensions

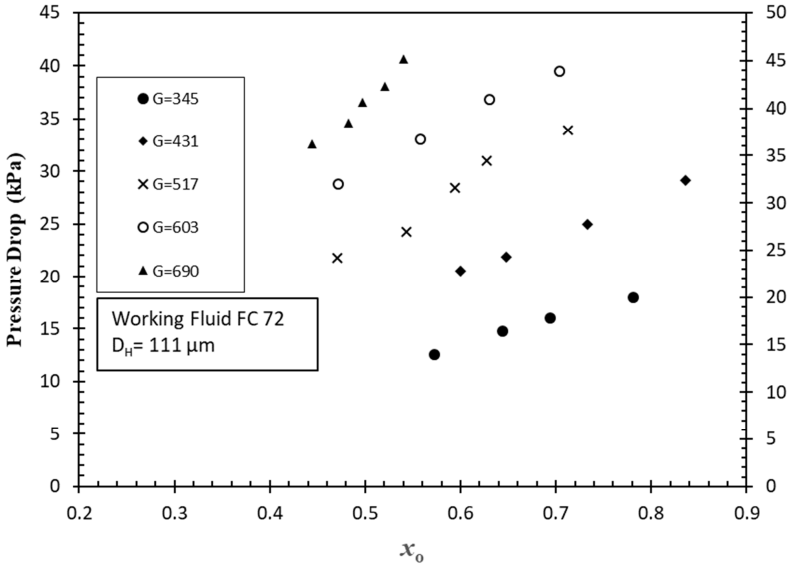

Fig. 7.2: Experimental total pressure drop with the exit vapor quality. Working Fluid: FC-72; $D_H = 111\mu$m; G=431-690 kg/m^{2}s; q_{eff}=4–8.5 W/cm^2

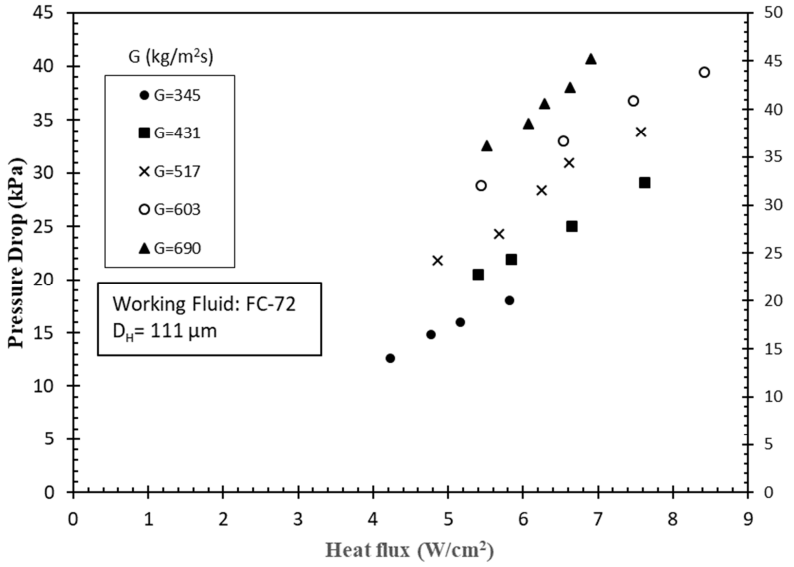

Fig. 7.3: Experimental total pressure drop with the wall heat.Working Fluid: FC-72; $D_H = 111\mu$m; G=431-690 kg/m^{2}s; q_{eff}=4–8.5 W/cm^2

(150 × 150 μm), the interaction of these forces becomes significant. In the present study, the channel dimension (D_H = 111μm) and flow rates (0.2–0.4 ml/min) are quite low, thus resulting in observations similar to those of Markal et al. (2016). Park et al. (2012) stated that heat flux negligibly affected the pressure drop under identical mass flux and vapor quality conditions, indicating that most of the pressure drop was caused by friction. However, their calculation of thermodynamic vapor quality was based on the effect of heat flux only, without considering the effect of flashing. This assumption is valid in case of low pressure drops only. The pressure drops in their experiments were high, causing the significant effect of flashing on the vapor quality.

7.2 Validation of a new approach with experimental data

7.2.1 Water as the working fluid

Experiments were conducted on a single microchannel with D_H = 111μm with mass flux range 205–410 kg/m^{2}s and heat flux range 7.5–19.5 W/cm^2. In the experiments, outlet pressure was considered to be atmospheric pressure. In Figure 6.4, experimental data is compared with the existing modelling approach with different C-correlations from literature (Mishima and Hibiki, 1996; Lee and Lee, 2001; Qu and Mudawar, 2003b; Lee and Mudawar, 2005; Li and Wu, 2011; Kim and Mudawar, 2013b; Li and Hibiki, 2017), where properties are evaluated at system pressure, and effect of flashing was not incorporated. It is observed that almost all the C-correlations predict the data with a high percentage of MAE (26–33%). The reason for such errors in the prediction of two-phase pressure drop was the accumulation of errors from the different parameters associated with the pressure drop calculation. Experimental two-phase pressure drop was in the range of 10–36 kPa, which, for water as the working fluid, causes a change in the saturation temperature in the range of about $4-9$°C along the length. Therefore, if the system pressure is considered instead of local pressure, the errors in v_g and h_f will be in the range of 4–6% and 8–11%, respectively. Existing modelling approach does not incorporate the effect of flashing; consequently, the thermodynamic quality (x) calculated with these models will be less than the actual value. Therefore, errors associated with v_g, h_f and x, result in significant error accumulation in the prediction of two-phase pressure drop.

The new approach is applied to the existing C-correlations from literature and compared with the experimental data (Figure 7.5), and substantial improvement in their predictions is observed. It is found that the new approach reduces the range of MAE for all the correlations to 7.5–13.5%. As discussed earlier, the new approach is based on the evaluation of thermophysical properties (v_g, h_f) at local pressure, the effect of flashing on the thermodynamic quality, and the effect of heat flux on the two-phase multiplier. Thus, this modelling approach is more realistic than the existing one.

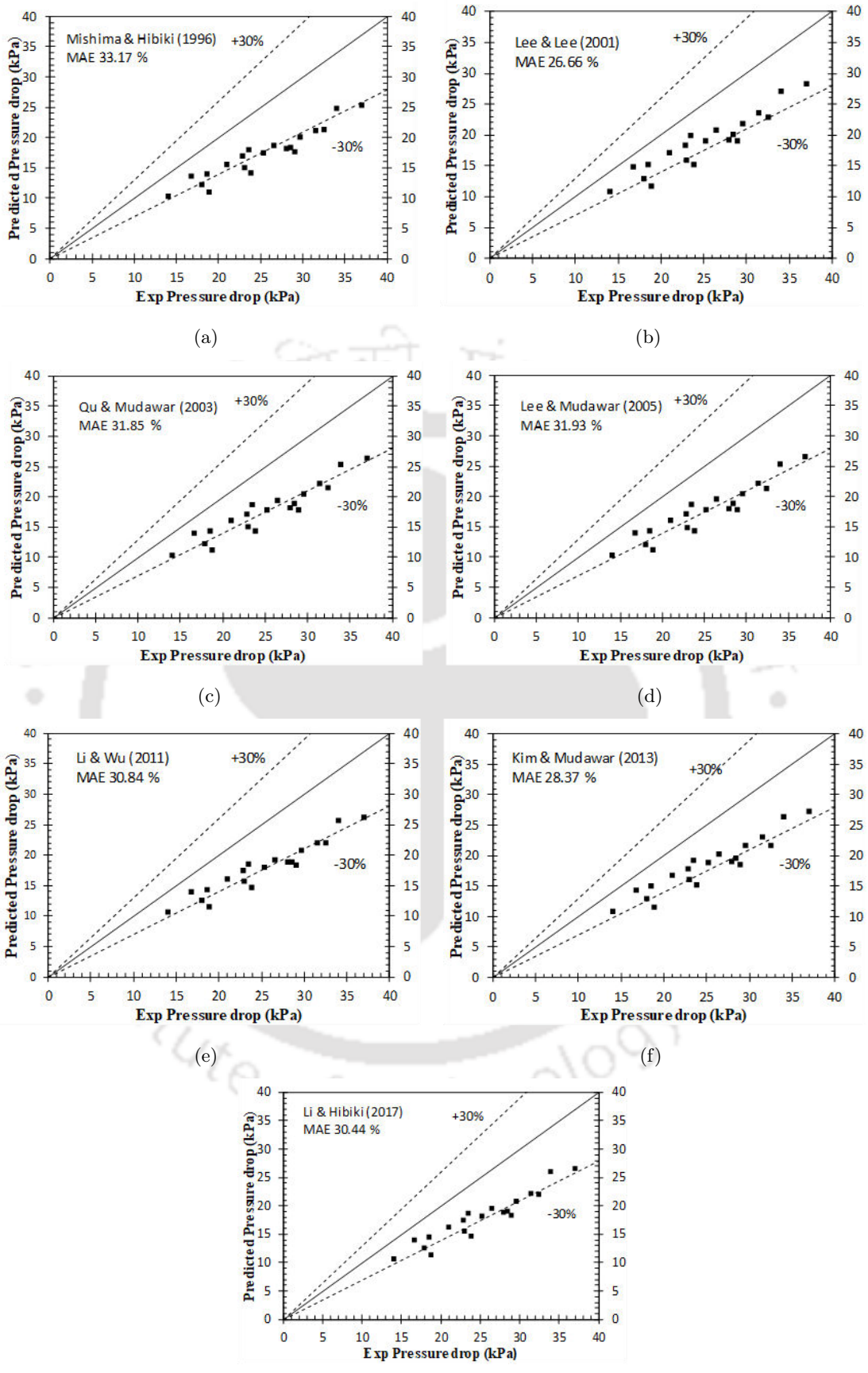

Fig. 7.4: Models from existing literature are compared with present experimental data.Working Fluid: DI water; $D_H = 111$ μm; G=205–410 kg/m^{2}s; q_{eff}=7.5–19.5 W/cm^2

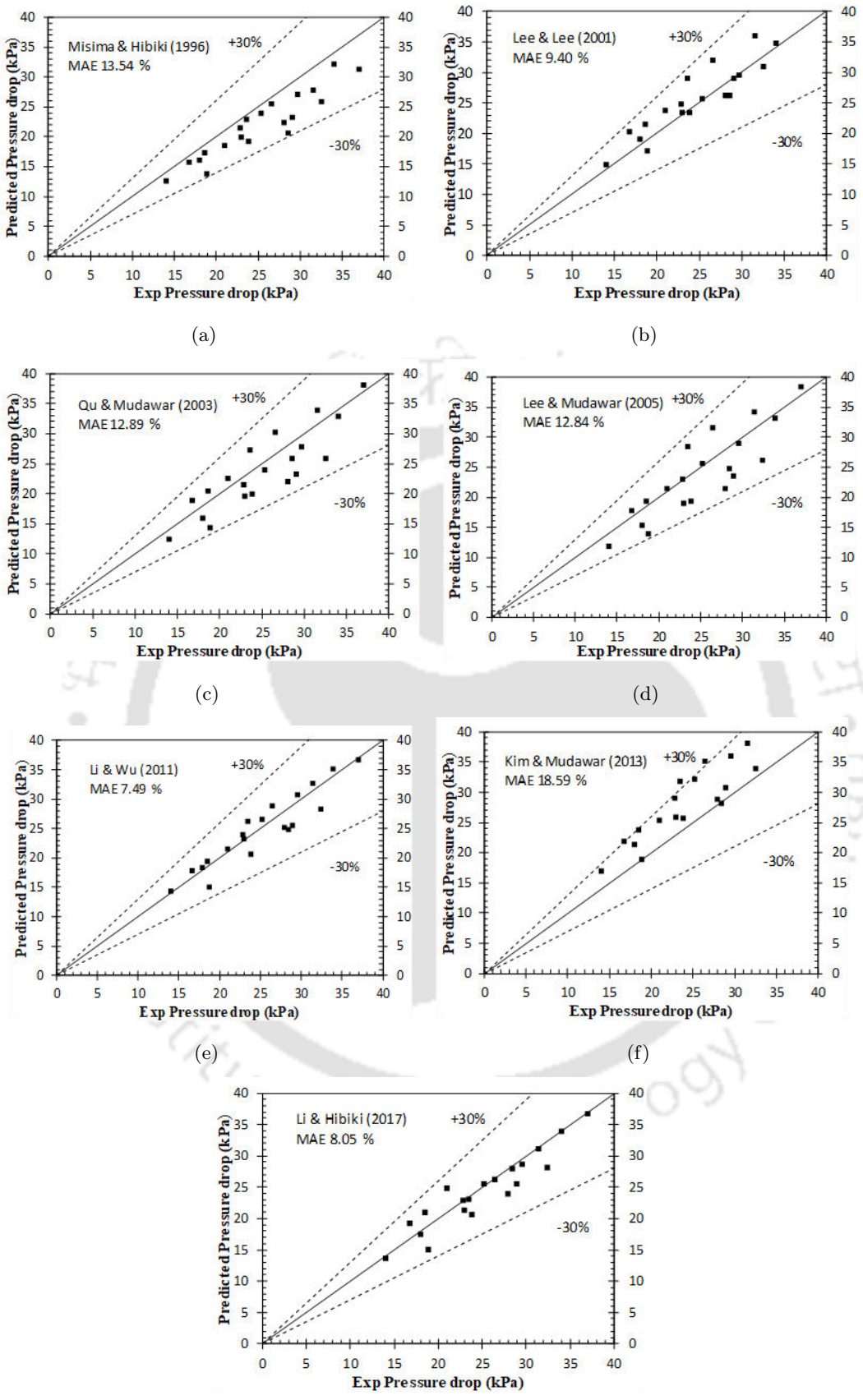

Fig. 7.5: Models with local properties, flashing effect and heating effect in existing models are compared with present experimental data. DI water; $D_H = 111$ μm; G=205–410 kg/m^{2}s; q_{eff}=7.5–19.5 W/cm^2

7.2.2 FC-72 as the working fluid

Experiments were conducted on a single microchannel with $D_H = 111$ μm with mass flux range 431–690 kg/m^{2}s and heat flux range 4–8.5 W/cm^2. In the experiments, outlet pressure was considered to be atmospheric. For water, the assumption of the ideal gas equation is valid since the compressibility factor (Z) is close to unity for the present working range of pressure. For FC-72, compressibility factor is not equal to one for the present working condition but constant within the range. Therefore, as discussed in Chapter 4, the generalized modelling approach combined with different C-correlations (listed in Table 7.1) is compared with experimental data (Figure 7.6). It was observed that almost all the correlations predict the data with high MAE (36–50%). The reason for this prediction with such error in the two-phase pressure drop is an accumulation of uncertainties from the different parameters associated with the pressure drop calculation. Experimental two-phase pressure drop was in the range of 10–46 kPa, which, for FC-72 as the working fluid, causes a change in the saturation temperature in the range of about 4–9°C along the length. Therefore, if the system pressure was considered instead of local pressure, the uncertainties in v_g and h_f will be in the range of 12–25% and 9–15%, respectively. Existing modelling approach did not incorporate the effect of flashing, and consequently, the thermodynamic quality (x) calculated with these models will be less than the actual value. Therefore, uncertainties associated with v_g, h_f and x, caused a considerable error in the prediction of two-phase pressure drop.

The present approach was applied to the existing correlations (listed in Table 7.1) and compared with the experimental data in Figure 7.7, significant improvement in their predictions was observed. It was found that the new approach reduces the range of MAE for all the correlations to 8.4–36%. As discussed earlier, the present approach is based on the evaluation of thermophysical properties (v_g and h_f) at local pressure, and the effect of flashing on the thermodynamic quality.

It is observed that incorporation of the effect of local properties and flashing improved the prediction to a great extent. In Table 7.1, comparison of MAE (%) of all the models reveals that model M6 showed the lowest MAE (8.4%). This model used the correlation of Kim and Mudawar (2013b) for the Chisholm parameter C, which incorporated the effect of heat flux on C. This was based on an earlier analysis (Kim and Mudawar, 2012) of the fundamental differences in flow structure between flow boiling and adiabatic flows. Therefore, further modification is done on the other models (M1–M5, M7), in order to improve their predictions. As discussed in chapter 4, an empirical correlation (Tarasova et al., 1966), relating the value of ϕ_{fo}^2 for heated and unheated tubes combined with these models (M1–M5, M7). Then the results of these modified models were compared with the experimental data. From Figure 7.8 and Table 7.1, it is observed that the effect of heat flux on ϕ_{fo}^2 improves the predictions of the models.

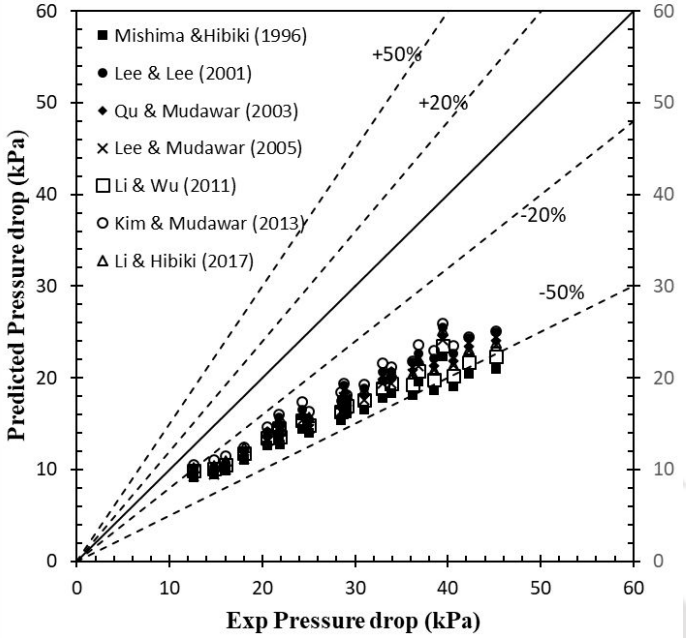

Fig. 7.6: Comparison of the existing correlations from the literature with present experimental data considering properties at system pressure. Working Fluid: FC-72; $D_H = 111$ μm; G=431–690 kg/m^{2}s; q_{eff}=4–8.5 W/cm^2

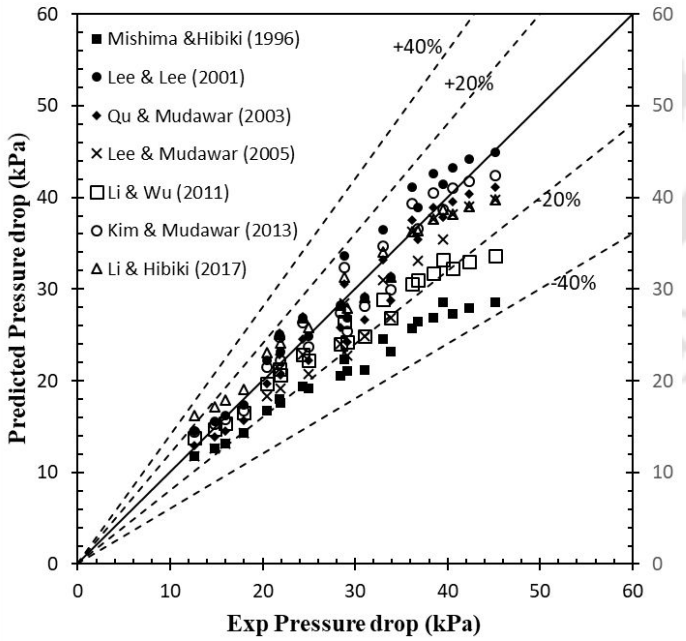

Fig. 7.7: Comparison of the existing correlations from the literature with present experimental data considering effect of flashing and local thermophysical properties. Working Fluid: FC-72; $D_H = 111$ μm; G=431–690 kg/m^{2}s; q_{eff}=4–8.5 W/cm^2

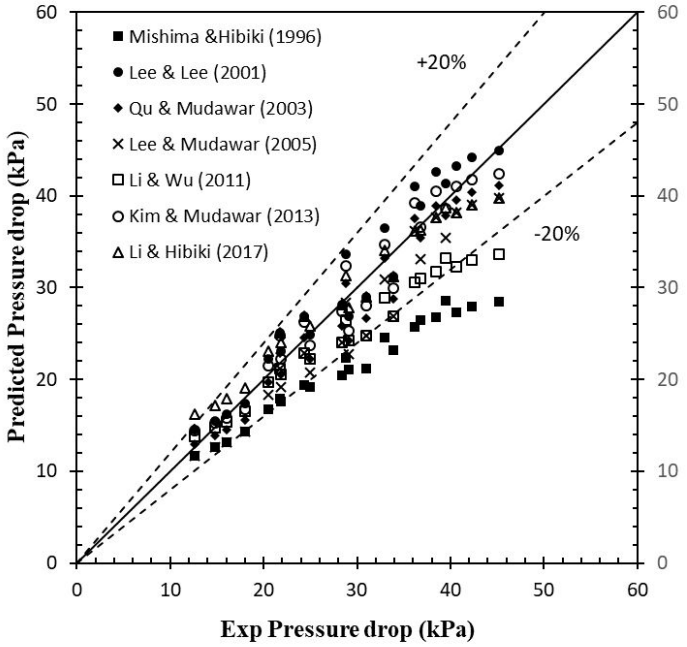

Fig. 7.8: Comparison of the existing correlations with present experimental data considering effect of flashing as well as effect of heating in the two-phase multiplier. Working Fluid: Working Fluid: FC-72; $D_H = 111$ μm; G=431–690 kg/m^{2}s; q_{eff}=4–8.5 W/cm^2

Tab. 7.1: List of MAE in pressure drop calculation for different C-correlations (Experimental data for FC-72)

Model nomenclature [References]	Equations for Chisholm Parameter (Liquid Laminar and Gas Laminar)	MAE (%) SYP	MAE (%) LOP	MAE (%) LOPH
M1 (Mishima and Hibiki, 1996)	$C = 21(1 - e^{319D_H})$	50.89	35.96	18.67
M2 (Lee and Lee, 2001)	$C = 6.185 \times 10^{-2} Re_{fo}^{0.726}$	46.85	16.62	9.45
M3 (Qu and Mudawar, 2003b)	$C = 21(1 - e^{319D_H}) \times (0.00418G + 0.06613)$	44.86	21.85	11.24
M4 (Lee and Mudawar, 2005)	$C = 2.16 Re_{fo}^{0.047} We_{fo}^{0.60}$	46.85	26.79	12.76
M5 Li and Wu (2011)	$C = 5.6 Bd^{0.28}$ for $Bd < 0.1$	46.72	27.28	14.65
M6 (Kim and Mudawar, 2013b)	$C_{boil} = 3.5 \times 10^{-5} Re_{fo}^{0.44} Su_{go}^{0.5} (\rho_f/\rho_g)^{0.48} \times \left[1 + 530 We_{fo}^{0.52} (Bo(P_H/P_F))\right]$	36.71	8.41	8.41

M7 (Li and Hibiki, 2017)	$C = 41.7 Nu_{\mu_{TP}}^{0.66} Re_{TP}^{0.42} x^{0.21}$ $Nu_{TP} = \mu_{TP} / \left(\rho_{TP} \sigma \sqrt{\sigma / g \Delta\rho}\right)^{0.5}$ $1/\mu_{TP} = (1-x)/\mu_f + x/\mu_g$ $\rho_{TP} = (1-x)/\rho_f + x\rho_g$	43.08	16.33	9.26

SYP = System Pressure; LOP= Local Pressure; LOPH = Local Pressure with Heat

7.3 Summary

Flow boiling experiments were performed using two working fluids (water and FC-72) with mass flux 205–690 kg/m^{2}s and heat flux 4.5–19.5 kW/m^2. The pressure drops observed for both the working fluids were large, facilitating validation of the new modelling approaches. The vapour phase of water can be considered ideal gas at present operating pressure, and the new modelling approach was validated with the flow boiling pressure drop data for water. On the other hand, the vapour phase of FC-72 did not behave like an ideal gas, but the compressibility factor remains constant for the operating conditions used. The pressure drop data for the FC-72 was used to validate the generalized modelling approach. It was observed that both the new methodologies improve the predictions significantly over the existing approach.

Chapter 8

Development and Validation of a Sample Correlation for Heat Transfer

Flow boiling heat transfer experiments are conducted in a microchannel for water and FC-72, and the local heat transfer coefficient is evaluated. To illustrate the new modelling approach for flow boiling heat transfer, a sample correlation is formulated by modifying a randomly chosen existing correlation (randomly chosen) using the experimental data from the literature. It is found that the correlation formulated with the new methodology improves the prediction over the original existing correlation chosen, for both the fluids. Further, the new sample correlation was tested for experimental data from literature and it was observed that for some data sets the predictions were good and for some it was poor, which implies a need of further improvement considering extensive data set for different ranges of fluid properties, shape, size, surface properties, pressure drop.

8.1 Flow Boiling Heat Transfer in a microchannel

Flow boiling heat transfer in trapezoidal a microchannel is experimentally investigated for water as well as FC-72. Effects of heat flux, mass flux and thermodynamic quality on flow boiling heat transfer are studied and dominating heat transfer mechanisms are identified for different cases.

Experiments are conducted for a single microchannel having $D_H = 111$ μm; length of the channel is 20 mm. A thermocouple is attached at 16 mm from the inlet at the bottom wall to measure the wall temperature. To evaluate the local heat transfer coefficient at that location, saturation temperature is evaluated by the new predictive approach discussed in chapter 4. Heat flux measurements are also done with proper calibration of heat loss.

In Figure 8.1 (a) and (b), the variation of local heat transfer coefficient (at 16 mm from the inlet) with thermodynamic quality (x) at different mass flux is presented for water and FC-72 respectively. Here, local h_{TP} is evaluated considering local saturation temperature (using the model described in Chapter 4), and the effect of flashing is considered in x. It is observed that for both the fluid, heat transfer coefficient decreases with increasing x and the effect of mass flux is not significant. On the other hand, if the same h_{TP} is plotted against heat flux (Figure 8.2), the effect of mass flux appeared significant (with increasing mass flux h_{TP} increases).

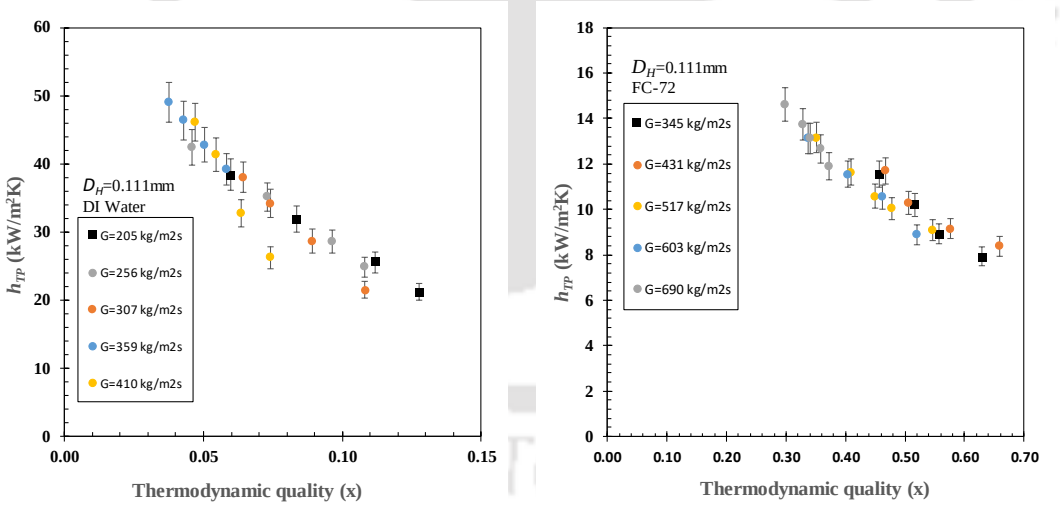

(a) (b)

Fig. 8.1: Local heat transfer coefficient vs thermodynamic quality at 16mm from inlet. (a)Fluid: DI water; $D_H = 111$ μm; G=205–410 kg/m^{2}s; q_{eff}=7.5-19.5 W/cm^2 (b)Working Fluid: FC-72; $D_H = 111$ μm; G=431–690 kg/m^{2}s; q_{eff}=4–8.5 W/cm^2

It can be observed from the Figure 8.1 that heat transfer coefficient decreases with increasing x. This trend is consistent with several previous experimental studies (Tran et al. (1996), Ravigururajan (1998), Kew and Cornwell (1997), Qu and Mudawar (2003a),

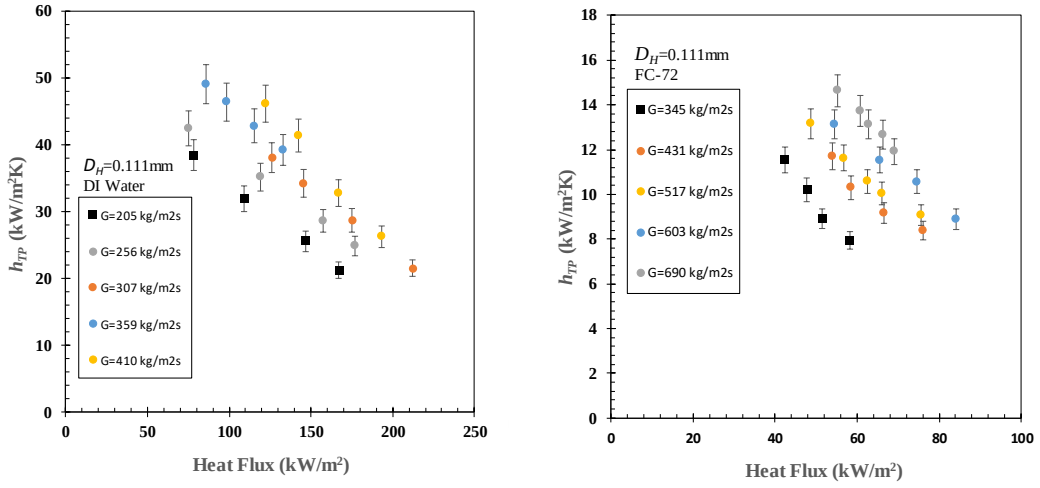

(a) (b)

Fig. 8.2: Local heat transfer coefficient vs Heat flux. (a)Fluid: DI water; $D_H = 111$ μm; G=205–410 kg/m^{2}s; q_{eff}=7.5-19.5 W/cm^2 (b)Working Fluid: FC-72; $D_H = 111$ μm; G=431–690 kg/m^{2}s; q_{eff}=4–8.5 W/cm^2

Zhuan and Wang (2013), Markal et al. (2016)). Ravigururajan (1998) attributed this phenomenon to possible blockage of the channel width (for a rectangular channel) by vapor bubbles. Kew and Cornwell (1997) and Warrier et al. (2002) explained this trend by local dry-out beneath the vapor bubbles. Qu and Mudawar (2003a)) explained this trend by the unique behavior of annular flow in micro-channels. In annular flow, the vapor flows along with the core of the channel, while liquid is comprised of two portions: the annular film along the channel wall, and droplets that are entrained in the vapor core. In case of flow boiling of water in micro-channels, an abrupt transition to annular flow occurred, and no bubbly flow was observed at moderate to high heat fluxes (Jiang et al. (2001), Qu and Mudawar (2004)). It is, therefore, possible that a large number of liquid droplets are broken off into the vapor core at the onset of annular flow development. The deposition of droplets upon the annular liquid film increases the film thickness in the stream-wise direction, resulting in the observed trend of decreasing h_{TP} with increasing x. Harirchian and Garimella (2009a) studied the heat transfer behaviour of FC 77 in microchannels and found that at high heat fluxes heat transfer coefficient was decreasing, which was due to an early partial wall dryout.

If the flow patterns inside the channel were not studied along with the heat transfer measurements then it is very difficult to precisely infer the mechanism (Karayiannis and Mahmoud (2017)). In the present study, from the graphical observations (figures 8.1 and 8.2) the mechanism involved can not be concluded precisely.

8.2 Boiling curve for a Microchannel

Boiling curves are plotted for the 111 μm microchannel in Figures 8.3 and 8.4 for water and FC-72 respectively, in terms of the variation of wall heat flux with the temperature difference between wall and saturated temperature at the 16 mm from the inlet. The results are plotted at four mass fluxes for water and five for FC-72. It is observed that for both the fluid (water and FC-72) and the condition mentioned, the temperature difference between wall and saturated temperature increases heat flux also increases. Galvis and Culham (2012) also observed the same trend of the boiling curve, with water as the working fluid and explained that during this region convective boiling dominates more than the nucleate boiling region since the effect of mass flux dominates. Without the flow patterns observation, the dominant heat transfer mechanism cannot be determined accurately.

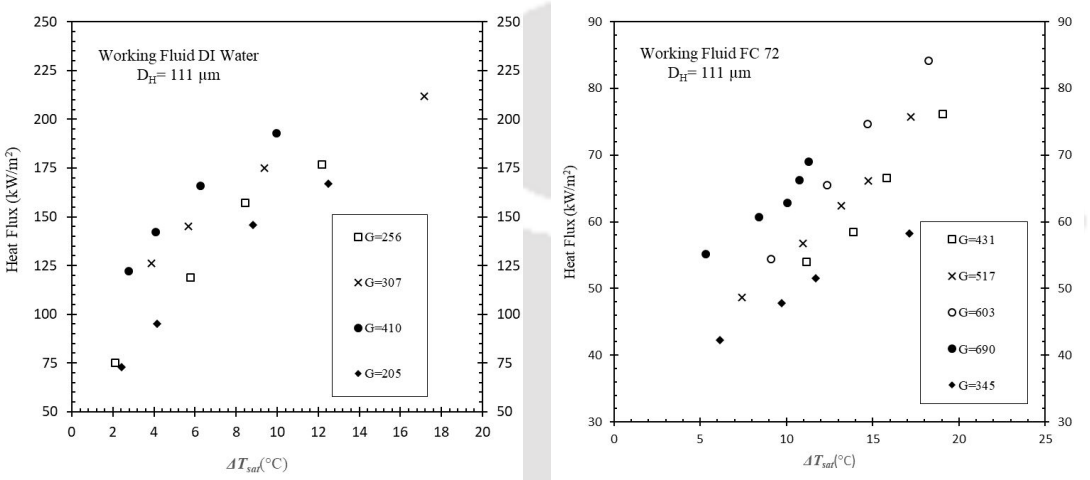

(a) (b)

Fig. 8.3: Boiling curve for a microchannel (a)Fluid: DI water; $D_H = 111$ μm; G=205–410 kg/m^{2}s; q_{eff}=7.5-19.5 W/cm^2 (b)Working Fluid: FC-72; $D_H = 111$ μm; G=431–690 kg/m^{2}s; q_{eff}=4–8.5 W/cm^2

8.3 Development of a new sample correlation

To formulate a heat transfer correlation, correct reduction of heat transfer coefficient from the experimentally measured quantities is important. As per Equation (8.1), to evaluate local heat transfer, accurate estimation of the heat flux, local wall temperature and local saturation temperature (at local pressure) is required.

$$h_{TP}(z) = \frac{q_{eff}}{T_w(z) - T_f(z)} \tag{8.1}$$

In most cases of flow boiling in microchannels (as discussed in Chapter 3), an axial

pressure profile was assumed instead of local measurements of saturation pressure were not reported. For simplicity, a linear pressure profile (Equation (8.2)) is assumed in most of the cases.

$$p_{sat}(z) = p_o + \frac{L - z}{L - L_{sub}} \left(p_{sat}(z_{sub} - p_o)\right) \tag{8.2}$$

This necessitates an accurate predictive approach for two-phase pressure drop. For large pressure drop cases, the effect of local thermophysical properties and effect of flashing in thermodynamic equilibrium quality are significant. Considering these effects, in chapter 4, new modelling approaches for different fluids are developed. In the present study, the axial pressure profile is estimated using the present modelling approach with the Chisholm parameter correlation of Kim and Mudawar (2013a).

In this section, the application of the new modelling approach is illustrated by developing a sample correlation for the local heat transfer coefficient for flow boiling in microchannels. As mentioned in Chapter 4, the first step is to select the form of the correlation, which can be taken from any of the existing correlations, or a new form based on the phenomena involved. Here a correlation (Fang et al. (2015)) is randomly chosen from the existing correlations were listed in Table 3.2 and modified with the new approach. The objective of this demonstration is to develop a sample correlation that is able to predict heat transfer coefficient for large pressure drop cases accurately. Therefore, limited (only 179 data points) experimental data points from the literature (Mirmanto, 2014, 2016) involving a large pressure drop was used for regression analysis (to minimize the MAE) and the modified form of the correlation was obtained. During data reduction, local saturation temperature was evaluated by the pressure modelling approach described in Chapter 4, where the axial variation of thermochemical properties and effect of flashing are considered. Thermodynamic quality is another important derived parameter in two-phase heat transfer evaluation, and for large pressure drop cases, the effect of flashing is significant in x (as discussed in chapter 4). Therefore, in the formulation of the sample correlation, the effect is incorporated using the equation (4.15). The modified form of equation is given by (8.3–8.7).

$$h_{TP} = Nu \frac{k_f}{D_H} \tag{8.3}$$

$$Nu = 0.000578(S + F)Re_f Fa^{0.84} Pr_f^{0.047} / \ln U \tag{8.4}$$

$$S = 139.7 Bo^{0.69} M^{0.51} \left(\frac{\rho_f}{\rho_g}\right)^{0.214} \tag{8.5}$$

$$F = x\left(\frac{x}{1-x}\right)^{1.18}\left(\frac{\rho_f}{\rho_g}\right)^{0.34} \tag{8.6}$$

$$U = 1.02\left(\frac{\mu_{f,w}}{\mu_{l,w}}\right)^{0.88} \tag{8.7}$$

8.4 Comparison of the new modelling approach with experimental results

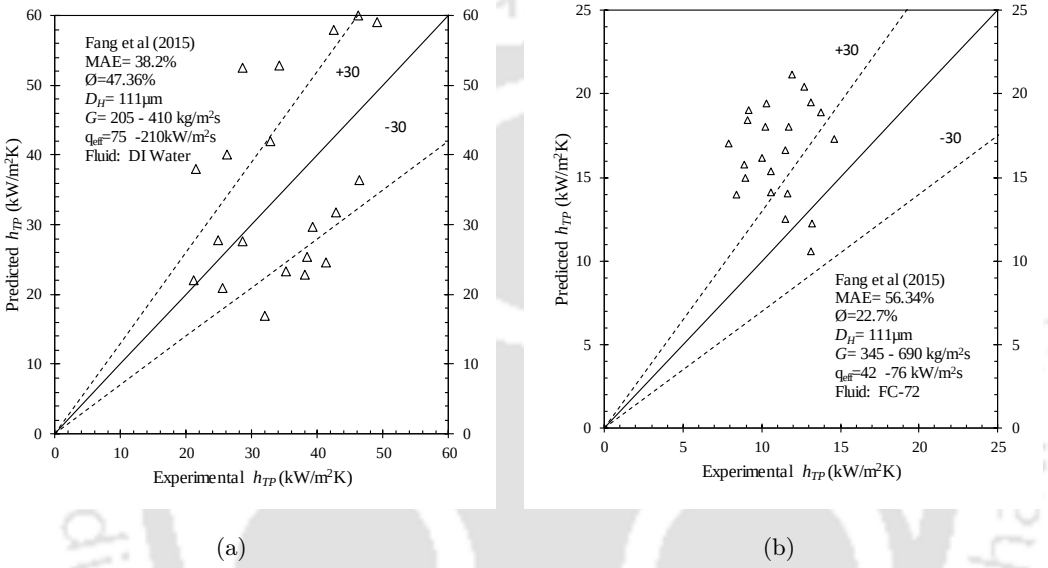

(a) (b)

Fig. 8.4: Experimental h_{TP} compared with Fang et al. (2015) (a) for water (b) FC-72

In Figures 8.4(a) and (b), the original correlation of Fang et al (2015)(listed in table 3.2) was compared with present experimental data (h_{TP}) for water and FC-72 respectively. It was observed that for both the cases, the correlation predicted the data points with a high margin of error (For water, MAE= 38.2% & ϕ=47.6 % and for FC-72 MAE= 52.34% & ϕ=22.7%). In Figures 8.5(a) and (b), experimental local heat transfer coefficient is compared with the present sample correlation formulated by new methodology (Equation (8.3–8.7)) for water and FC-72, respectively. The prediction of the new sample correlation for water (MAE= 21% and ϕ=84 %) as well as FC-72 (MAE= 13.75% and ϕ=95 %) is improved as compared to the original correlation (Fang et al. (2015)). For both the cases, pressure drops observed are high (10–45 kPa). Therefore, linear pressure profile assumption contribute a significant error. These experimental data points are not used during the formulation of the present sample correlation, and thus, it gives an independent mode of validation. The present experimental data set are less in number. Therefore, this sample correlation further tested with the experimental data points from the literature

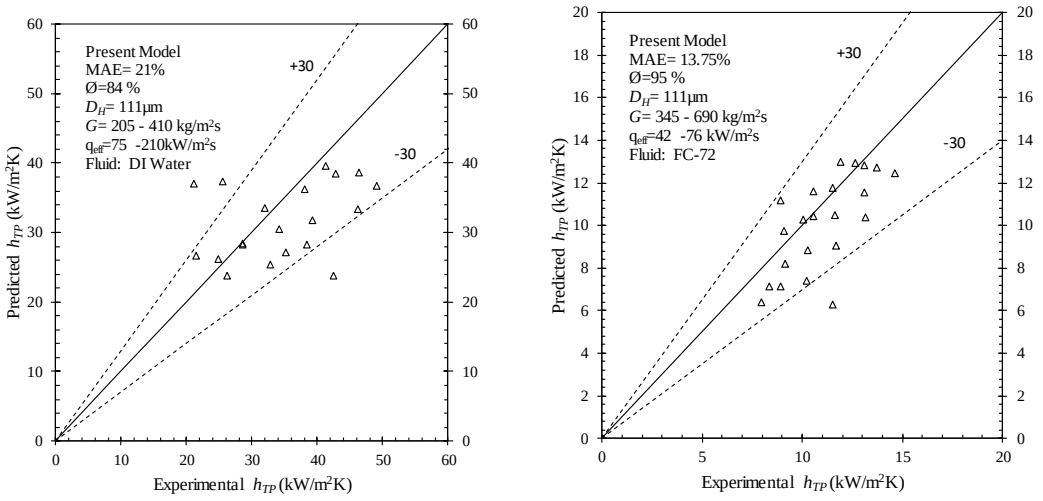

(a) (b)

Fig. 8.5: h_{TP} with new approach compared with the present experimental data (a) for water (b) FC-72

(Qu and Mudawar (2003a), Markal et al. (2019)). It is observed from the Figure 8.6 (a) that the sample correlation predicts the data from (Qu and Mudawar (2003a) with good accuracy (MAE= 19.5% and ϕ=88.42%) but it shows significant error (MAE= 104.2% and ϕ=27.27%) in predicting the experimental data from Markal et al. (2019) (Figure: 8.6 (b)). It implies that the new sample correlation required further improvement using large experimental data sets (different fluids, D_H, aspect ratio, surface characteristics, etc.).

The new modelling approach can be used to develop correlations for flow boiling heat transfer in microchannels with a large pressure drop. This will require extensive experimentation involving a large pressure drop for the development of correlations and independent experimental data for their validation.

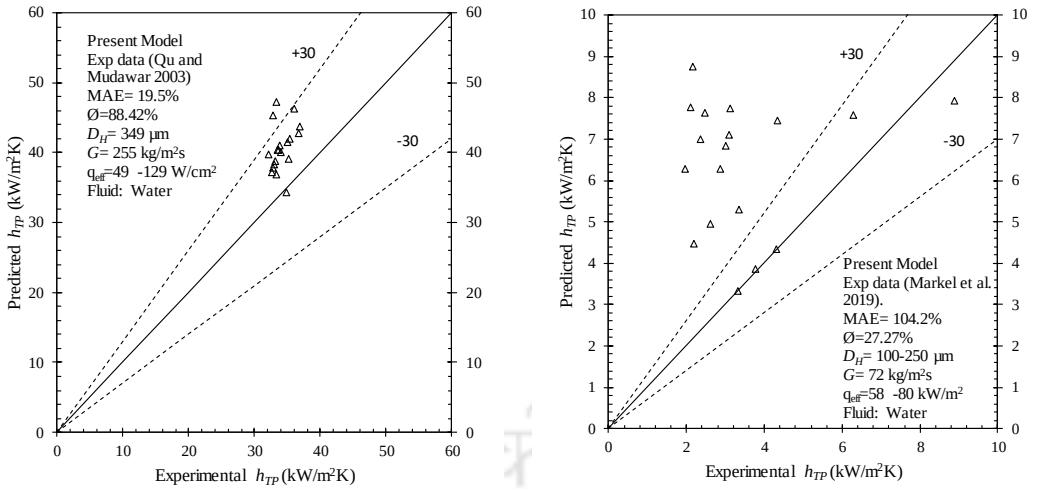

(a) (b)

Fig. 8.6: Present sample correlation is compared with experimental h_{TP} (a) Qu and Mudawar (2003a) (b) Markal et al. (2019)

8.5 Summary

Flow boiling experiments are performed using two working fluids (water and FC-72) with mass flux 205–690 kg/m^{2}s and heat flux 4.5–19.5 kW/m^2. The local heat transfer coefficient was evaluated at 16 mm from the inlet using the new pressure modelling approach. To illustrate the new modelling approach for flow boiling heat transfer, a sample correlation was formulated by modifying a randomly chosen existing correlation (from Table 3.2) using the experimental data from the literature. It was found that the correlation formulated with the new modelling approach improves the prediction over the original existing correlation (Fang et al. (2015)) chosen, for both the fluids.The new sample correlation was tested for experimental data from literature and , and it was observed that the predictions were better for some data sets but poor for some other data sets, which implies a need of further improvement in the formulation of h_{TP} considering extensive data set for different ranges of fluid properties, shape, size, surface properties, pressure drop.

Chapter 9

Conclusion and Future Scope

9.1 Conclusions

An extensive review is done on flow and heat transfer in microchannels. Thus, the need for improvements in flow boiling pressure drop and heat transfer modelling, especially for large pressure drop cases, is assessed. New predictive approaches for flow boiling pressure drop and heat transfer in microchannels are developed and validated by conducting experiments with a large pressure drop in a microchannel using water and FC-72.

Fluid flow and heat transfer in miniature channels is of significant scientific interest and flow boiling in microchannels have the capabilities of removing high heat fluxes. The phase change process in a microchannel enhances heat transfer in cooling systems of electronic devices, thus allowing the devices to function at high power densities. Design of these miniature devices requires a proper estimation of two-phase heat transfer, which, in turn, necessitates accurate prediction of two-phase pressure drop.

Experimental data from the literature show that, depending upon the parameters, the two-phase pressure drop in microchannels can reach up to nearly 100 kPa. For that range, if the system pressure were considered then (for water as the working fluid), there would be an error (MAE) of 40% in v_g and 30% in h_f. As these two quantities play an important role in the estimation of pressure drop and thermodynamic quality, they must be evaluated at the local pressure to get an accurate prediction of flow boiling pressure drop. Due to the axial variation of thermophysical properties, the effect of flashing becomes significant. To estimate these effects for large pressure drop, experimental data from the literature (Mirmanto, 2016, 2014) are compared with the existing approach for pressure drop, using property evaluation at the system pressure and without considering the flashing effect. It is observed that MAE is low (10–17%) for small pressure drop and MAE is high (37–44%) for the large pressure drop.

The axial profile of the local heat transfer coefficient is greatly influenced by the local

pressure. The existing approach uses a linear pressure profile to evaluate local saturation temperature while formulating correlations for flow boiling heat transfer coefficient. This approach is compared with the experimental data from the literature (Mirmanto, 2014, 2016), where saturation temperatures were measured locally. The predictions are found to be good for small pressure drop but significantly erroneous in case of a large pressure drop. This indicates the necessity of a new modelling approach for pressure drop that can facilitate an accurate prediction of flow boiling heat transfer, especially for a large pressure drop.

A new methodology is developed, which is simple but successful to evaluate flow boiling pressure drop. The idea is to incorporate the effect of local thermophysical properties and flashing on the pressure gradient. This method uses the separated flow model by employing different correlations from the literature for the Chisholm parameter. In this way, a significant improvement is observed in the prediction of large pressure drop data from the literature. The literature has revealed differences in flow structure between boiling and non-boiling flows. Hence, further improvement of the pressure drop model is done by modifying the two-phase multiplier with the heating effect for flow boiling. Comparison with experimental data from the literature shows a significant reduction of MAE (%).

The above modelling approach assumes ideal gas behaviour of the vapour phase of the working fluid and uses the Clausius-Clapeyron equation to relate local saturation pressure and temperature. By relaxing this assumption, a modified form of the Clausius-Clapeyron equation is developed to characterize the saturation line on the P-T plane for fluids whose vapour phase has a nearly constant compressibility factor in the range of operation. Hence, a generalized modelling approach is developed, which can predict the pressure drop for a variety of fluids.

Using the new modelling approach, the axial pressure profile is estimated, and the saturation temperature is evaluated locally. Hence, the variables associated with heat transfer correlations are calculated accurately, using local thermophysical properties and the thermodynamic quality accounting for flashing. These steps make the formulation procedure of correlations more realistic. The effectiveness of the modelling approach is established by comparing with the experimental local heat transfer coefficient from the literature and shows a significant improvement over the existing approach.

To validate these new models for flow boiling pressure drop and heat transfer in microchannels, experiments are conducted on a single microchannel with a hydraulic diameter of 111 μm. The fabrication of the test sections is done using a microfabrication facility available at CEN, IIT Bombay. Heat loss calibration and uncertainty analysis are done to ensure the correctness of the measurements. Single-phase pressure drop and heat transfer experiments are conducted to validate the previous correlations for trapezoidal microchannel. For heat transfer, correlation from Wu and Cheng (2003a) gives good agreement with

the present experimental data. A new sample correlation of friction factor for the trapezoidal microchannel with the non-adiabatic condition is developed. These correlations of single-phase pressure drop and heat transfer can be used for the development of two-phase correlations.

Flow boiling experiments are performed using two working fluids (water and FC-72) with mass flux 205–690 kg/m^{2}s and heat flux 4.5–19.5 kW/m^2. The pressure drops observed for both the working fluids are large, facilitating validation of the new modelling approaches. The vapour phase of water can be considered ideal gas at present operating pressure, and the new modelling approach is validated with the flow boiling pressure drop data for water. On the other hand, the vapour phase of FC-72 does not behave like an ideal gas, but the compressibility factor remains constant for the operating conditions used. The pressure drop data for the FC-72 is used to validate the generalized modelling approach. It is observed that both the new methodologies improve the predictions over the existing approach.

Flow boiling heat transfer experiments are conducted in the same microchannel for both the fluids (water and FC-72) and the local heat transfer coefficient is evaluated at 16 mm from the inlet. To illustrate the new modelling approach for flow boiling heat transfer, a sample correlation was formulated by modifying a randomly chosen existing correlation using the experimental data from the literature. It was found that the correlation formulated with the new modelling approach improves the prediction over the original existing correlation (Fang et al. (2015)) chosen, for both the fluids. The new sample correlation was tested for experimental data from literature and , and it was observed that the predictions were better for some data sets but poor for some other data sets, which implies a need of further improvement in the formulation of h_{TP} considering extensive data set for different ranges of fluid properties, shape, size, surface properties, pressure drop.

Thus, the new pressure drop and heat transfer modelling approaches presented here, along with their experimental validation, demonstrate that the effect of local thermophysical properties and flashing are significant for large pressure drop cases, and predictions can be improved considerably by incorporating these effects. These methods are obtained by relaxing some of the assumptions made in the existing methods, maintaining mathematical simplicity and computational inexpensively.

9.2 Future Scope

In the present work, the methodologies to develop flow boiling pressure drop and heat transfer correlation are developed and illustrated with examples. Based on the research experiences following possible ideas are stated.

- By conducting flow boiling experiments on miniature channels for different channel size and for different fluids, a large database can be obtained and using the present modelling approach, generalized correlations for flow boiling pressure drop and heat transfer coefficient can be developed.
- For very small microchannels (less than 1 μm), there is a possibility that slip on the wall can occur depending upon the Knudsen number. For such cases, In Appendix A, a modelling approach to predict the two-phase pressure drop and heat transfer are developed considering the effect of slip on the wall. The pressure drop is modelled using the homogeneous equilibrium model, and the two-phase friction factor is modified, introducing the Knudsen number.
- Transient behavior of flow boiling pressure drop and heat transfer can be observed in mini/microchannels experimentally, and 1D unsteady mathematical model can be developed for the same.

Appendix A

Predictive Approach for Miniature Channels with Slip Flow

For the past century, the no-slip boundary condition has been assumed to be appropriate for most macroscopic flows. But recent developments in microfluidic and nanofluidic devices have renewed interest in the problem of slip, where its influence is expected to be significant even as the Reynolds number Re tends to zero (Priezjev and Troian, 2006). New modelling approaches to predict flow boiling pressure drop and heat transfer in very small microchannels have been proposed where the no slip condition is not valid and incorporate the effect of local thermophysical properties and flashing on the pressure gradient. For simplicity, homogeneous equilibrium model is adopted for the present study. A new two phase friction factor is suggested by incorporating effect of slip in the wall. Using this pressure drop model, local saturation temperature and local thermodynamic properties are evaluated and local heat transfer coefficient is predicted. It is observed that for large pressure drop, new modelling approaches for pressure drop and heat transfer give significant difference in the predictions when it compared to the existing modelling approaches.

A.1 Modelling approach for Flow Boiling Pressure Drop

In the boiling region due to saturated boiling that produces a net vapor generation resulting in an increase in pressure drop as compared to purely liquid flow. Using the homogeneous equilibrium model, the liquid and vapor phases are assumed to form a homogeneous mixture with equal and uniform velocities and property values for the liquid and vapor phases are the saturated values at the local pressure. Consider the channel shown in Figure A.1. From energy balance the vapor quality x can be expressed by Equation (A.1) which accounts for axial changes in quality due to heat input as well as flashing that results from enthalpy changes with the pressure.

$$\frac{dx}{dz} = \frac{1}{h_{fg}} \left[\frac{q_{eff} P_H}{GA} - \frac{dh_f}{dp} \frac{dp}{dz} \right] \tag{A.1}$$

Assuming the properties (v_g and h_f) within the saturated region are functions of only the local pressure, pressure gradient is expressed by Equation (A.2)

$$-\frac{dp}{dz} = \frac{\left(\frac{f_{TP,new} G^2 v_f}{2D_H}\right)\left(1 + x\frac{v_{vg}}{v_f} + \frac{G q_{eff} P_H v_{fg}}{A h_{fg}}\right)}{1 + G^2 x \frac{dv_g}{dp} - \frac{G^2 v_{fg}}{h_{fg}} \frac{dh_f}{dp}} \tag{A.2}$$

Equations (A.1) and (A.2) are coupled and can be solved by using 4$^{\text{th}}$ order explicit Runge-Kutta method. But beforehand, dh_f/dp and dv_g/dp was evaluated using Equations (A.3) and (A.4). In the present study two-phase friction co-efficient is modified incorporating the surface tension (Weber number) and slip in the wall (Knudsen number) and it is expressed by Equation (A.5) and Equation (A.6). This new predicted two-phase friction factor ($f_{TP,new}$) determined by curve fitting of experimental data from literature from Revellin and Thome (2007).

$$\frac{dv_g}{dp} = \frac{RT}{p^2} \left[\frac{RT}{h_{fg}} - 1 \right] \tag{A.3}$$

$$\frac{dh_f}{dp} = C_{v,f} \frac{RT^2}{p h_{fg}} + v_f \tag{A.4}$$

$$f_{TP,new} = \frac{12 We^{-0.35}}{(1 + 6K')\, Re'_{TP}} \tag{A.5}$$

$$\frac{1}{K'} = \frac{x}{Kn\eta} + \frac{1 - x}{L_s} \tag{A.6}$$

In Re'_{TP}, viscosity considered is mixture viscosity and it is given by Equation (A.7)

$$\frac{1}{\mu} = \frac{x}{\mu_g} + \frac{1 - x}{\mu_f} \tag{A.7}$$

A.1.1 Results And Discussion

The present model is compared with the homogeneous equilibrium model considering thermodynamic properties at system pressure and no effect of flashing. For the calculation, water is taken as working fluid model and the parameters are listed in Table A.1. For smaller pressure drop (especially for bigger channels), present model almost predict same as homogeneous equilibrium model with constant properties and without any modification. The differences between the two modelling approaches become significant once the size of channel decrease or pressure drop become large (Figure A.1). The present model properties are calculated at local pressure which represents the true phenomenon and inclusion of surface tension and slip make the model more realistic and it can be a suitable choice for microchannels heat sink design.

Tab. A.1: Model parameters

Parameter	Value / Range
Heat Flux	1 to 20 W/cm^2
Mass Flux	200 kg/m^2 s
Inlet Temperature	60°C
Inlet Pressure	3 bar

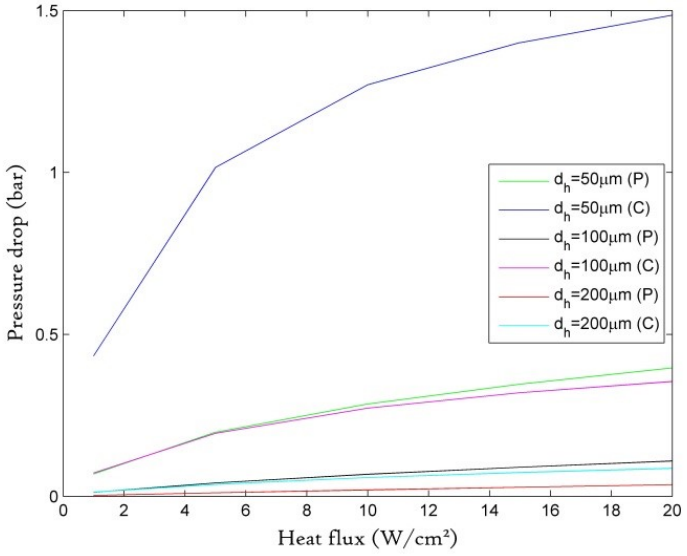

Fig. A.1: Pressure drop predication at different hydraulic diameter. (P= present model, C= HEM with constant properties and without modification)

Not only pressure drop, exit quality is also depends on local pressure as well as local thermodynamic properties. In Figure A.2 it is observed that there is significant deviation in x_{out} is observed as compared to x_{out} considering constant properties for small hydraulic diameter It is because for lower hydraulic diameter, pressure drop is high and property variation is significant and effect of flashing become significant.

A.2 Modelling approach for Flow Boiling Heat Transfer

The trend of local heat transfer coefficients basically depends on the local saturation pressure (or saturation temperature) inside the channel and the wall temperature. Meanwhile, there is no accurate correlation to predict the local saturation pressures (temperatures) along the channel (Mirmanto, 2014). Therefore, existing approaches considered the saturation pressure distribution decreases linearly in the two phase region. In the present study, local saturation pressure is evaluated from the pressure model described in above section and saturation temperature is calcualted from equation (A.8)

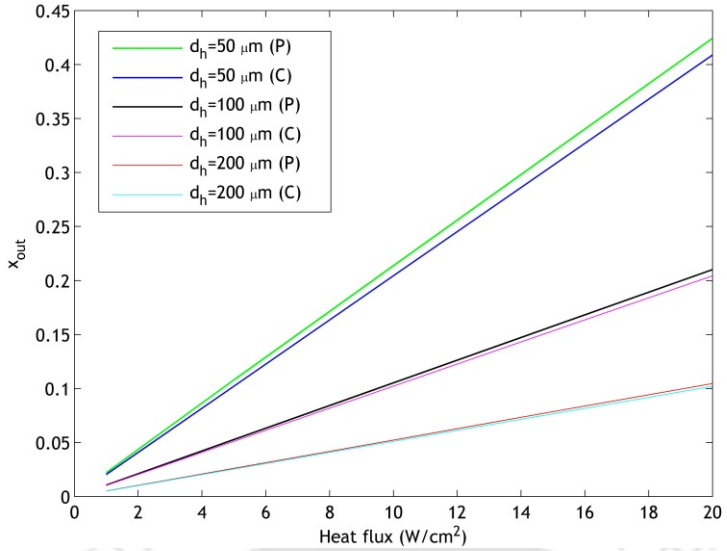

Fig. A.2: Thermodynamic exit quality predication at different hydraulic diameter (P= present model, C= HEM with constant properties and without modification)

$$T = \left[\frac{1}{T_{ref}} - \frac{R}{h_{fg}} ln\left(\frac{p}{p_{ref}}\right)\right] \tag{A.8}$$

In the boiling region due to saturated boiling that produces a net vapor generation resulting in an increase in pressure drop as compared to purely liquid flow. Using the homogeneous equilibrium model, the liquid and vapor phases are assumed to form a homogeneous mixture with equal and uniform velocities and property values for the liquid and vapor phases are the saturated values at the local pressure. From energy balance the vapor quality x can be expressed by equation (A.1) which accounts for axial changes in quality due to heat input as well as flashing that results from enthalpy changes with pressure. Fang et al. (2015) compiles a database of 1055 data points of water flow boiling heat transfer in mini/microchannel and given a correlations of flow boiling heat transfer coefficient. Therefore in this study, two phase heat transfer coefficient (h_{TP}) was evaluated by using the correlation given by Fang et al. (2015) and it is expressed by equation (A.9 – A.13)

$$h_{TP} = Nu\frac{k_f}{D_H} \tag{A.9}$$

$$Nu = 0.00061(S+F)Re_f Fa^{0.11} Pr_f^{0.4}/\ln U) \tag{A.10}$$

$$S = 142.5Bo^{0.9}M^{0.55}\left(\frac{\rho_f}{\rho_g}\right)^{0.33} \tag{A.11}$$

$$F = x\left(\frac{x}{1-x}\right)^{0.9}\left(\frac{\rho_f}{\rho_g}\right)^{0.35} \tag{A.12}$$

$$U = 1.02\left(\frac{\mu_{f,w}}{\mu_{l,w}}\right) \tag{A.13}$$

Present model was examined with model given by Fang et al. (2015) (linear pressure profile) for two different of hydraulic diameter of 50 μm and 100 μm and model parameters were listed in Table A.1. Microchannels were considered as square and three side wall heating is assumed.

A.2.1 Results and Discussion

In Figure A3 present model and model without the effect of pressure profile for constant mass flux is compared for two different hydraulic diameter. Heat transfer coefficient was evaluated at 0.03 m from the inlet. It can be seen that for both the cases h_{TP} increases with heat flux. This can be explain on the basis of previous experimental data from literature that the dominating heat transfer mechanism was nucleate boiling. For the same inlet condition and same length perdition of present model with pressure profile independent model was good for 100 μm channel but shows deviation for 50 μm channel. Reason for that can be explained on the basis of pressure drop. Since for the 100 μm channel pressure drop range was 0.13 bar to 0.19 bar so effect of saturation temperature change due to pressure drop was not significant on heat transfer coefficient. On the other hand pressure drop range for 50 μm channel was 0.24 to 0.48 bar which was much higher than 100 μm channel. Therefore, large pressure drop influence the saturation temperature as well as in the local thermophysical properties for which there came a significant deviation between present model and pressure profile independent model specially in higher heat flux.

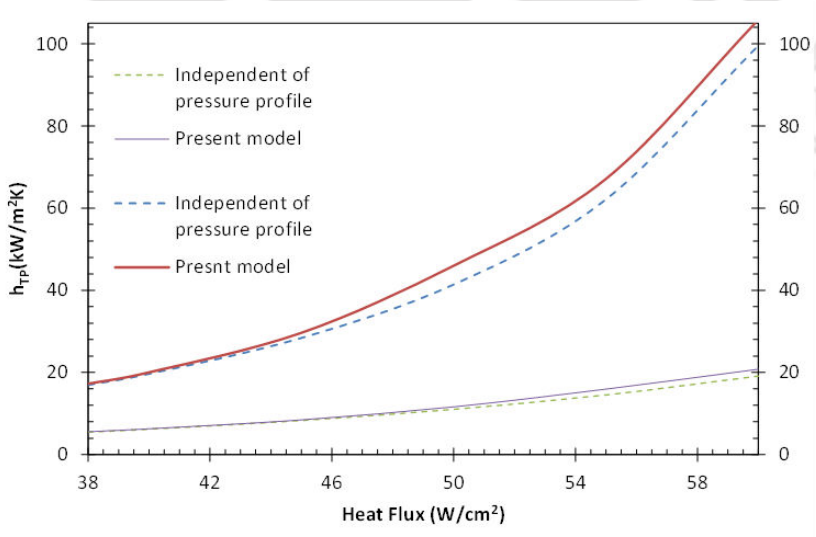

Fig. A.3: Comparison between the present model and model without the effect of pressure profile for constant mass flux

Appendix B

Appendix B

B.1 Improvement of the new modelling approach with the incorporation of heating effect

Improvement of the new modelling approach (local thermophysical properties and flashing) with the incorporation of heating effect on ϕ_{fo}^2 for large pressure drop case is shown in the Figure B.1.

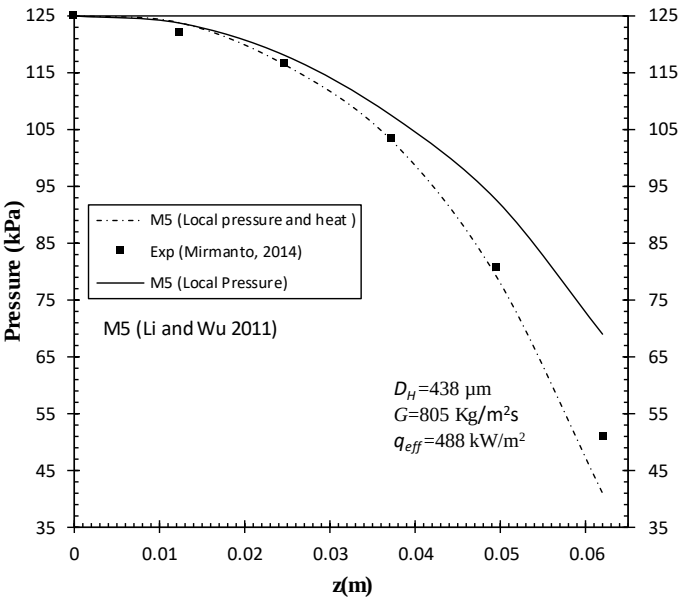

Fig. B.1: Improvement of a model from the literature (li and Wu, 2011) , with local properties, flashing effect and heating effect on ϕ_{fo}^2 for large pressure drop case. Fluid: DI water

B.2 Experimental data points

The figure B.2 contains all the experimental flow boiling pressure drop and heat transfer data points for water and FC-72.

Water as working fluid			
G	q_eff	hTP exp	Exp DP
kg/m^2s	kw/m^2	kW/m^2K	kPa
205.1	78.16	38.35	14.09
205.1	109.25	31.91	18.06
205.1	146.56	25.52	23.06
205.1	167.10	21.19	28.06
256.4	75.16	42.41	18.91
256.4	119.25	35.11	23.91
256.4	157.56	28.56	29.06
256.4	177.10	24.83	32.56
307.7	126.19	38.01	22.91
307.7	145.24	34.13	25.31
307.7	175.14	28.64	29.66
307.7	212.35	21.49	34.06
359.0	85.70	49.06	16.81
359.0	98.49	46.33	18.61
359.0	115.16	42.76	21.06
359.0	133.22	39.17	28.56
410.3	122.52	46.11	23.56
410.3	142.31	41.35	26.56
410.3	166.87	32.74	31.56
410.3	193.58	26.19	37.06

FC-72 as working fluid			
G	q_eff	hTP exp	Exp DP
kg/m^2s	kw/m^2	kW/m^2K	kPa
345.0	42.31	11.53	12.60
345.0	47.78	10.20	14.81
345.0	51.57	8.92	16.00
345.0	58.20	7.93	18.00
431.0	54.00	11.70	20.50
431.0	58.49	10.30	21.90
431.0	66.53	9.16	25.00
431.0	76.19	8.38	29.10
517.0	48.65	13.16	21.80
517.0	56.77	11.63	24.30
517.0	62.46	10.58	28.43
517.0	66.15	10.03	31.00
517.0	75.70	9.09	33.90
603.0	54.42	13.13	28.80
603.0	65.45	11.53	33.00
603.0	74.70	10.55	36.80
603.0	84.13	8.89	39.50
690.0	55.18	14.63	36.20
690.0	60.67	13.75	38.50
690.0	62.88	13.12	40.60
690.0	66.28	12.67	42.30
690.0	69.01	11.91	45.20

Fig. B.2: Experimental flow boiling pressure drop and heat transfer data points for water and FC-72.

B.3 Comparison of generalized model with the ideal-gas flow based model

Comparison of generalized model with the ideal-gas flow based model is shown in Figure B.3 . The experimental data used for validation was for FC-72 whose vapour phase does not behave like ideal gas. It was observed that the generalized model predicts better than the ideal-gas flow based model.

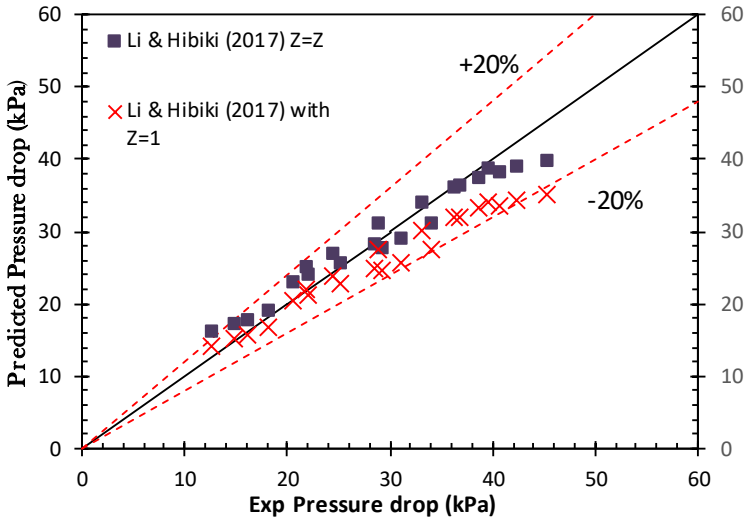

Fig. B.3: Comparison of generalized model with the ideal-gas flow based model

Bibliography

Adham, A. M., Mohd-Ghazali, N., and Ahmad, R. (2013). Thermal and hydrodynamic analysis of microchannel heat sinks: A review. *Renewable and Sustainable Energy Reviews*, 21:614–622.

Agostini, B. and Bontemps, A. (2005). Vertical flow boiling of refrigerant R134a in small channels. *Int. J. Heat Fluid Flow*, 26:296–306.

Al-Shemmeri, T. (2012). *Engineering Fluid Mechanics*. Ventus Publishing ApS.

Al-Zaidi, A. H., Mahmoud, M. M., and Karayiannis, T. G. (2019). Flow boiling of hfe-7100 in microchannels: Experimental study and comparison with correlations. *International Journal of Heat and Mass Transfer*, 140:100 – 128.

Alam, T., Lee, P. S., Yap, C. R., and Jin, L. (2012). Experimental investigation of local flow boiling heat transfer and pressure drop characteristics in microgap channel. *Int. J. of Multiphase Flow*, 42:164–174.

Asadi, M., Xie, G., and Sunden, B. (2014). A review of heat transfer and pressure drop characteristics of single and two-phase microchannels. *International Journal of Heat and Mass Transfer*, 79:34–53.

Baldassari, C. and Marengo, M. (2013). Flow boiling in microchannels and microgravity. *Progress in Energy and Combustion Science*, 39:1–36.

Bertsch, S. S., Groll, E. A., and Garimella, S. V. (2009). A composite heat transfer correlation for saturated flow boiling in small channels. *Int. J. Heat Mass Transfer*, 52:2110–2118.

Bhide, R. R., Singh, S. G., Sridharan, A., Duttagupta, S. P., and Agrawal, A. (2009). Pressure drop and heat transfer characteristics of boiling water in sub-hundred-micron channel. *Experimental Thermal and Fluid Science*, 33:963–975.

Bigham, S. and Moghaddam, S. (2017). Physics of the Microchannel Flow Boiling Process and Comparison With the Existing Theories. *J. Heat Transfer*, 139(11):111503. Paper No: HT-16-1594; doi: 10.1115/1.4036655.

Brauner, N. and Maron, D. M. (1992). Identification of the range of âĂŸsmall diametersâĂŹ conduits, regarding two-phase flow pattern transitions. *International Communications in Heat and Mass Transfer*, 19(1):29 – 39.

Chen, C. (1966). Correlation for boiling heat transfer to saturated fluids in convective flow. *I&EC Process Des. Dev.*, 5(3):322–329.

Chen, L., Tian, Y., and Karayiannis, T. (2006). The effect of tube diameter on vertical two-phase flow regimes in small tubes. *International Journal of Heat and Mass Transfer*, 49(21):4220 – 4230.

Chen, T. and Garimella, S. V. (2007). Flow boiling heat transfer to a dielectric coolant in a microchannel heat sink. *IEEE Transactions on Components and Packaging Technologies*, 30(1):24–31.

Chen, T. and Garimella, S. V. (2011). Local heat transfer distribution and effect of instabilities during flow boiling in a silicon microchannel heat sink. *International Journal of Heat and Mass Transfer*, 54:3179–3190.

Cioncolini, A. and Thome, J. R. (2017). Pressure drop prediction in annular two-phase flow in macroscale tubes and channels. *Int. J. of Multiphase Flow*, 89:321–330.

Coleman, H. and Steele, W. J. (2009). *Experimentation and Uncertainty Analysis for Engineers, 3rd Edition*. John Wiley and Sons, Inc.,.

Collier, J. G. and Thome, J. R. (1994). *Convective Boiling and Condensation*. Oxford University Press, Oxford, third edition.

Cooper, M. G. (1984). Saturation nucleate pool boiling âĂŞ a simple correlation. *I. Chem. Eng. Symp. Ser.*, 86:785–793.

Cornwell, P. and Kew, P. (1993). *Boiling in small parallel channels, in: P.A. Pilavachi (Ed.), Energy Efficiency in Process Technology,*. Elsevier Applied Science, London,.

D., L. and V., G. S. (2006). Flow boiling heat transfer in microchannels. *ASME. J. Heat Transfer*, 129(10):1321–1332.

Dário, E. R., Passos, J. C., Simón, M. L. S., and Tadrist, L. (2016). Pressure drop during flow boiling inside parallel microchannels. *Int. J. Refrigeration*, 72:111–123.

Ducoulombier, M., Colasson, S., Bonjour, J., and Haberschill, P. (2011a). Carbon dioxide flow boiling in a single microchannel - part i: Pressure drops. *Experimental Thermal and Fluid Science*, 35:581–596.

Ducoulombier, M., Colasson, S., Bonjour, J., and Haberschill, P. (2011b). Carbon dioxide flow boiling in a single microchannel - part II: heat transfer. *Exp. Therm. Fluid Sci*, 35:597–611.

Duryodhan, V. S., Singh, A., Singh, S. G., and Agrawal, A. (2015). Convective heat transfer in diverging and converging microchannels. *Int. J. Heat Mass Transfer*, 80:424âĂŞ438.

Fang, X., Zhou, Z., and Wang, H. (2015). Heat transfer correlation for saturated flow boiling of water. *Applied Thermal Engineering*, 76:147–156.

Fayyadh, E., Mahmoud, M., Sefiane, K., and Karayiannis, T. (2017). Flow boiling heat transfer of r134a in multi microchannels. *International Journal of Heat and Mass Transfer*, 110:422 – 436.

Fukano, T. and Kariyasaki, A. (1993). Characteristics of gas-liquid two-phase flow in a capillary tube. *Nuclear Engineering and Design*, 141:59–68.

Galvis, E. and Culham, R. (2012). Measurements and flow pattern visualizations of two-phase flow boiling in single channel microevaporators. *International Journal of Multiphase Flow*, 42:52–61.

Gao, P., Person, S. L., and Favre-Marinet, M. (2002). Scale effects on hydrodynamics and heat transfer in two-dimensional mini and microchannels. *Int. J. of Thermal Sciences*, 41:1017–1027.

Harirchian, T. and Garimella, S. V. (2008). Microchannel size effects on local flow boiling heat transfer to a dielectric fluid. *Int. J. Heat Mass Transfer*, 51:3724–3435.

Harirchian, T. and Garimella, S. V. (2009a). The critical role of channel cross-sectional area in microchannel flow boiling heat transfer. *International Journal of Multiphase Flow*, 35(10):904 – 913.

Harirchian, T. and Garimella, S. V. (2009b). Effects of channel dimension, heat flux, and mass flux on flow boiling regimes in microchannels. *Int. J. Multiphase Flow*, 35:349–362.

Harirchian, T. and Garimella, S. V. (2010). A comprehensive flow regime map for microchannel flow boiling with quantitative transition criteria. *International Journal of Heat and Mass Transfer*, 53:2694–2702.

Huh, C. and Kim, M. H. (2007). Pressure Drop, Boiling Heat Transfer and Flow Patterns during Flow Boiling in a Single Microchannel. *Heat Transfer Engineering*, 28 (8-9):730–737.

Huo, X., Chen, L., Tian, Y. S., and Karayiannis, T. G. (2004). Flow boiling and flow regimes in small diameter tubes. *Applied Thermal Engineering*, 24:1225–1239.

Jang, Y., Park, C., Lee, Y., and Kim, Y. (2008). Flow boiling heat transfer coefficients and pressure drops of FC-72 in small channel heat sinks. *Int. J. Refrig*, 31:1033–1041.

Jayaramu, P., Gedupudi, S., and Das, S. K. (2019). Influence of heating surface characteristics on flow boiling in a copper microchannel: Experimental investigation and assessment of correlations. *International Journal of Heat and Mass Transfer*, 128:290 – 318.

Jiang, J., Hao, Y., and Shi, M. (2008). Fluid flow and heat transfer characteristics in rectangular microchannel. *Heat Transfer-Asian Research*, 37:197–207.

Jiang, L., Wong, M., and Zohar, Y. (2001). Forced convection boiling in a microchannel heat sink. *J. Microelectromech. Syst*, 10:80–87.

Jiang, X. N., Zhou, Z. Y., Huang, X. Y., and Liu, C. (1997). Laminar flow through microchannels used for microscale cooling systems. *Proceeding of the Electronic Packaging Technology Conference, EPTC*, pages 119–122.

Kadam, S. T. and Kumar, R. (2014). Twenty first century cooling solution: Microchannel heat sinks. *Int. J. Thermal Sciences*, 85:73–92.

Kandlikar, S. G. and Grande, W. J. (2003). Evolution of microchannel flow passages thermos hydraulic performance and fabrication technology. *Heat Transfer Eng*, 24:3–17.

Karayiannis, T. and Mahmoud, M. (2017). Flow boiling in microchannels: Fundamentals and applications. *Applied Thermal Engineering*, 115:1372 – 1397.

Kawahara, A., Chung, P., and Kawaji, M. (2002). Investigation of two-phase flow pattern, void fraction and pressure drop in a microchannel. *International Journal of Multiphase Flow*, 28(9):1411 – 1435.

Keepaiboon, C., Thiangtham, P., Mahian, O., DalkÄślÄśÃğ, A. S., and Wongwises, S. (2016). Pressure drop characteristics of r134a during flow boiling in a single rectangular micro-channel. *International Communications in Heat and Mass Transfer*, 71:245 – 253.

Kew, P. A. and Cornwell, K. (1997). Correlations for the prediction of boiling heat transfer in small-diameter channels. *Applied Thermal Engineering*, 17(8):705–715.

Kim, S. M. and Mudawar, I. (2012). Flow condensation in parallel micro-channels - Part 1: Experimental results and assessment of pressure drop correlations. *Int. J. Heat Mass Transfer*, 55:971–983.

Kim, S. M. and Mudawar, I. (2013a). Universal approach to predicting heat transfer coefficient for condensing mini/micro-channel flow. *Int. J. Heat Mass Transfer*, 56:238–250.

Kim, S. M. and Mudawar, I. (2013b). Universal approach to predicting two-phase frictional pressure drop for mini/micro-channel saturated flow boiling. *Int. J. Heat Mass Transfer*, 58:718–734.

Korniliou, S., Mackenzie-Dover, C., Harmand, S., Duursma, G., Christy, J., Terry, J., Walton, A., and Sefiane, K. (2019). Local wall temperature mapping during flow boiling in a transparent microchannel. *International Journal of Thermal Sciences*, 135:344 – 361.

Lazarek, G. M. and Black, S. H. (1982). Evaporative heat transfer, pressure drop and critical heat flux in a small vertical tube with R113. *Int. J. Heat Mass Transfer*, 25:945–960.

Lee, H. J. and Lee, S. Y. (2001). Pressure drop correlations for two-phase flow within horizontal rectangular channels with small heights. *Int. J. Multiphase Flow*, 27:783–796.

Lee, J. and Mudawar, I. (2005). Two-phase flow in high-heat-flux micro-channel heat sink for refrigeration cooling applications: Part I-pressure drop characteristics. *Int. J. Heat Mass Transfer*, 48:928–940.

Lee, P. S. and Garimella, S. V. (2008). Saturated flow boiling heat transfer and pressure drop in silicon microchannel arrays. *Int. J. Heat Mass Transfer*, 51:789–806.

Lelea, D., Nishio, S., and Takano, K. (2004). The experimental research on micro-tube heat transfer and fluid flow of distilled water. *Int. J. Heat Mass Transfer*, 47:2817âĂŞ2830.

Li, W. and Wu, Z. (2010). A general criterion for evaporative heat transfer in micro/mini-channels. *Int. J. Heat Mass Transfer*, 53(9):1967–1976.

Li, W. and Wu, Z. (2011). Generalized adiabatic pressure drop correlation in evaporative micro/mini-channels. *Experimental Thermal and Fluid Science*, 35:866–872.

Li, X. and Hibiki, T. (2017). Frictional pressure drop correlation for two-phase flows in mini and micro single-channels. *Int. J. of Multiphase Flow*, 90:29–45.

Lim, T.-W., You, S.-S., Choi, J.-H., and Kim, H.-S. (2015). Experimental investigation of heat transfer in two-phase flow boiling. *Experimental Heat Transfer*, 28:23–36.

Lin, S., Kew, P. A., and Cornwell, K. (2001). Flow Boiling of Refrigerant R141B in Small Tubes. *Chemical Engineering Research and Design*, 79:417–424.

Lin, S., Kwok, C. C. K., Li, R. Y., Chen, Z. H., and Chen, Z. Y. (1991). Local frictional pressure drop during vaporization of R-12 through capillary tubes. *Int. J. Multiphase Flow*, 17:95–102.

Liu, Z. and Winterton, R. H. S. (1991). A general correlation for saturated and subcooled flow boiling in tubes and annuli, based on a nucleate pool boiling equation. *Int. J. Heat Mass Transfer*, 34:2759–2766.

M., M., Kenning, D. B. R., Lewis, J. S., and Karayiannis, T. G. (2012). Pressure drop and heat transfer characteristics for single-phase developing flow of water in rectangular microchannels. *Journal of Physics: Conference Series*, 395:012085.

Mahmoud, M. M. and Karayiannis, T. G. (2013a). Heat transfer correlation for flow boiling in small to micro tubes. *International Journal of Heat and Mass Transfer*, 66:553 – 574.

Mahmoud, M. M. and Karayiannis, T. G. (2013b). Heat transfer correlation for flow boiling in small to micro tubes. *Int. J. Heat Mass Transfer*, 66:553–574.

Mahmoud, M. M., Karayiannis, T. G., and Kenning, D. B. R. (2013). Flow boiling pressure drop of r134a in microdiameter tubes: Experimental results and assessment of correlations. *Heat Transfer Engineering*, 35:178–192.

Markal, B., Aydin, O., and Avci, M. (2016). An experimental investigation of saturated flow boiling heat transfer and pressure drop in square microchannels. *Int. J. Refrigeration*, 65:1–11.

Markal, B., Aydin, O., and Avci, M. (2019). Effect of hydraulic diameter on flow boiling in rectangular microchannels. *Heat and Mass Transfer*, 55(4):1033–1044.

Markal, B. Aydin, O. A. M. (2017). Prediction of heat transfer coefficient in saturated flow boiling heat transfer in parallel rectangular microchannel heat sinks: an experimental study. *Heat Transf. Eng.*, 38:1415–1428.

Megahed, A. and Hassan, I. (2009). Two-phase pressure drop and flow visualization of FC-72 in a silicon microchannel heat sink. *Int. J. Heat Fluid Flow*, 30:1171–1182.

Mehendale, S., Jacobi, A.M., and Shah, R. (2000). Fluid flow and heat transfer at micro- and meso-scales with application to heat exchanger design. *ASME. Appl. Mech. Rev.*, 53:175–193.

Mirmanto, M. (2014). Heat transfer coefficient calculated using a linear pressure gradient assumption and measurement for flow boiling in microchannels. *Int. J. Heat Mass Transfer*, 79:269–278.

Mirmanto, M. (2016). Local pressure measurements and heat transfer coefficients of flow boiling in a rectangular microchannel. *Heat Mass Transfer*, 52:73–83.

Mishan, Y., Mosyak, A., Pogrebnyak, E., and Hetsroi, G. (2007). Effect of developing flow and thermal regimes on momentum and heat transfer in micro scale heat sinks. *Int. J. Heat Mass Transfer*, 50:3100–3114.

Mishima, K. and Hibiki, T. (1996). Some characteristics of air-water two-phase flow in small diameter vertical tubes. *Int. J. Multiphase Flow*, 22:703–712.

Moharana, M. M., Agrawal, G., and Khandekar, S. (2011). Axial conduction in single phase simultaneously developing flow in a rectangular mini-channel array. *Int. J. of Thermal Sciences*, 50:1001–1012.

Mudawar, I. (2011). Two-phase microchannel heat sinks: Theory, applications, and limitations. *ASME. J. Electron. Packag*, 133(4):041002–31.

Oh, H. K. and Son, C. H. (2011). Evaporation flow pattern and heat transfer of R-22 and R-134a in small diameter tubes. *Heat Mass Transfer*, 47:703–717.

Ong, C. and Thome, J. (2011). Macro-to-microchannel transition in two-phase flow: Part 1 âĂŞ two-phase flow patterns and film thickness measurements. *Experimental Thermal and Fluid Science*, 35(1):37 – 47.

Ong, C. L. and Thome, J. R. (2009). Flow boiling heat transfer of R134a, R236fa and R245fa in a horizontal 1.030mm circular channel. *Experimental Thermal and Fluid Science*, 33:651–663.

Park, C. Y., Jang, C. Y., Kim, B., and Kim, Y. (2012). Flow boiling heat transfer coefficients and pressure drop of FC-72 in microchannels. *Int. J. of Multiphase Flow*, 39:45–54.

Park, H., Pak, J. J., Son, S. Y., Lim, G., and Song, I. (2003). Fabrication of a microchannel integrated with inner sensors and the analysis of its laminar flow characteristics. *Sens. Actuators A Phys.*, 103 (3):317–329.

Peng, X. F. and Peterson, G. P. (1996). Convective heat transfer and flow friction for water flow in microchannels structures. *Int. J. Heat Mass Transfer*, 36(12):2599–2608.

Pike-Wilson, E. and Karayiannis, T. (2014). Flow boiling of r245fa in 1.1mm diameter stainless steel, brass and copper tubes. *Experimental Thermal and Fluid Science*, 59:166 – 183.

Priezjev, N. V. and Troian, S. M. (2006). Influence of periodic wall roughness on the slip behavior at liquid/solid interfaces: molecular-scale simulations versus continuum predictions. *Journal of fluid Mechanics*, 554:25–46.

Qu, W. and Mudawar, I. (2003a). Flow boiling heat transfer in two-phase micro-channel heat sinksâĂŞâĂŞi. experimental investigation and assessment of correlation methods. *International Journal of Heat and Mass Transfer*, 46(15):2755 – 2771.

Qu, W. and Mudawar, I. (2003b). Measurements and prediction of pressure drop in two-phase micro-channel heat sinks. *Int. J. Heat Mass Transfer*, 46:2737–2753.

Qu, W. and Mudawar, I. (2004). Transport phenomena in two-phase micro-channel heat sinks. *J. Electron. Packag. Trans. ASME*, 126:213–224.

Rathnasamy, R., Arakeri, J. H., and Srinivasan, K. (2005). Experimental investigation of fluid flow in long rectangular micro-channels. *Proceedings of the Institution of Mechanical Engineers, Part E: Journal of Process Mechanical Engineering*, 219:227–235.

Ravigururajan, T. (1998). Impact of channel geometry on two-phase flow heat transfer characteristics of refrigerants in microchannel heat exchangers. *ASME. J. Heat Transfer*, 120(2):485–491.

Revellin, R. and Thome, J. R. (2007). A new type of diabatic flow pattern map for boiling heat transfer in microchannels. *Journal of Micromechanics and Microengineering*, 17 (4):788.

Sahara, A. M., Wissinka, J., Mahmoud, M. M., Karayiannisa, T. G., S., M., and Ishakd, A. (2017). Effect of hydraulic diameter and aspect ratio on single phase flow and heat transfer in a rectangular microchannel. *Applied Thermal Engineering*, 115:793–814.

Saurel, R., Petitpas, F., and Abgrall, R. (2008). Modelling phase transition in metastable liquids: application to cavitating and flashing flows. *J. Fluid Mech*, 607:313–350.

Shah, M. M. (1982). Chart correlation for saturated boiling heat transfer: equations and further study. *ASHRAE Trans*, 88:185–196.

Shah, M. M. (2017). Unified correlation for heat transfer during boiling in plain mini/micro and conventional channels. *International Journal of Refrigeration*, 74:606 – 626.

Shah, R. and Sekulic, D. (2003). *Fundamentals of Heat Exchanger Design*. John Willey and Sons,.

Shah, R. K. and London, A. L. (1978). *Laminar Flow Forced Convection in Ducts Supplement 1 to Advances in Heat Transfer*. Academic Press, New York.

Shen, S., Xu, J. L., Zhou, J. J., and Chen, Y. (2006). Flow and heat transfer in microchannels with rough wall surface. *J. Energy Convers. Manage*, 47:1311–1325.

Silverio, V. and Moreira, A. L. N. (2008). Friction losses and heat transfer in laminar microchannel single-phase liquid flow. *Proceedings of 6th International ASME Conference on Nanochannels, Microchannels and Minichannels, Darmstadt, Germany.*

Singh, S., Kulkarni, A., Duttagupta, S., Puranik, B., and Agrawal, A. (2008). Impact of aspect ratio on flow boiling of water in rectangular microchannels. *Experimental Thermal and Fluid Science*, 33(1):153 – 160.

Singh, S. G., Bhide, R., Puranik, B., Duttagupta, S. P., and Agrawal, A. (2009). Two phase flow pressure drop characteristics in trapezoidal silicon microchannels. *IEEE Trans. Component Packaging Technology*, 32 (4).

Smpertegui-Tapia, D. F. and Ribatski, G. (2017). Two-phase frictional pressure drop in horizontal micro-scale channels: Experimental data analysis and prediction method development. *International Journal of Refrigeration*, 79:143 – 163.

Steinke, M. E. and Kandlikar, S. G. (2004). An experimental investigation of flow boiling characteristics of water in parallel microchannels. *Journal of Heat Transfer-Transactions of the ASME*, 126:518–526.

Steinke, M. E. and Kandlikar, S. G. (2006). Single-phase liquid friction factors in microchannels. *Int. J. Therm. Sci*, 45:1073–1083.

Suo, M. and Griffith, P. (1964). Griffith p. two-phase flow in capillary tubes. *ASME. J. Basic Eng*, 86(3):576–582.

Thiangtham, P., Keepaiboon, C., Kiatpachai, P., Asirvatham, L. G., Mahian, O., Dalkilic, A. S., and Wongwises, S. (2016). An experimental study on two-phase flow patterns and heat transfer characteristics during boiling of r134a flowing through a multi-microchannel heat sink. *International Journal of Heat and Mass Transfer*, 98:390 – 400.

Thome, J. R. (2004). Boiling in microchannels: a review of experiment and theory. *Int. J. Heat and Fluid Flow*, 25:128–139.

Tibirica, C. and Ribatski, G. (2015). Flow boiling phenomenological differences between micro-and macroscale channels. *Heat Transfer Eng.*, 36(1):937–942.

Toh, K. C., Chen, X. Y., and Chai, J. C. (2002). Numerical computation of fluid flow and heat transfer in microchannels. *Int. J. Heat Mass Transfer*, 45:5133âĂŞ5141.

Tran, T., Wambsganss, M., and France, D. (1996). Small circular- and rectangular-channel boiling with two refrigerants. *International Journal of Multiphase Flow*, 22(3):485 – 498.

Triplett, K., Ghiaasiaan, S., Abdel-Khalik, S., and Sadowski, D. (1999). GasâĂŞliquid two-phase flow in microchannels part i: two-phase flow patterns. *International Journal of Multiphase Flow*, 25(3):377 – 394.

Tuckerman, D. B. and Pease, R. F. (1981). High performance heat sinking for VLSI. *IEEE Electron. Dev. Lett. EDL*, 2:126–129.

Ullmann, A. and Brauner, N. (2007). The prediction of flow pattern maps in minichannels. *Multiphase Sci. Technol*, 19(1):49âĂŞ73.

Urbanek, W., Zemel, J. N., and Bau, H. H. (1993). An investigation of the temperature dependence of Poiseuille numbers in microchannel flow. *J. Micro-mech Microeng*, 3:206–209.

Wang, B. X. and Peng, X. F. (1994). Experimental investigation on liquid forced convection heat transfer through microchannels. *Int. J. Heat Mass Transfer Supplementary*, 37 (1):73–82.

Wang, G., Cheng, P., and Wu, H. (2007). Unstable and stable flow boiling in parallel microchannels and in a single microchannel. *International Journal of Heat and Mass Transfer*, 50(21):4297 – 4310.

Wang, S., Chen, H., and Chen, C. (2018). Flow Boiling Heat Transfer of HFE7000 in Manifold Microchannels through Integrating Three-dimensional Flow and Silicon Nanowires. *17th IEEE Intersociety Conference on Thermal and Thermomechanical Phenomena in Electronic Systems (ITherm), San Diego, CA*, pages 630–638.

Warrier, G. R., Dhir, V. K., and Momoda, L. A. (2002). Heat transfer and pressure drop in narrow rectangular channels. *Exp. Thermal and Fluid Science*, 26:53–64.

Wu, H. and Cheng, P. (2003a). An experimental study of convective heat transfer in silicon microchannels with different surface conditions. *Int. J. Heat Mass Transfer*, 46(14):2547–2556.

Wu, H. Y. and Cheng, P. (2003b). Friction factors in smooth trapezoidal silicon microchannels with different aspect ratios. *Int. J. Heat Mass Transfer*, 46:2519–2525.

Xu, Y. and Fang, X. (2012). A new correlation of two-phase frictional pressure drop for evaporating flow in pipes. *Int. J. Refrigeration*, 35:2039–2050.

Xu, Y., Fang, X., Li, G., Li, D., and Yuan, Y. (2016). An experimental study of flow boiling heat transfer of R134a and evaluation of existing correlations. *International Journal of Heat and Mass Transfer*, 92:1143–1157.

Zhuan, R. and Wang, W. (2013). Boiling heat transfer characteristics in a microchannel array heat sink with low mass flow rate. *Applied Thermal Engineering*, 51(1):65 – 74.